MERIDIONAL HEAT TRANSPORT BY WIND-DRIVEN GYRES IN THE OCEANIC MIXED LAYER

by

FRANCIS BRUNO TOURNEUR

Eng. Degree in Marine Environment
Ecole Nationale Supérieure de Techniques Avancées
1986

DEA in Meteorology and Oceanography
Université Paris VI
1986

SUBMITTED TO THE DEPARTMENT OF METEOROLOGY
IN PARTIAL FULFILLMENT OF
THE REQUIREMENTS FOR THE DEGREE
OF

MASTER OF SCIENCE

at the

MASSACHUSETTS INSTITUTE OF TECHNOLOGY

September 1989

Signature of Author_____
Department of Earth, Atmospheric, and Planetary Sciences
July 30, 1989

Certified by_____
Reginald E. Newell, Professor of Meteorology, Thesis Supervisor

Accepted by_____
Tom Jordan, Chairman, Departmental Committee on Graduate Students

This thesis is dedicated
to the memory
of
Susan Ary

"Nothing living should ever be treated with contempt.
Whatever it is that lives, a person, a tree, or a bird,
should be touched gently,
because the time is short."

Elizabeth Goudge

MERIDIONAL HEAT TRANSPORT BY WIND-DRIVEN GYRES IN THE OCEANIC MIXED LAYER

by

Francis Bruno Tourneur

Submitted to the Department of Meteorology
in June 1989, in partial fulfillment of
the requirements for the degree
of

Master of Science

ABSTRACT

Oceanic temperature profiles covering the North Atlantic and North Pacific Oceans from 10°N to 56°N for the period 1949 - 1979 are processed and a seasonal climatology of the mixed-layer depth of the ocean is determined. It is subsequently used to see how much of the seasonal cycle of the total meridional heat transport within the top 300 meter of the ocean could be explained by a horizontal zonal overturning cell in the oceanic mixed layer. It is shown that the seasonal signature of this transport is partially retrieved and we identify the regions and processes that are dominant in this approach.

Thesis Supervisor : Reginald E. Newell
Title : Professor of Meteorology

ACKNOWLEDGEMENTS :

I would like to take this opportunity to sincerely thank my advisor, Professor Reginald Newell, whose broad interest and unflagging enthusiasm for science have been of great inspiration throughout my stay at MIT. Without his encouragements, care, constant availability, this thesis would have never been started. My thanks also go to many friends, colleagues and great people I met during this year and a half at MIT. They were there in the good times and the bad. Their moral support and friendship were precious to me. I would like to name here : Jane Hsiung, Ron Miller, Jane Mc Nabb, Nilton Renno, Jim Rydock, Steve Walker, Shuntai Zhou, Wu Zhongxiang, and many others. I really appreciated the long distance phoned friendship from Jim. Special thanks go to Mrs Dorothea Franzosa for opening her home to me and giving me the heartwarming atmosphere of a family.

Finally the person I wish to thank most is Susan Ary, to whom this thesis is dedicated.

Table of Content :

Abstract 3
Acknowledgements 4
Table of content 5
List of figures 6

I. Introduction 9
II. The Data Sets 12
2.1) COADS 12
2.1.1) Data density 13
2.1.2) Seasonal fields of SST 14
2.1.3) Wind system over the North Atlantic and North Pacific 15
2.2) MOODS 15
2.2.1) Data density 17

III. Computation of the mixed-layer depth
3.1) Preliminary treatment 19
3.2) Filtering procedure 24
3.3) Interpolation 26
3.4) Results and discussion 27
3.4.1) Basic physics of the mixed layer 27
3.4.2) Results 29

IV. Meridional heat flux calculation
4.1) Introduction 32
4.2) Computation of the standing gyre oceanic heat transport 33
4.3) Derivation of the current speed from the wind data 34
4.4) Water density calculation 35
4.5) Preliminary results 35
4.6) Mass Balance conservation 39
4.7) Adjusted results 43
4.8) Other possible contributors 46

V. Conclusion 47
VI. Figures 49
VII. References 83
VIII. Annexes 86

List of figures :

Figures 1a, 1b, 1c :
Number of reports per month for respectively the Atlantic, the Pacific and global oceans. (from COADS documentation).

Figure 2 :
Total number of individual SST measurements in each grid square for January over the 1854 - 1948 and 1949 - 1979 periods. (Atlantic and Pacific).

Figure 3 :
Number of years with SST observation for January over the 1854 - 1948 and 1949 - 1979 periods. (Atlantic and Pacific).

Figure 4 :
Sea surface temperature over the Atlantic Ocean : winter, spring, summer and fall. Long-term means over the 1949 -1979 period.

Figure 5 :
Sea surface temperature over the Pacific Ocean : winter, spring, summer and fall. Long-term means over the 1949 -1979 period.

Figure 6 :
Amplitude of the SST seasonal cycle, based on long-term means over the 1949 - 1979 period. (Atlantic and Pacific Oceans).

Figure 7 :
Long-term averaged seasonal wind over the North Atlantic Ocean. Winter, spring, summer and fall.

Figure 8 :
Long-term averaged seasonal wind over the North Pacific Ocean. Winter, spring, summer and fall.

Figure 9 :
Number of vertical soundings in the North Atlantic basin in January and July 1949, 1964 and 1973.

Figure 10 :
Number of vertical soundings in the North Pacific basin in January and July 1949, 1964 and 1978.

Figure 11 :
A sampling-based rejection criterion.

Figure 12 :
Mixed-layer depth climatology for the North Atlantic Ocean. Winter, spring, summer and fall.

Figure 13 :
Mixed-layer depth climatology for the North Pacific Ocean. Winter, spring, summer and fall.

Figure 14 :
Amplitude of the mixed-layer depth seasonal cycle, based on long-term means over the 1949 - 1979 period. (Atlantic and Pacific Oceans).

Figure 15 :
Long-term standing gyre heat transport contribution and standard deviation for the Atlantic Ocean.

Figure 16 :
Long-term standing gyre heat transport contribution and standard deviation for the Pacific Ocean.

Figure 17 :
Zonal averages of meridional transport, 0-300m for the Atlantic and Pacific Oceans. (from Hsiung et al 1988).

Figure 18 :
Distribution of the standing gyre contribution for selected months over the North Atlantic Ocean. (Climatologies).

Figure 19 :
Distribution of the standing gyre contribution for selected months over the North Pacific Ocean. (Climatologies).

Figure 20 :
Idealized seasonal cycle of the mixed-layer depth and the northeasterly winds in the upwelling areas off Africa and South California.

Figure 21 :
Long term mass imbalances and standard deviation for the Atlantic Ocean.

Figure 22 :
Long term mass imbalances and standard deviation for the Pacific Ocean.

Figure 23 :
Main path of the Kuroshio and Gulf-stream systems. From Hideo Kawai 1972.

Figure 24 :
Boundary current and other zones used for mass balance correction. (Atlantic and Pacific).

Figure 25 :
Long-term adjusted standing gyre heat transport contribution and standard deviation for the Atlantic Ocean.

Figure 26 :
Long-term adjusted standing gyre heat transport contribution and standard deviation for the Pacific Ocean.

Figure 27 :
Long-term sea surface temperature anomalies for the North Atlantic and North Pacific Ocean.

I) INTRODUCTION

Recent concerns about the Earth's climate have brought out the necessity to better understand the role that the ocean has in carrying from the equator to the pole the heat required to balance the ocean-atmosphere system. At the present time, although many estimations have been made, using various types of methods (Bryan 1962, Budyko 1963, Oort and Vonder Haar 1976, Hsiung et al 1989), much remains to be determined about the magnitude and variability of its contribution. In this study, we will investigate the seasonal cycle of the heat transport by the oceans.

The ocean heat transport is a transfer of thermal energy and its seasonal or interannual variations are likely to depend on features that are closely related to the oceanic mixed layer, since it is the region of the ocean the most subject to smaller time-scale fluctuations. The net heat transport is basically the result of an exchange of water masses, having different temperatures, between latitudes. A positive flux will then be driven by a northward flow of water at one temperature and by a southward flow at a lower temperature. The question to be addressed is at which depths those exchanges occur. Do they all take place within the surface mixed layer, as part of the general surface circulation imposed by the large scale horizontal gyre forcing, a kind of horizontal zonal overturning, or do the poleward or equatorward flows necessary to account for the observed seasonal cycle occur at different depths ?

It is well known that strong cooling coupled with enhanced evaporation forces at higher latitudes in the Atlantic ocean for the Northern Hemisphere an equatorward flow of colder, denser water. However, it is clearly improbable that this deep water circulation may affect the magnitude of the heat fluxes on a seasonal or interannual basis. A decadal timescale would be more appropriate. As a matter of fact, any flow occurring below the so-called seasonal thermocline is unlikely to produce any changes over a season or so. Hence we are dealing with only the top 300 meters of the ocean. What are now the water mass circulations to invoke

within that 0-300 meter layer in order to explain our seasonal cycle ?

Undoubtedly any features within the mixed layer of the ocean are of major importance for time-scales of the order of a season. The mixed layer is the interface between the atmosphere and the interior ocean and any forcing, of mechanical or thermodynamical nature, has to go first through that layer, before it can act upon the water at deeper levels. The mixed layer removes in the meantime a significant part of the energy supplied by the atmosphere and only that which remains can be transferred further down with more or less delay. It is unclear, however, how much of the seasonal variability can be explained by contributions within the mixed layer only. This will be the topic of the present study.

We will tackle this question by using an approach classical in meteorology, where it is known as the standing eddy formulation. In the present case, it will consist in computing the transport of heat due to correlations in the horizontal plane between the temperature and meridional mass transport fields within the mixed layer of the ocean. The mass transport field will be determined from surface wind speed data, by means of an observations based relationship. Those wind data are drawn from the Comprehensive Ocean Atmosphere Data Set, which also provides the sea surface temperature data. As part of the mass transport calculation, mixed-layer depths will be determined by processing vertical oceanographic profiles from the Master Oceanographic Observation Data Set. The North Atlantic and North Pacific oceans were selected for this study and more precisely the latitude band between 10°N and 56°N. The reasons for choosing those limits are various. The first one is a better coverage over a sufficient long period of time, namely 1949 - 1979. The second one is that the forcing of the gyre is a subtropical feature. Besides the relationship mentioned above does not hold at latitudes within $\pm 10^{\circ}$ from the equator, and finally beyond 56°N the criterion that we applied for our mixed-layer depth determination is less valid.

Chapter II of this thesis gives a description of the history, content and quality of the data sets. Long term seasonal means of the sea surface temperature and wind fields are also presented as support for further

references. Chapter III details the procedure used to derive the mixed-layer depth data and discusses the main mechanisms that control its evolution. The associated long-term means are provided and the reader may find in annexe 2 the corresponding standard deviation as well as some other informations useful to get a feel of the quality of the derivation. Chapter IV deals with the meridional heat flux computation outlined before. A description of the method and assumptions is given and a specific treatment of the western boundary current contribution is made. Finally the conclusion summarizes the principal results.

II) THE DATA SETS

In this study, data from the Master Oceanographic Observation Data Set, hereafter referred to as MOODS, were used for computing the mixed- layer depth for the North Atlantic and North Pacific Oceans. Data on sea surface temperature and wind speed were derived from the Comprehensive Ocean Atmosphere Data Set (COADS). We shall describe in this chapter the most important features of these data sets and present the preliminary processing procedures that lead to the final quantities used as input in our "standing gyre" approach of the meridional oceanic heat transport.

2.1) The COADS data set :

About seventy million of weather reports taken near the ocean surface primarily from merchant ships have been included in building this data base . It covers a 126 year period, from 1854 to 1979. The basic data sources which were integrated into COADS are listed below :

Input	Million	Sources
Atlas	38.6	NCDC
HSST		
(Historical Sea Surface		
Temperature Data Project)	25.2	NCDC(Germany)
Old TDF-11 (Supl. B & C)	7	NCDC
Monterey Telecommunication	4	NCDC
Ocean Station Vessels, and		
Supplements	0.9	NCDC
Marsden Square 486 Pre-1940	0.07	NCDC
Marsden Square 105 Post-1928	0.1	NCDC
National Oceanographic Data Center		
(NODC) Surface, and Supplement	2	NCDC
Australian Ship Data (file 1)	0.2	Australia
Japanese Ship Data	0.13	MIT
IMMPC (international Exchange)	3	NCDC
South African Whaling	0.1	NCAR
Eltanin	0.001	NCDC
'70s Decade	18	NCDC
IMMPC (international Exchange)*	0.9	NCDC
Ocean Station Vessel Z*	0.004	NCDC
Australian Ship Data (file 2)*	0.2	Australia
Buoy Data*	0.3	NCDC
'70s Decade Mislocated Data*	0.003	NCDC
	100.**	

* Additions solely to 1970 - 1979 decade.

** The approximate total includes 26.58 million relatively certain duplicates, and some seriously defective or mis-sorted reports, which, were removed by intial processing steps.

(From Coads Documentation)

Within each report up to eight observed quantities have been summarized on a monthly scale in 2 degree latitude by 2 degree longitude squares. They are : sea surface temperature (SST), air temperature, sea level pressure, total cloudiness and specific humidity, the eastward and northward components of the wind speed taken at the typical level of 10 m above the ocean surface. For each of these monthly averaged values, the standard deviation and number of observations available were provided.

2.1.1)Data density :

The number of reports per month over the 1854-1979 period is shown on figure 1, for respectively the Atlantic Ocean (a), the Pacific Ocean (b) and the global ocean (c). Large fluctuations appear, with for instance a peak at about 230 thousands of reports per month in 1968 and a stabilization in the 1970's at about 150 thousands observations per months if we look at the global ocean curve. The large increase in the mid 60's is due to the input of data from countries linked by a World Meteorological Organization agreement to collect marine reports. The decrease in 1970 might be due in part to the time lag for entering the up-to-date TDF-11 data in this data set. Besides the input from the Soviet Union seems to have been stopped at that time also.

In terms of degree of coverage in space, the 1949-1979 period is overwhelmingly better described than the 1854-1948 one, with the bulk of the data coinciding with the well traveled North Atlantic and North Pacific Oceans. Beyond 65°N or south of 20°N the data are concentrated along narrow ship routes with large data gaps in between.

Figure 2 shows the total number of SST measurements in January at each grid square for both periods. January is generally the month with the least number of observations. Bearing in mind that the values for the first period are actually sums over 95 years as opposed to the 31 years of the second one, the density in space is in average about 20 times better during the latter period for the Atlantic Ocean and even more for the

Pacific Ocean. A maximum number is found off the coasts of Virginia during the 1949 -1979 period, while its analogue for the previous period is located at the mouth of the French Channel, where different ship routes are converging. In the Pacific Ocean, the maxima occur off Nagasaki (Japan) with about 2900 measurements during the first period and off San Diego with approximately 8000 observations for the second period.

In the average the Atlantic Ocean is slightly better described, with gradients for the spatial density less sharp than for the Pacific Ocean. These differences are strengthened if we consider the first period.

We also present on figure 3 the number of years with observations at each grid square for the month of January as an indicator of the quality of the temporal coverage at that location. In the Atlantic, about 75% of the basin has a full temporal coverage for the latter period, while this percentage drops to nothing if we considered the former period, and only one quarter enjoys a 50% temporal coverage. In the Pacific, if we look at the years 1854 to 1948, no square presents a 75% coverage (i.e 72 years with data) and only a few percent reach the 50% level. About 45% of the boxes have a full coverage during the next period, but with an averaged number of observations per year less than for the Atlantic.

In view of the previous remarks, it was decided to limit the study to the 1949-1979 period, provided that this period also presents a reasonably good density of data both in time and space for the oceanographic data set (MOODS), which will be the case but to a lesser extent as we shall see next.

2.1.2)Seasonal fields of SST :

We present in figure 4 and 5 the climatologies associated with the SST fields for each season and basin, as a support of our heat flux investigation.

The influence of latitude, currents and upwelling is evident. Along the African and Western American coasts, intense upwellings give anomalously cold waters compared to the zonal means. In addition, advection of cold water within the surface layer may play a role also. The thermal signature of the Gulf Stream and Kuroshio is clearly apparent, with a tilting of the isotherms towards the North East sharper than that which one would expect otherwise.

Without temperature advection through a current or upwelling, the distribution of the SST would be zonal as is the case in all the regions that are not altered by the above factors.

Strong seasonal variations are encountered in the northwestern side of both oceans, with amplitudes of more than 12°C, as illustrated in figure 6. This feature can be ascribed to strong continental influences. Besides, the annual variation of SST in the upwelling regions follows the variation in wind intensity as we shall see next.

2.1.3) Wind systems over the North Atlantic and Pacific : (figures 7 and 8)

Both oceans are in summer under the influence of a basinwide anticyclonic wind circulation. In the Pacific this gyre extends from the American coast to about 140°E where it joins the northward wind system associated with the Asian summer monsoon. It is centered at 150°W, 37°N. Its Atlantic homologue covers the whole width of the basin with a center around (35°W, 35°N). In winter, this anticyclonic circulation weakens and its influence on the basin is replaced by that of a now stronger cyclonic system located above 30° N and centered at about 52°N, 182°W in the Pacific Ocean and around Iceland for the Atlantic Ocean.

2.2) The MOODS data set :

The Master Oceanographic Data Set is the result of a four year program of gathering and processing temperature and sound velocity depth profile observations, undertaken under the monitoring of the Fleet Numerical Oceanographic Center (FNOC). Under its auspices more than 3.5 million of MBT, XBT, AXBT,

hydrocast and STD records have been collected. The meaning of the previous acronyms and others can be found in appendix I. We summarize in the table below all the sources and corresponding update levels that have contributed to make out of MOODS the most complete and up-to-date set of oceanographic subsurface data until 1981 or so.

SOURCES	NUMBER OF OBS.	YEARS - UPDATING
MBT100	161,000	1942-1968
CSI30M	1,602	1958-1979
FNOC MESSAGE	1,108,749	1965-1981/2
NODC MBT	963,994	1942-1980
NODC SDII	623,067	1980
FNOC XBT	211,735	1963-1981/7
NODC STD	1,715	1967-1977
BRITISH MBT/XBT	132,611	1978/4
NODC CARD MBT(WHOI)	14,752	1943-1959
AUST OLD	3,284	1960-1972
NEW AUST MBT DATA	58,746	1943-1979/10
NODC XBT	338,739	1980
NEW AUST XBT	20,316	1967-1979
JAPAN MBT/XBT	56,801	1970-1978
LAMONT XBT	121	1976
ARGENTINA	797	1977-1978
JAPAN	34	1964-1975
NODC SDI	17,621	1923-1978
SOUTH AFRICA	12,900	1959-1969
JAPAN	25	1969-1973
NEW FRENCH MBT/XBT	35,358	1952-1975/10
KOREAN HYDRO	18,817	1961-1977
JAPANESE PUBLISHED DATA	200	1961-1966
FOSTER STD	89	1975-1976
OLD FRENCH MBT	8,903	1952-1967
NORWAY HYDRO	1,858	1948-1957
NODC KRUNCH STD	8,286	1972-1978
	3,802,120	

2.2.1) Data density :

Although it is the most complete data set of its kind available up to 1981, MOODS presents some serious weaknesses due to the lack of data. The bulk of the soundings is concentrated in the Northern Hemisphere with about 90% of the total number of observations. The maps on figure 9 to 10 are intended to give an idea of the distribution of the data both in time and space. We selected the years 1949 and 1973 as typical of the least covered, and the best covered years in the Atlantic respectively. 1964 stands here as representative of a mean coverage. 1978 was the best described year for the Pacific Ocean.

A number of interesting features emerge from these maps. There is a significant increase with time of the number of observations gathered. In addition, more soundings are made during the summer than during the winter. The best covered period spreads over June, July and August, which we have taken to be the summer season. On the contrary, January is the least favoured month of the year. The decrease in the number of observations in the later years results primarily from the delay with which new collected data are incorporated into the data set. The Atlantic Ocean is generally better described than the Pacific Ocean.

This data set presents in addition some very distinct aspects as opposed to a collection of surface observations. The latter can generally be made by merchant ship in an extensive and routine manner and present an upward trend with regards to the number of observations with time, generally everywhere, except for particular locations and over limited periods of time (e.g. wars...), while the former shows highly fluctuating data distributions both in time and space, with, however, still an upward trend, but a very jagged one, even on a monthly scale. Certain areas, even large ones, could be observed for the purpose of some localized scientific interest only during a given month over, say, 5 years and never again afterwards. Generally we have observed a significant correlation between the time of the year a sounding was performed and its location. This makes any attempt of studying annual cycles on a monthly basis strongly biased.

Therefore at the most only a seasonal basis could be considered, providing that the quantities to be derived do not vary a lot from a month to an other.

Dealing with this type of data set presents nevertheless some advantages. One of those is an improved accuracy. Our temperatures at depth were given with an accuracy of about 0.06 °C, as opposed to typically a few tenths of a degree centigrade for COADS for which data were collected by ships of opportunity on their way to their usual business of commerce. On the other hand, it should be noted that the mixture of soundings from different origins, countries or scientific institutions, the various methods or instrumentations used yield potentially inhomogeneous data, not to mention the large discrepancies observed in the vertical samplings.

III) COMPUTATION OF THE MIXED-LAYER DEPTH

3.1) Preliminary treatment :

Altogether about two millions of profiles have been analyzed for both the Atlantic and the Pacific Ocean. Any measurement made within the top one meter of the ocean was considered as a surface temperature data. For each of those soundings, the mixed-layer depth was taken to be the level at which the temperature was 0.5 °C less than the surface temperature. This criterion seems appropriate to describe the temperature of an isothermal oceanic upper layer to which the mixed layer could be identified. This does not hold at high latitudes for instance, as we shall see later on.

To determine the depth of the mixed layer, we linearly interpolated the temperature between the levels available. By using this simplified vertical description, we strengthen the effects that the sampling could introduce on the accuracy of our depth determination, making necessary some adapted data quality controls.

First of all we asked the profiles to meet certain basic requirements, such as to supply surface temperature data, or to extend to a level at which the temperature is at least 0.5 °C less than its surface value. Besides, we retained only the profiles that presented at least three levels, one of those having to lie within the 0-300 m layer. Those objective criteria are by no means self-sufficient. They yield, however, the elimination of an unexpectedly large number of soundings, as evidenced by the following tables for each of the oceans under study :

a) Atlantic Ocean :

Month	Number of data processed per month	Number of data discarded	Rejection rate (%)
JANUARY	45,791	15,919	34.8
FEBRUARY	55,470	20,426	36.8
MARCH	67,153	25,100	37.8
APRIL	65,274	18,725	28.7
MAY	85,241	11,771	13.8
JUNE	87,807	3,970	4.5
JULY	89,864	2,358	2.6
AUGUST	76,213	2,366	3.1
SEPTEMBER	74,987	4,657	6.2
OCTOBER	70,103	6,057	8.6
NOVEMBER	67,884	9,433	13.9
DECEMBER	42,152	9,170	21.8
	827,939	129,952	15.7

b) Pacific Ocean :

Month	Number of data processed per month	Number of data discarded	Rejection rate (%)
JANUARY	68,410	11,533	16.9
FEBRUARY	79,599	14,973	18.8
MARCH	91,303	13,876	15.2
APRIL	105,382	9,736	9.2
MAY	110,472	4,286	3.9
JUNE	110,934	1,955	1.8
JULY	106,932	1,423	1.3
AUGUST	106,891	1,550	1.5
SEPTEMBER	101,468	2,964	2.9
OCTOBER	95,582	4,513	4.7
NOVEMBER	81,640	5,947	7.3
DECEMBER	55,991	7,845	14.0
	1,114,415	80,601	7.2

The next constraint we applied was directly related to the sampling interval. A larger or smaller sampling distance may, indeed, lead to serious uncertainties in the depth determination. In the case shown on figure 11, data are provided at the surface as well as at about 26 m. The depth of the mixed layer is necessarily above the 26 m level where the decrement in temperature from the surface value is larger than 0.5°C. But it entirely relies upon whether or not an intermediate level is provided and the accuracy with which it would be described . The solid line illustrates the case where no intermediate datum is known and yields a mixed-layer depth of 6.10 meter. Now, depending on which intermediate sampling may be available our determination could give a priori any value between 0 and 26 meter. The constructions shown yield 3.52 or 24.62 meter. Therefore it appears necessary to limit the sampling interval to a degree that should depend on the level at which the mixed-layer depth derived from our 0.5°C criterion is lying.

We will allow a more coarse sampling as the depth increases.

We chose the simple function : $\dfrac{50. \times \text{Depth}}{90. + \text{Depth}}$

For a mixed layer at 6.10 meter, this distance should not exceed 3.17 meter. This index was crudely set to ascertain a reasonable accuracy and resolution for the expected range of depths to be determined, namely 0 to 300 meters. This choice ensures an accuracy of about 12.5% at around 300 meters (about 38 m), but only 50% at 10 meters (5 m). It is thought to provide a good trade-off between the accuracy and the concern to keep in the meantime sufficient data.

The rejection rate associated with this additional criterion are given in the following table :

a) Atlantic Ocean :

Month	Number of data processed per month	Number of data discarded	Rejection rate (%)
JANUARY	45,791	2,784	6.1
FEBRUARY	55,470	4,046	7.3
MARCH	67,153	5,776	8.6
APRIL	65,274	6,906	10.6
MAY	85,241	10,699	12.6
JUNE	87,807	12,841	14.6
JULY	89,864	12,851	14.3
AUGUST	76,213	9,418	12.4
SEPTEMBER	74,987	5,446	7.3
OCTOBER	70,103	2,993	4.3
NOVEMBER	67,884	2,331	3.4
DECEMBER	42,152	1,969	4.7
	827,939	78,060	9.4

b) Pacific Ocean :

Month	Number of data processed per month	Number of data discarded	Rejection rate (%)
JANUARY	68,410	4,537	5.7
FEBRUARY	79,599	2,156	3.9
MARCH	91,303	3,173	4.6
APRIL	105,382	7,073	7.8
MAY	110,472	8,426	8.0
JUNE	110,934	13,482	12.2
JULY	106,932	16,391	14.8
AUGUST	106,891	18,766	17.5
SEPTEMBER	101,468	17,181	16.1
OCTOBER	95,582	9,630	9.5
NOVEMBER	81,640	4,330	4.5
DECEMBER	55,991	2,850	3.5
	1,114,415	107,995	9.7

Finally, we estimated that a temperature based criterion would not be appropriate to determine bases deeper than 300 meters, for it is probable that in the cases of an isothermal thickness of 300 meters or more for the regions under study (North Pacific and North Atlantic between 10°N and 56°N) we would be in the very northern parts of the basins where salinity is likely to become an important factor in controlling the convective stirring process.

The temperature is there typically uniform over thicker and thicker layer, while a strong halocline may lie near the surface, as a result of river runoff or excess precipitation. On the right is given an illustration of the above remark. It is obvious then, that a temperature based criterion would break down and a cutoff at 300 meters allows us to stay within the domain where temperature can be considered as a good index of the depth of mixing.

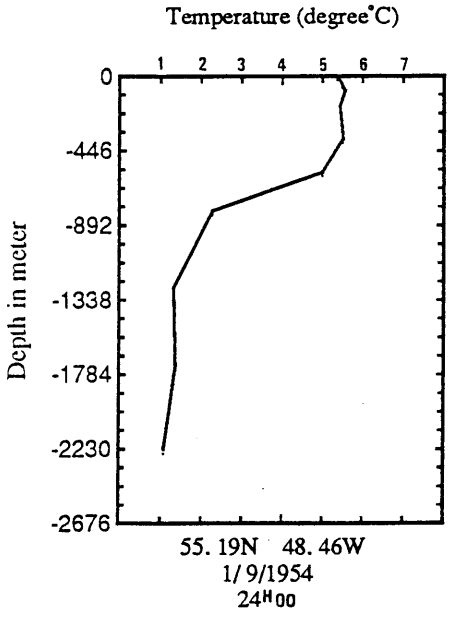

The next step was to organize the data using 2°latitude by 2°longitude boxes for each season of each year of the 1949-1979 period. Once this was done, we proceeded to an extensive filtering procedure intended to eliminate bad data, followed by a 1-step interpolation in order to fill some missing or removed data, while still avoiding the propagation of "neighborhood effects" or contamination. Both these phases will be developed next.

3.2) The filtering procedure :

The first action was to calculate for each season of each year the mean mixed-layer depth at each grid square. If only one value was available, the square was given the missing value flag. We then computed the standard deviation from the aforementioned mean.

If the number of data for a given box was less than 10, each of those data was compared to a weighted average of the mean values obtained for the neighboring boxes. Each adjacent square received a different weight according to its distance from the central square and its number of mixed-layer depth data. Our hypothesis was that if that number is large, then the corresponding mean may be more reliable and should be given a larger weight.

Let N_i be the number of data at box i , M_i the mean value of these data, and W_i the weighted average attached to this box. This weighted average was computed as follows :

M_1 N_1	M_2 N_2	M_3 N_3
M_8 N_8	M_0 N_0	M_4 N_4
M_7 N_7	M_6 N_6	M_5 N_5

for corner boxes : $$W_{\substack{k=1,3,5,7}} = \frac{N_k}{\sqrt{2}\sum_{i=1,m} N_i}$$

for others : $$W_{\substack{\iota=2,4,6,8}} = \frac{N_\iota}{\sum_{i=1,m} N_i}$$

weighted average : $$\Pi = \sum_{i=1}^{m} \frac{W_i M_i}{m}$$

m : number of adjacent boxes with an available mean value.

The test was performed even if m was equal to 1. If one of the mixed-layer depths for a given box was different from the weighted averaged mixed-layer depth of the surrounding by more than 15 meters, it was discarded. If not, it was integrated into the computation of the mean mixed-layer depth for that square.

If now, the number of data for a box was more than 10, but the relevant standard deviation for that box was greater than 5 m, an additional test was performed. We first assume that the mixed-layer depth data within each square were normally distributed. Then we computed for each datum of each box a standardized variable, which measured its deviation from the box mean in units of the appropriate standard deviation, namely :

$$\psi = \frac{Mld - (\overline{Mld})_{box}}{(Std)_{box}}$$

The standard deviation we are using throughout this study is defined as :

$$Std = \sqrt{(1/N)\,\Sigma_i (a_i - \bar{a})^2}$$

where N is the number of values (a_i) taken by the variable a and $\bar{a}$ their mean.

If ψ was found to be larger than 1.96 (which should occur for at the most 5% of the data under the Gaussian assumption) and if in addition that datum fails the weighted average test described before, it was rejected. The reasons for using two tests are that all the data for a given square may be too far from the surrounding mean, without being necessarily bad data. They could possibly be ascribed to some smaller scale features at

the lower limit of our resolution capability. On the other hand, even if it is less probable, a particular datum for a given box could be anomalous for that square but, however,close to the surrounding mean. This would happen if all the other data for that square were bad or in case again of a smaller scale system. Being unable to decide whether the data are bad or not for the above cases, it was decided to keep them.

Each time an update was made necessary, the statistical parameters (mean and standard deviation) were accordingly corrected for further use in the filtering procedure.

All the aforementioned conditions were set after extensive trial analyses and hand checkings to make sure that all the corrections were justified and that the filtering did not result in a too drastic reduction of the number of data. We estimate that about 5% of the data were removed.

3.3) Interpolation :

Each missing data was replaced by the weighted averaged mixed-layer depth value computed for the surrounding boxes, under the condition that at least three adjacent boxes had data.

3.4) Discussion and Results :

In this section we present the results of the mixed-layer depth determinations, whose procedure has just been detailed. Long term means for each season and both oceans are displayed. It is beyond the scope of this study to give a complete and extensive description of the mixed-layer physics and the present treatment has to be seen within the framework of an investigation of the standing gyre contribution for the upper layer oceanic heat transport. We will, therefore, provide only a brief outline of the main factors that may control the mixed-layer behavior and explain some of the features of the mixed layer patterns, which are displayed in figures 12 and 13.

3.4.1) Basic physics of the mixed layer :

The mixed layer is basically maintained by turbulence.

The ocean may be represented ideally as a two-layer fluid, with denser water in the lower layer and lighter water above.(This simple picture is associated with the thermohaline circulation induced by a cooling at higher latitude and a large scale upwelling in the ocean interior, which gives closure for mass balance.) This structure is particularly stable and turbulent kinetic energy is necessary to locally break down this stability and mix waters from each layer.

Kinetic energy may arise from wind forcing or convection related to buoyancy forcing. As opposed to the atmosphere where convection is induced by surface heating, convection in the ocean is driving by surface cooling, which increases the water density and allows water to subsequently sink with respect to lighter water. Evaporation, by increasing the salinity, also increases the density. Note that in the atmosphere , evaporation also acts as a booster for convection, for it lightens ascending particles, making further ascending motions easier.

Surface cooling results from a negative balance between radiational loss by infrared emission, latent heat loss by surface evaporation and absorption of solar energy, the latter taking place within a very thin layer near the ocean surface. Therefore convection is enhanced at night since the solar input is lacking.

The action of the surface cooling is to lower the center of gravity of the water column by compressing the fluid it contains. When this center is lowered, the concomitant potential energy released is converted into turbulent kinetic energy.

The other factor, we said, is the wind which drives a flux of momentum into the ocean. The air blowing over the ocean surface is slowed down by friction, while the surface oceanic layer is speeded up. This velocity shear is used to generate turbulent kinetic energy.

Waves and currents actually make this idealized view less simple. Surface waves are generated by the wind through the absorption of a fraction of its momentum. This fraction of momentum is thus lost for local conversion into turbulent kinetic energy, and will be recovered for that purpose only when the waves break, which may be a long distance further. When the waves break, they also mix air bubbles, which will enhance convection and turbulent kinetic energy creation. Internal waves affect also the local distribution of the turbulent kinetic energy, but have no impact on a global scale. In addition, horizontal advection is usually associated with a deeper mixed layer, since it strengthens the water stirring.

The turbulence generated develops a well mixed upper layer, whose thickening may be inhibited, however, by upwelling, driven by the curl of the wind stress. At the bottom of the mixed layer, water from the denser layer of the ocean is stirred with lighter water above, the potential energy of the water column rises. This increase is made possible by consumption of turbulent kinetic energy. When the supply of turbulent kinetic energy goes down, a lesser amount of potential energy is available to bring upward water particles from below the mixed-layer bottom and therefore the stirring that occurs at that interface (which is not a material

surface) involves lighter water particles. This means that this interface has to rise and the thickness of the layer diminishes.

This fairly basic treatment of the mixed layer physics will allow us to explain now some of the major features evidenced on figure 12 and 13.

3.4.2) Results :

The mixed layer presents a uniform or quasi-uniform vertical structure with respect to various parameters. It is highly fluctuating, with possible time scales as small as a day or less, and therefore it is necessary to use a fair amount of data to be able to reach an estimation of its vertical extension that is representative of , say, a seasonal cycle. We believe that for most of our selected areas this level of data was obtained, or the problem was overcome by use of intercomparison criteria between adjacent $2^{\circ} \times 2^{\circ}$ squares. The reader will find in annexe 2 a statistical description of our data under the form of number of observations and standard deviation, that should give a feel of the locations where the level of seasonal representativeness may not be met.

The mixed layer does vary with latitude, longitude and season, from around 200 m for the North Atlantic winter to less than 15 m for the North West Atlantic and Pacific summer. The maximum thickness is reached in winter and decreased then rapidly to the summertime minimum value. This change is an illustration of the stabilizing effect of the solar heating. Our seasonal study can not show evidence of the intermonthly changes, which are, however, very important. The erosion of the mixed layer between the maximum value at the end of the wintertime cooling and the summertime minimum needs only 3 months (April to June) to complete. Outside this sharp variation period, the evolution is slow. The amplitude of the seasonal cycle (figure 14) may reach more than 130 m in both basins, with the areas of maximum variation coinciding generally with those of maximum wintertime depths. This is a consequence of a fairly uniform small

mixed-layer depth in the summer (25 m for latitudes above 20°N). If we compare figure 14 with figure 6, it appears that areas of maximum annual mixed-layer depth variations are not areas of maximum annual SST changes, for surface cooling or warming is not the only factor in controlling the mixed layer thickness.

The Atlantic maps show, in addition, a band of higher mixed layer values spreading accross the basin from the North East to the South West, above 30°N. This is consistent with the study made by Lamb (1984). This pattern can be explained in part by the fact that this area is located at the confrontation line between polar air and warmer equatorial air masses. Southward incursion of cold air, also dry for it blows over continental areas, yields strong surface cooling and subsequent mixed layer deepening. Note that the Gulf Stream region has as a matter of fact the highest evaporative loss in the world ocean (Hsiung 1983). In addition this water belongs to the high salinity water masses of the Sargasso sea. Therefore the variations of density with temperature will be sharper, leading to more powerful vertical displacements. Another favoring element in driving convection within the Sargasso sea is its slow motion, which will lead to enhanced evaporation and buoyancy fluxes.

On the northern side of this band, lower mixed- layer depth values are due to an increased stratification that partly inhibits convection. This stratification results from the presence of relatively fresh water in the upper layer in consequence of river runoffs or excess of precipitation over evaporation.

In both oceans the areas of upwelling are clearly identified by patterns of minimum mixed-layer depth values, illustrating the inhibiting effect of vertical transports on the depth of mixing. They hug the coasts of Africa and Western United States. Again we find a minimum in mixed-layer depth concomitant with the peaking of the upwelling activity in summer, with typical values of less than 25 m at that time.

The region of maximum mixed-layer depth in the Northern Pacific Ocean in winter and spring centered around 180°W, 43°N coincides with stronger winds and is far enough from the coasts so that the inhibiting effect of fresh water is not felt.

Comparisons with previous studies are made difficult by the fact that usually each author has his own definition of the mixed layer and hence applies to its determination some specific criterion. Levitus (1982) based his mixed-layer depth computation on a $\Delta T=0.5^{\circ}$ criterion. However his results are given for March and September, which for our study are pivot months and hence their particularities are somehow swallowed into the averaged features of the seasons that they belong to. This is a problem especially for March, after which the mixed-layer depth is expected to decrease very rapidly. Note that Levitus (1982) had in his disposal only half the amount of data we used in the present investigation. However, with the above restrictions, both studies bear some resemblance, with the difference that his values are generally larger than ours. It might be due only to the length of the period over which the temporal averages where computed. This raises again the question on how many data one needs to be able to determine the mixed layer depth on a monthly basis, without being too much affected by the impact of local and sudden storms that may induce a strong deepening of the mixed layer for a short time.

IV) MERIDIONAL HEAT FLUX COMPUTATION :

4.1) Introduction

Our purpose in this chapter is to investigate the impact that the atmospheric gyre scale circulation exerts on the meridional oceanic heat transport and to go towards a better understanding of the seasonal cycle of this transport as described in Hsiung et al (1989).

The idea underneath our study is fairly simple. The oceanic circulation and vertical temperature profiles do not undergo seasonal changes below a depth where the so-called seasonal thermocline lies. Above, changes in wind forcing or solar heating induce marked seasonal fluctuations. The Ekman theory is then of major importance in parameterizing the oceanic transport that results from the wind stress distribution. However, this classical theory fails in giving a good representation of the depth to which the Ekman based transport takes place, believed to be in general much smaller than the actual mixed-layer depth, not to mention the much too exagerated decay of the current with depth predicted by that theory. Thus any attempt to estimate meridional heat transports in the upper layer of the ocean from an Ekman point of view would yield a large underestimation of their magnitude and encourage us to disregard their contribution in oceanic heat budget calculation (De Szoeke et al. 1981).

We therefore decided to use mixed-layer depth data, surface winds speeds and surface temperatures to compute what is felt to hold one of the strongest relative seasonal cycles among all the terms that work together to build the oceanic heat budget, namely a correlation between the meridional mass transport and temperature fields within the mixed layer of the oceans as a result of zonal circulation. An empirically deduced formula (Pickard and Pond 1983) was used to compute the surface current velocities, assumed to be uniform within the mixed layer.

4.2) Computation of the standing gyre oceanic heat transport :

We define by standing gyre heat transport the term that in the heat budget represents the correlation in the horizontal plane between the temperature and the northward mass transport fields within the mixed layer, namely :

(1)
$$H_g = \int_{\lambda_{west}}^{\lambda_{east}} \int_{-D(\lambda,\phi)}^{0} C \cdot T^{*} \, (\rho V dz)^{*} d\lambda$$

where D is the depth of the mixed layer, ρ the density of seawater, v the current velocity, T the temperature, z the vertical coordinate, λ the longitude, ϕ the latitude, and c the specific heat of seawater taken as 4218 J/KgK .

$(.)^{*}$ denotes the deviation from the zonal average.

At this point several assumptions are made. First we suppose that the temperature is uniform or quasi-uniform within the mixed layer. This was indeed the criterion on which we based our mixed-layer depth computation. In addition, we assume that the density is independent of depth within this layer. It is therefore inferred that the salinity has to be quasi-constant also. Since we derived the mixed-layer depth for only those locations that were not controlled by salinity, the above requirement is implicitly satisfied.

In addition we made the hypothesis that the mixed layer does not present any vertical velocity shear. In a first approximation, this is justified and many authors have been using it (Schopf and Cane, 1983). However, stirring mechanical quantities, like momentum, is different from mixing thermodynamics properties. Some authors have as a matter of fact shown evidence of significant velocity shears within the well mixed layer. Niiler (1977) and Pollard (1977) found that the assumption of vertical uniform horizontal velocity does not hold for shear in excess of 10^{-3} - 10^{-2} sec^{-1}, which is not unusual in the ocean (Halpern (1980)). Nevertheless,

because of turbulent momentum transport, shears are likely to be smaller. To view the mixed layer as a slab appears, however, as a better approximation than the classical picture of an e-folding velocity decay over a depth corresponding to the Ekman layer depth.

Finally T and V were taken as the surface values.

With these assumptions, expression (1) can be reduced to : $$H_q = C \cdot \int_{\lambda_{west}}^{\lambda_{east}} \overline{T}^{*} \cdot (\rho V D)^{*} \, d\lambda$$

4.3) Derivation of the current speed from the wind speed data :

Observational studies of surface current speed have shown that to a reasonable approximation the current velocity $\underset{\sim}{V}$ is related to the wind speed $\underset{\sim}{W}$ by the following relationship : (Pond and Pickard 1983).

$$|\underset{\sim}{V}| = \frac{0.0127}{(\sin|\phi|)^{1/2}} \cdot |\underset{\sim}{W}|$$

outside $\pm$ 10° latitude from the equator.

We furthermore assume that the water transport crossing a zonal surface element, $\rho \underset{\sim}{V} dz \, d\lambda$ was directed 30° to the right of the surface wind direction. 45° is the angle given by the Ekman theory. However , due to the limitations of the theory, the expected 45° angle is rarely observed in nature and the rotation direction is likely to be somewhat smaller. We took 30° for an estimated averaged most probable direction. A trial analysis showed that the angle was of minor importance on our results, but this point deserves further study.

Thus, the meridional elementary water transport became :

$$\rho V dz \, d\lambda = \frac{0.0127}{(\sin|\phi|)^{1/2}} \cdot |\underset{\sim}{W}| \cdot \sin(\psi - 30^{\circ}) \, dz \, d\lambda$$

where ψ is the angle associated with the wind direction.

4.4) Water density calculation :

For each square ρ was computed using the surface temperature available at that box. If no temperature was present, the box was given the mean density of its zonal belt. Since no data on salinity were ready to be used, we took for each box a salinity value that was an estimation of its mean over the whole basin, namely 34.5% for the Pacific and 36% for the Atlantic.

The formula applied for its computation is given below :

$$\begin{aligned}
\rho = 999.842594 &+ 0.06793952 \times T \\
&- 0.009095290 \times T^2 \\
&+ 0.0001001685 \times T^3 \\
&- 0.000001120083 \times T^4 \\
&+ 0.000000006536332 \times T^5 \\
&+ 0.824493 \times S \\
&- 0.0040899 \times S \times T \\
&+ 0.000076438 \times S \times T^2 \\
&- 0.00000082467 \times S \times T^3 \\
&+ 0.0000000053875 \times S \times T^4 \\
&- 0.00572466 \times S^{3/2} \\
&+ 0.00010227 \times S^{3/2} \times T \\
&- 0.0000016546 \times S^{3/2} \times T^2 \\
&+ 0.00048314 \times S^2
\end{aligned}$$

From Pond & Pickard 1983.

4.5) Preliminary results :

The discussion and results presented in this section are understood as incomplete, since they have been drawn without the necessary mass transport conservation principle to be satisfied. However, it already provides a good insight at some of the physics involved in this standing gyre approach for the meridional heat transport. Most of the features we shall present here will not be denied later on by application of the zonal mass balance criterion. In the next section, that mass balance will be forced by introducing into our model a western boundary current. Since then, the velocities for this current are likely to be quite large compared to interior

ocean surface velocities, and the anomaly of temperature positive, we shall generate a rather strong possible correlation between our temperature and mass transport fields, due to the occurrence of positive temperature anomalies in that western boundary area. This will have a strong impact on our initial results and hence any features which appear within the belt having a boundary current correction should not be considered as conclusive at this stage but may be used as a reference to assess the ultimate impact of the mass balance adjustement.

Figure 15 and figure 16 contain respectively the results for the North Atlantic and North Pacific, in terms of long term means over the 1949 - 1979 period. In addition the corresponding standard deviations are provided. They show a maximum at high latitudes in wintertime due to sparse data especially during that season. This yields fairly uncertain heat transport values for those regions, which are the only locations where negative values are obtained : 30°N - 38°N in winter, above 38°N the rest of the year for the Atlantic, 30°N to 37°N in winter, 40°N to 48°N in spring and summer for the Pacific. Below those latitudes, values are positive and show a maximum in May for the Atlantic. For the Pacific, and bearing in mind the uncertainties on our data, the maximum is found at around 30°N somewhere between April and September, without a particular month to present a significant peaking value.

The computation of heat flux from Hsiung et al (1989) reproduced on figure 17 show a relative maximum in September for the Pacific. Note that data on figure 17 represent the total meridional heat transport as opposed to ours . They differ as a matter of fact by a factor of 10 or so. From just wind or temperature consideration, we would expect a stronger correlation to occur in summer since as shown on figure 4 the isotherms are very much tilted and the development of the gyre is peaking. We have to keep in mind that it is actually the tilt of the isotherms on the edges of the basin , where the strongest winds are expected with opposite directions on each side, that only matters. Remember that a positive correlation means colder water moving southwards and warmer water moving northwards. However, the depth of the mixed layer is reduced by a factor of 4 between winter and summer, which yields a modulation of the same rate or so on the heat

transport. Therefore maxima somewhat shifted in time from a summer occurrence do make sense.

The transports accross latitude belts have about the same size in the Atlantic and Pacific. However about three times less heat per square meter is carried northwards in the Pacific than in the Atlantic through correlation between the temperature and mass transport fields, since with these units our results are normalized by the the width of the oceans, the Pacific being in the average three times broader than the Atlantic. Again, this should be confirmed by the adjusted results to really be conclusive.

At this point, it is interesting to look more carefully at the spatial distribution of the correlation term, in order to get a more precise feeling of the regions that count in each month and of the processes that may explain the observed distribution. Figures 18 and 19 show those regions and how their importance is modulated with the time of the year. The most significant result is the overwhelming influence of the upwelling areas, which actually contribute more than 75% to the total value of this heat component. The intensity of their contribution follows the annual cycle of the strength of the northeasterlies over the upwelling regions, more powerful in summer or so. This fact would be consistent with a peaking value for the correlation term occuring in late spring-summer. However the impact from the mixed-layer depth is likely to be the main controlling factor. Figure 20 shows an idealized picture of the concomitant variations of the surface current speeds over the upwelling areas and the mixed-layer depth during the year. The mixed-layer depth and surface speed curves are qualitatively drawn from figures 12, 13 and 8, 9 respectively. For each parameter, only the month to month variations matter here and the curves are therefore, for conveniency, expressed in arbitrary units. We note that, while the differences between the currents are not very large between spring and fall off southern California or off Africa, the differences in mixed-layer depths are indeed clearly larger.

FIGURE 20.

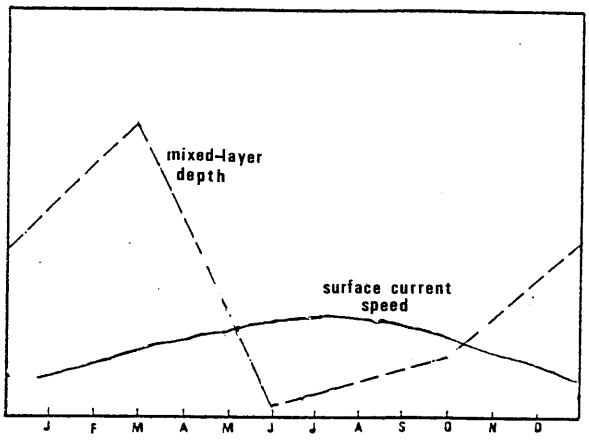

Note that figures 18 and 19 show also the importance of the western side of the oceans, where continental influence may drive a strong winter cooling both by latent heat or sensible heat release, since the air blowing from those land areas is very dry and cold. This feature is more obvious in the Pacific ocean than in the Atlantic and is consistent with the heat loss investigation of Hsiung (1986).

All those key areas do affect the standing gyre heat component through the tilt of the isotherms that they drive. The depth of the mixed layer constitutes a modulating factor. The positive peaks obtained are due primarily to the upwellings, while the negative ones are driven by negative net heat losses on northwards moving flows. All these processes are as a matter of fact closely related to coastlines proximity and do not extend over the open ocean over more than 1/4 of its width. Hence most of the open ocean may be neglected for an exploration of the standing gyre contribution or at least a deep knowledge of the winds, temperature or mixed-layer depth is not crucial. This is a very important result, since it allows us to concentrate our efforts of collecting data only on a much smaller area. We did for the present investigation, however, a computation over the whole basin.

4-6) Mass balance conservation :

All the previous results, as we mentioned, have been derived while omitting the necessary mass balance requirement. In order to prevent any accumulation of water in the ocean, we need to ensure a constant mass flux across every latitude belt. This constant value has to equal the assumed deep water transport, generated at the surface at high latitudes, when strong cooling coupled with enhanced evaporation initiates sinking of dense water in the Atlantic. As we saw, the salinity in the Pacific ocean at high latitudes is not large enough to support a deep convective activity and most of the water that sinks there is unlikely to reach a level below 1000 meters. Thus we will not consider any deep water return flow in the Pacific. However there is a flow from the Pacific into the Atlantic through the Bering Straits, which is estimated at about 1 Sverdrup. Therefore we will force a 1 Sv mass transport across each latitude for the Pacific. For the Atlantic, the strength of the deep flow is more controversal. The range of the estimates goes from a few Sverdrups (L. V. Worthington) up to 40 Sv (Riser et al. 1978). In this study we decided to follow Worthington's value of 7 Sv, for it was based on basinwide considerations on water masses. Estimates that are made only with local observations do not include possible deep water recirculation phenomena and may, therefore, be exaggerated One of the 7 Sv assumed by Worthington for the Atlantic Deep Water comes from the Pacific. Another one balances the mid-thermocline northward flow, so that the remaining 5 should move northwards within the mixed layer. We will therefore force a 5 Sverdrup mass transport across each latitude for the Atlantic.

4-6.1) Mass Imbalances - Results :

Figures 21 and 22 show the net mass transport across each latitude and month for respectively the Atlantic and the Pacific. Note that they are long term means over the 1949 - 1979 period and that the results do not incorporate the 1 or 5 Sverdrups developed above. We give also the corresponding standard deviations. They represent basically half the value of the mean.

The mass imbalance is due to two different phenomena . The first one is inherent to our computation and is related to the noise of the data. We estimated at 50 % its contribution to the total computed imbalance, by reference to the standard deviation level. We partitioned these noise imbalances over all the boxes along their corresponding latitude. The remaining 50 % are related to the net southerly drift of water which results from the part of the Sverdrup circulation that applies to the mixed layer. Negative values on the figures mean southward flow. To those values we have to subtract 5 Sverdrups, that is 50 10+8 kg/sec or so to get the actual imbalance. After those corrections, we can see that there is basically no net northward flow in the Atlantic at any of the latitudes considered, and only below 20°N in winter or 26°N in summer in the Pacific.

For both the Atlantic and Pacific, the bulk of the imbalances occurs in winter, at respectively 37°N and 33°N. They represent there a flow of 18 sverdrups in the Atlantic and 32 sverdrups in the Pacific. The summertime values are very small and account only for the escape flow of water. This seasonal cycle is partly consistent with the observations of the western boundary currents stronger in winter in their northern parts and weaker in fall in all regions (Fuglister 1951), although we do not really get minimum values in fall but rather in summer. For southern sections we get lower values in summer than in winter, which is consistent with Fuglister's observations. However due to the noise level, especially in winter at those latitudes, the relative variations may not be meaningful. Besides, we noted a downstream increasing mass transport consistent with the observed downstream pressure gradient that acts to accelerate the flow. For the Pacific, features are quite similar with the difference that everything is shifted southwards by about 4 or 5 degrees. The Kuroshio does as a matter of fact separate from the coast and moves eastwards at a lower latitude than the Gulf Stream (see for example figure 23).

The assumption we made then was that the negative mass imbalances, meaning net southward flow, are balanced by a northward flow in a western boundary current. The latitude limits we set for these boundary currents are 18°N to 40°N for the Atlantic and 14°N to 38°N for the Pacific . Outside these areas the negative net southward flow was balanced by a northerly drift of water over the whole width of the ocean. We

assumed that in that case the entire belt acts to reduce the imbalance, which is also decreasing as we move northwards. If a positive imbalance occurred, the corresponding southward flow correction was in a similar way split over the entire width, since no boundary current, that should implicitly be on the eastern side of the basin, could make up for such imbalances.

We show on figure 24 the areas over which the corrections were computed. In the narrowest regions of the stream, the width is about 120 km, and increased as we go closer to the outer limits of the domain in order to take into account a gradually zonal orientation.

The depth we took for the current was not the depth of the mixed layer given by our earlier computation. The main reason is that the net southward drift within the mixed layer of the open ocean is unlikely to return northwards with exactly the same physical properties, temperature and salinity, although it is improbable, however, that those properties will change drastically under evaporative processes and give a return flow much deeper than the mixed layer depth, already increased in the western boundary current areas, because of a stronger advection. The depth of the current was taken to be about 50 % larger than the depth of the mixed layer. In case the boundary current was occupying only one 2 degree grid square, the mixed-layer depth that we took was the mean value calculated with the value of the next adjacent box to its east, in order to diminish the dependency on only one data that is potentially affected by noise. The current speed was taken to be uniform over this depth.

For each box new velocities were computed by adding the initial ones to those required for mass conservation, namely : (Zones A,B,C are defined on figure 24)

1) zone C and A : (for noise correction)

$$Vel(\Phi) = \frac{-(I\ 2)}{d_{\Phi}\,(\varrho_i D_i)_{i=west,east}} \quad \text{in m/sec}$$

where d_{Φ} is the width of a grid square at latitude Φ. The velocity was the same for each square.

2) zone C : (for mass balance correction)

$$Vel'(\Phi) = \frac{-(I/2-50)}{n(\Phi)\cdot[\varrho_i D_i]_{n(\Phi)}}$$

$n(\Phi)$ is the number of squares considered for the boundary current at that latitude.
50 is the value we took for the deep water flow transport in kg/sec.

$[\rho_i D_i]_{n(\phi)}$ is the mean of (ρD) over those squares. The underlying idea is to replace in each square the actual ρD value, by the mean over the squares involved in the current. This is just to avoid a fictitious speed-up of the current in case of missing data, if the summation $\rho_i D_i$ is made only where data is available. Again the velocity is taken as uniform across the current.

3) zone B : (noise and mass balance corrections)

$$Vel''(\Phi) = \frac{-(I-50)}{\left(\sum_{west}^{east} \varrho_i D_i\right)\cdot d_{\phi}} \quad \text{in m/sec}$$

Finally each initial speed V was corrected by the above velocities, and the final velocities ϑ are :

zone A + C :

$$\vartheta = V + Vel'$$

zone B :

$$\vartheta = V + Vel''$$

The size of the corrections were of the order of 1 m/sec in the narrowest regions of the stream and a few centimeters per second elsewhere.

The last step was to recompute the long-term standing gyre heat contribution. The procedure used in the earlier stage was kept unchanged, only ϑ was substituted in place of V.

4-7) Final results :

The long-term averaged adjusted standing gyre contribution over the 1949 - 1979 period is shown on figures 25 and 26 as well as the associated standard deviation, respectively for the Atlantic and Pacific. Compared to what we obtained previously, the new standard deviations are generally smaller relatively to the means and the largest values are found in winter at high latitudes, because of sparse data and bigger interannual variability . We also provide on figure 27 a picture of the evolution of the mean anomalies of temperature over the boxes that are included into zones C and B (figure 24) at each latitude, in order to give to the reader a better understanding of the changes that have affected our initial results. As a matter of fact, even if the boundary current generated as part of the requirements for mass balance conservation is strong, the correction it will drive is unlikely to modify the original situation in case the temperature anomalies are small in that region. This fact is fairly well illustrated for the Pacific ocean where large mass imbalances, obtained

between 22°N and 48°N in wintertime, do not generate overwhelming heat fluxes since the anomalies of temperature are quite low there, only around 1.35°C. Briefly our mass balance correction acted to globally raise our heat fluxes by about 2 to 3 10+13 Watts from their initial values in that ocean.

As regards the Atlantic ocean, the old picture has been much more altered. The boundary correction took place in a region of higher temperature anomalies which resulted in a 10 10+13 Watts increase for the heat flux at 30°N, and gave a second peak between January and May at that latitude. In addition, the meridional gradient of heat flux there has been enhanced reflecting the large gradient in temperature anomalies encountered as we move northwards beyond 30°N.

It is interesting to note that for both oceans the maximum temperature anomalies in the boundary current region occur at about 30°N. The peak is centered for the Atlantic in April and in June - July for the Pacific. The anomalies are about 2 degree C smaller in the Pacific than in the Atlantic and hence, even if the mass imbalances are larger in the former, the situation in terms of heat flux is reversed, with the largest values occurring in the latter ocean. Above 40°N, in winter, however, the Pacific experiences a larger generation of positive correlation than the Atlantic. This difference already appeared in our earlier results but it has been reduced now by the mass adjustment made, which acted to diminish the southward flow of colder water.

4-7.1) Comparison with the total heat transport within the top 300 meters of the ocean : (Hsiung et al 1989) figure 17.

Hsiung et al calculated the divergence of the total heat transport within the top 300 meters of the ocean as a residual between the net surface heat flux and the rate of change of heat storage. They subsequently integrated this divergence from North to South and obtained the meridional heat transport every 5 degrees.

A quick look at our results shows that our heat term based on an horizontal circulation cell cannot be

responsible for the seasonal mean northward flux of heat evidenced in figure 17. Other features are likely, indeed, to produce a significant transport. This is the case for instance with the mid-ocean geostrophic flow, even if we consider its contribution at depths below the mixed layer. Our present purpose was only to see how well the seasonal cycle of the total meridional heat transport correlates with the seasonal variation of our standing gyre term. However, the strength of the deep water flow that we assumed is of great importance in our calculations. As a matter of fact, to take 20 Sv instead of 7 Sv would lead to values for our northward Atlantic heat flux up to roughly 3 times larger.

a) Atlantic Ocean :

Qualitatively the agreement between our results and Hsiung and al 1989 is fairly good below 20°N. We do get a peak around May and a slow decrease afterwards. This peak is however centered around 18°N in our computation and around 10°N in Hsiung's results. We showed that this peak may be explained by the contribution of the upwelling region off Africa. After looking at the standard deviations given in the Hsiung et al study, around 5 or 6 10+14 Watts in the 5°N - 20°N area in May - June , we do not disagree significantly. The main discrepancy is found in fact at the latitude of the boundary current. Further North, i.e. beyond 35°N our results are not anymore significant, because of large error bars. We still get a decrease with the time of the year, but our maximum in winter and spring do not appear on Hsiung's estimates.

b) Pacific Ocean :

Our positive maximum centered in winter at 43°N corresponds to an area of presumed negative flux in the Hsiung and al study. However their values, there, are given with a standard deviation of 3 or 4 10+14 Watts. The relative maxima centered at 30°N or so in May and July do not disagree much from their estimations. Nevertheless there is still a lot of features in the seasonal cycle of the total meridional net heat transport that our approach cannot explain.

4-8) Other possible factors :

The zonal circulation cell mechanism, though being an elegant way of studying the seasonal cycle of the meridional oceanic heat transport is not the only process that can generate a positive correlation between the mass transport and temperature fields within the 0 - 300 meter layer. It certainly represents the main mechanism in our mixed layer, but the picture is incomplete. If the assumption of an uniform horizontal velocity is good within the mixed layer it is by no means obvious that the same remains true below. Observations actually show,in many places, current or net drift with opposite direction at depth. In the same way, the temperature anomalies at depth could possibly have an opposite sign also. Hall and Bryden (1981) report, indeed, that below 100 meter the Florida Straits water presents a negative temperature anomaly, while the flow is still northward. This would generate a negative correlation and hence a southward heat flow. Hall and Bryden's direct estimates of ocean heat transport at 25°N in the Atlantic Ocean actually show that it is primarily due to a vertical circulation cell or more likely a diagonal one, since they do not rule out the importance of the horizontal component.

Although the returning flow between the mixed layer and a depth of 300 meter is relatively weak in terms of mass transport, its seasonal variations could possibly account for some of the unexplained features mentioned above .

We should also point out in this section that horizontal heat flux may not only proceed from organized differential drift but also from horizontal turbulence. Bortkovskii (1961) actually showed that the turbulent heat flow should not be neglected except for the upper 50 meter layer. Between 100 and 250 meters, its contribution is actually dominant by more than a factor 10. Although due to large errors arising from his method based on finite difference schemes with second derivatives, this mechanism is potentially important, all the more because it appears that the water within that 50 to 300 meter layer is an important element also to understand the seasonal cycle of the northward heat transport.

V. CONCLUSION :

This thesis was based on extensive data processing and analysis work. We first derived the mixed-layer depth from about 2 million vertical oceanographic profiles. This depth was assumed to be the level at which the temperature was 0.5°C less than at the surface. Not only did this first step provide more realistic data for further integrated vertical mass transport computations than the Ekman theory would have predicted, but also it constituted a good opportunity to update previous mixed-layer depth seasonal climatologies by using a significantly increased number of profiles. However, a lack of data still prevented us from refining the temporal resolution and describing a quantity that does vary sensibly on a monthly basis as well. Secondly, we wanted to see how much of the seasonal cycle of the total meridional heat transport within the 0 - 300 meter oceanic layer could be explained by a horizontal zonal overturning within the mixed layer of the ocean. We did not quite suceed in getting a full agreement but qualitatively some of the seasonal features of the total heat flux were resolved, for instance the maxima found at around 10 - 15°N in May in the Atlantic and 25°N in September in the Pacific, although some discrepancies may appear in the latitudes at which we found those maxima, respectively 18°N and 30°N.

One of our main results is to have shown that only very limited areas actually control the seasonal cycle through a standing gyre formulation , namely the upwelling regions off Africa and southern California in late spring and summer, and the North Western corner of the basins in winter especially for the Pacific Ocean. Thus, collecting data on smaller regions, while still allow to fully describe the phenomena. Indeed, this description will have the potential to yield more accurate results.

We also found that the contribution of the horizontal zonal overturning cell in driving northwards heat flux was larger in the Atlantic than in the Pacific, although the differences are rigourously not really significant owing to the relevant error bars. However, since our Atlantic deep flow may have been underestimated,

this difference could become significant. In the Atlantic this contribution may, indeed, reach up to 50 % of the total heat transport found by Hsiung et al. 1979. This stresses the importance of a better knowledge of the thermohaline circulation in heat budget studies.

It is suspected that a good deal of the unexplained features encountered in the seasonal cycle of the meridional heat transport within the top 300 meters of the ocean could be removed if slightly more sophisticated vertical profiles of temperature and current were used. This refined description of the upper ocean was unfortunately not available. However by using the data at our disposal, it would be interesting to look at a situation where the meridional mass transport would be described by use of the surface current to a depth corresponding to the mixed layer bottom and by residual from the Sverdrup relation predicted transport below. Though there is an uncertainty about the reality of a level of no motion which affects the Sverdrup theory, for our purpose this level would be equivalent to a level below which the anomalies of temperature from a zonal mean would be small enough to be zero. For the upper layer we would still use our surface temperature data, and for the lower layer, vertically averaged temperature anomalies, given at each depth by the MOODS profiles. This possible development will be left at that for now.

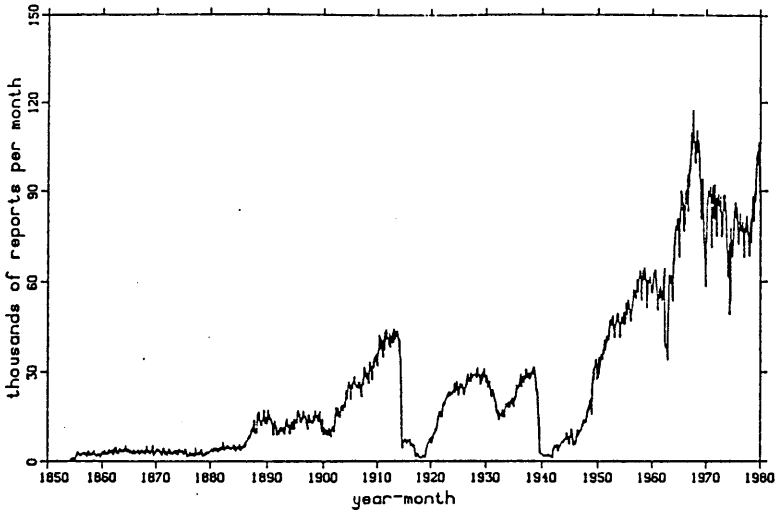

Figure 1-a. Basin 1 ATLANTIC reports after duplicate elimination.

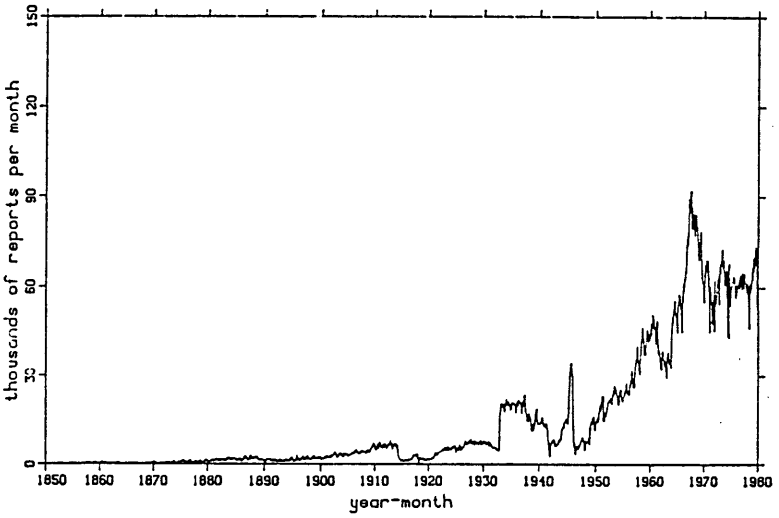

Figure 1-b. Basin 3 PACIFIC reports after duplicate elimination.

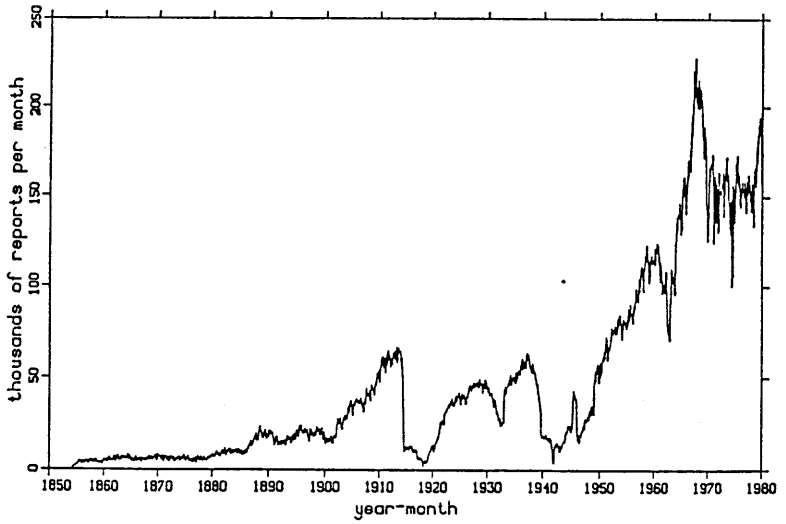

(From Coads Documentation)

Figure 1-c. Global reports after duplicate elimination.

Total number of individual sst measurements
in each grid square
for January, over the 1854 - 1948 period

SST

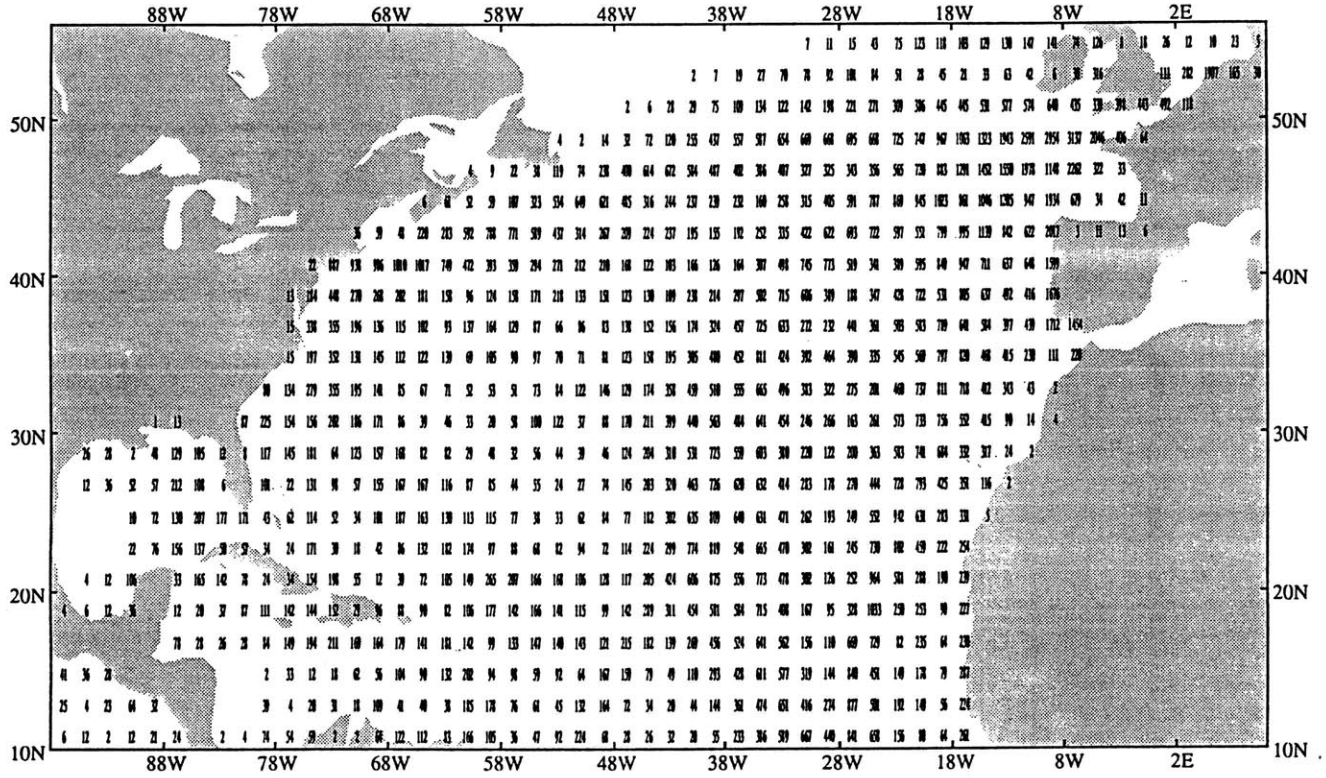

Total number of individual sst measurements
in each grid square
for January, over the 1949 - 1979 period

SST

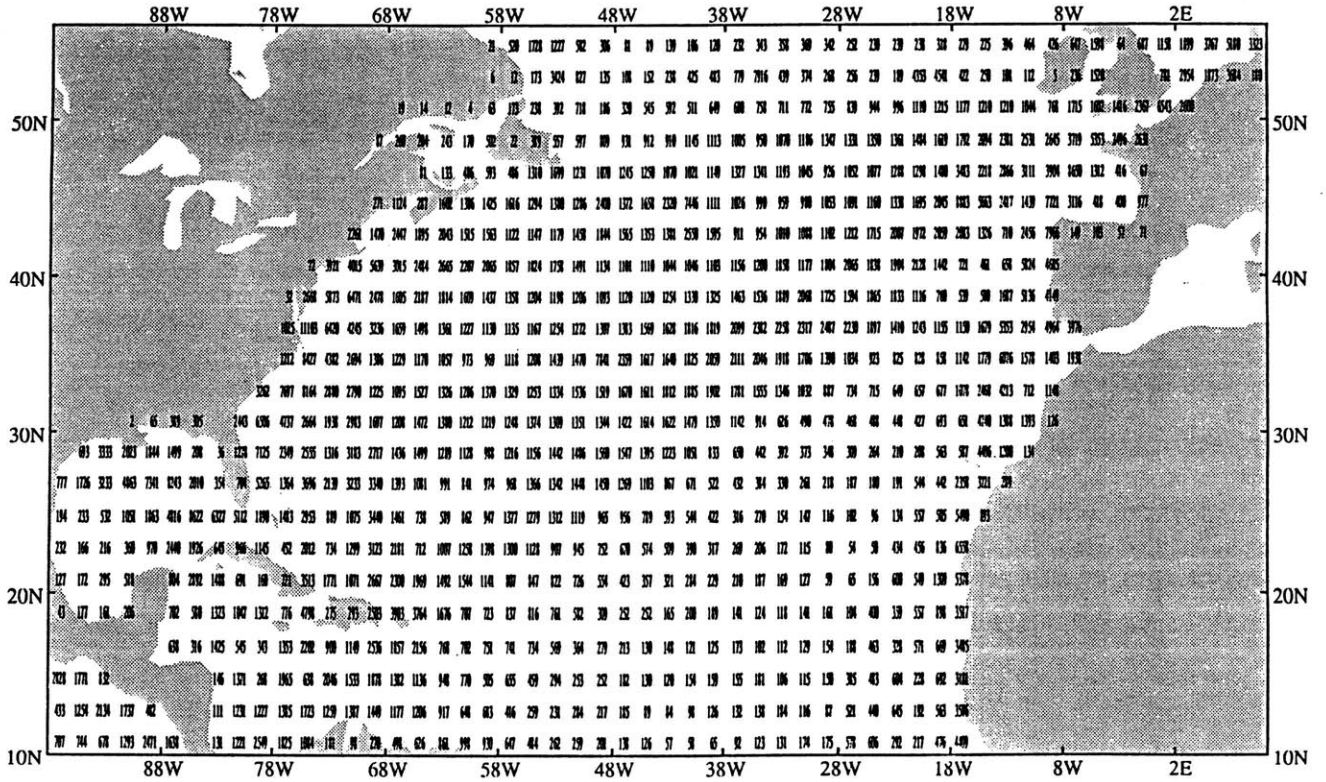

FIGURE 2.

FIGURE 2. (cont.)

Total number of individual sst measurements
in each grid square
for January, over the 1854 - 1948 period

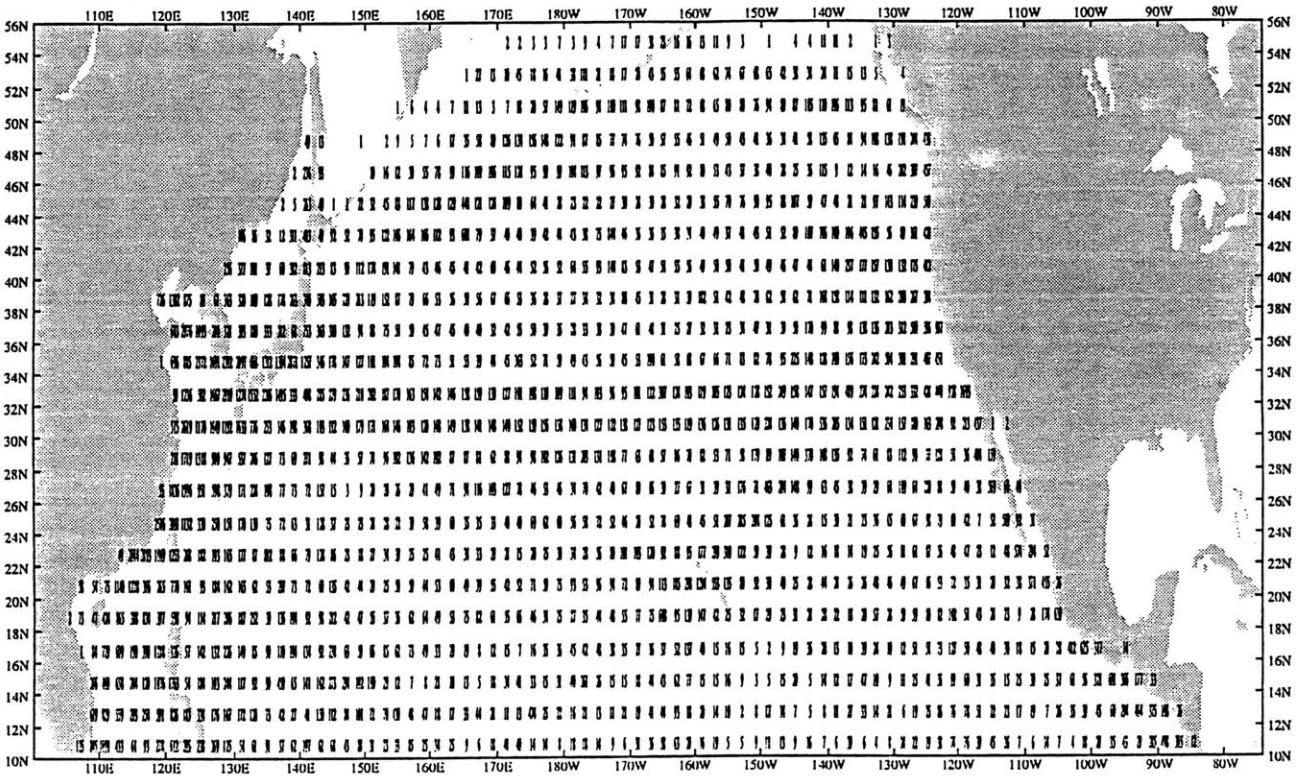

Total number of individual sst measurements
in each grid square
for January, over the 1949 - 1979 period

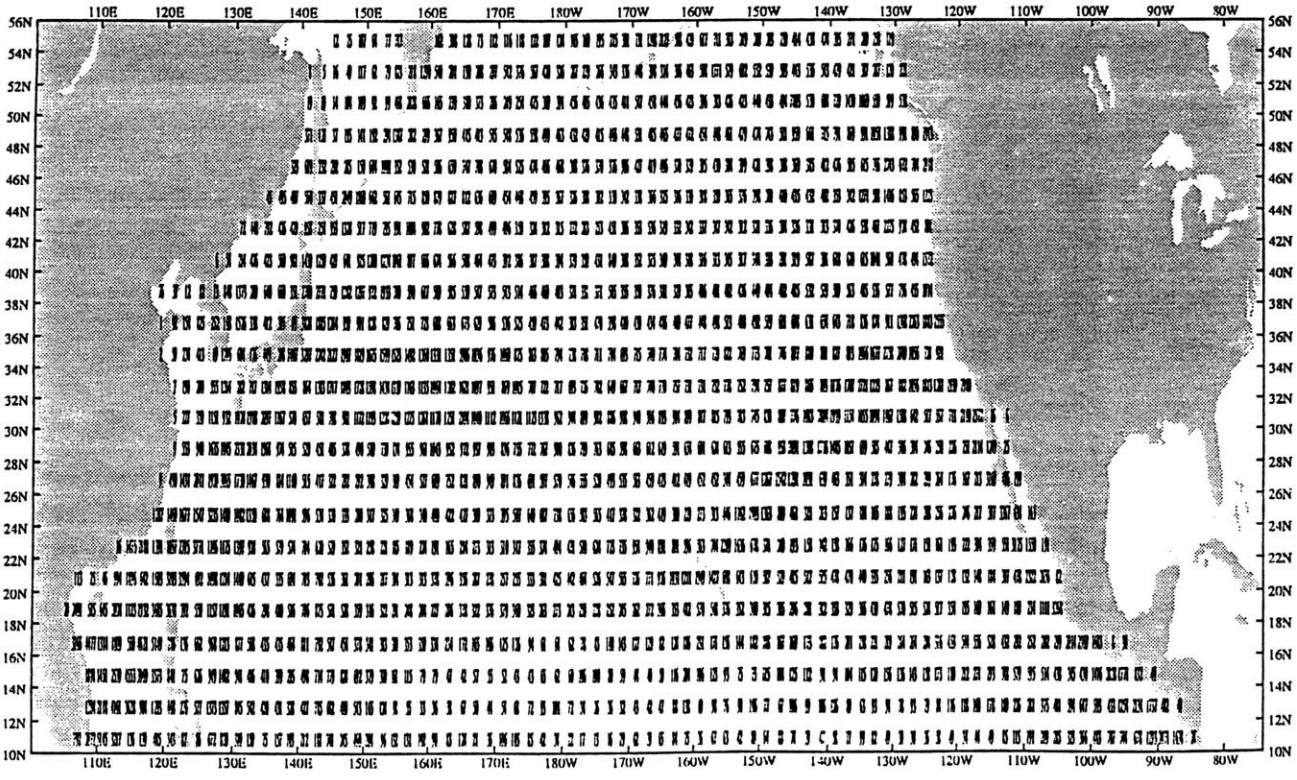

SST

FIGURE 3.

Number of years with observation
for January, over the 1854 - 1948 period

Max. Nr. = 95

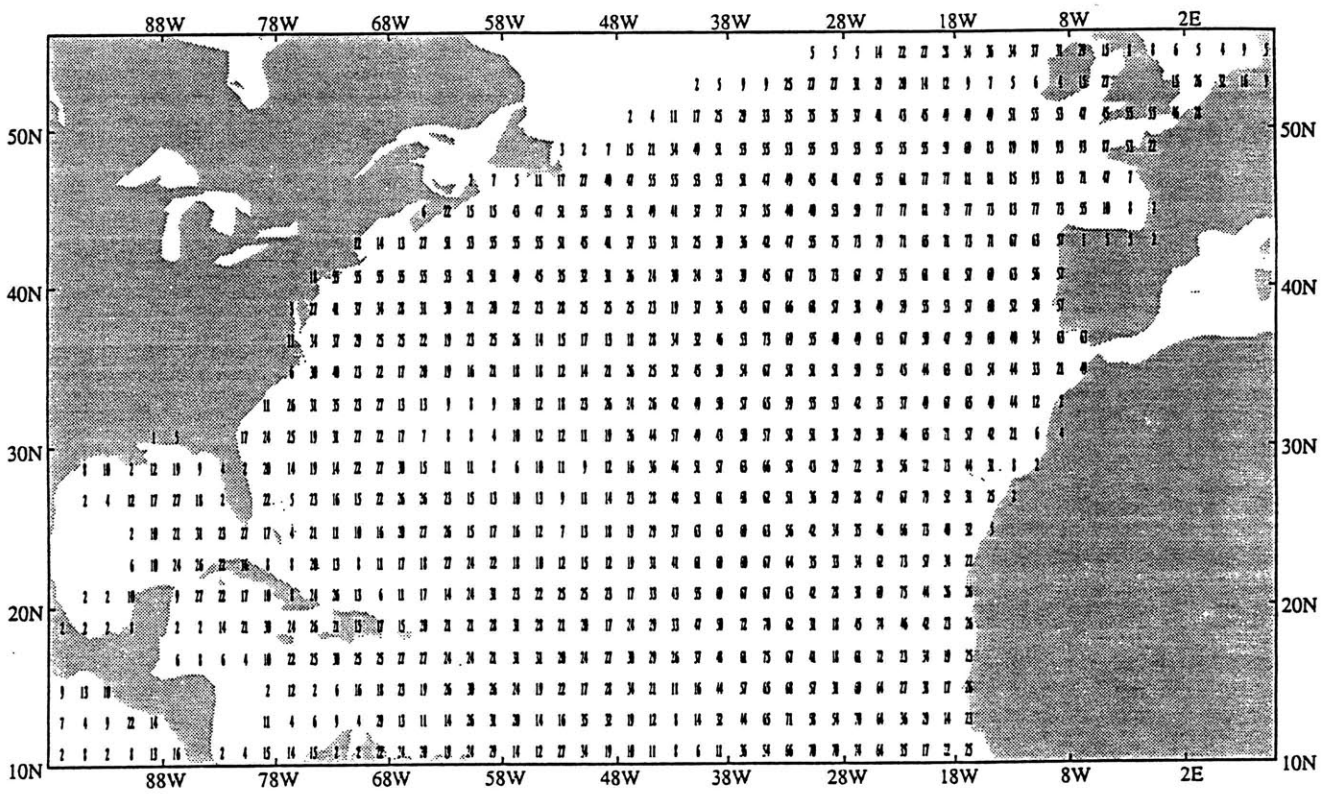

Number of years with observation
for January, over the 1949 - 1979 period

Max. Nr. = 31

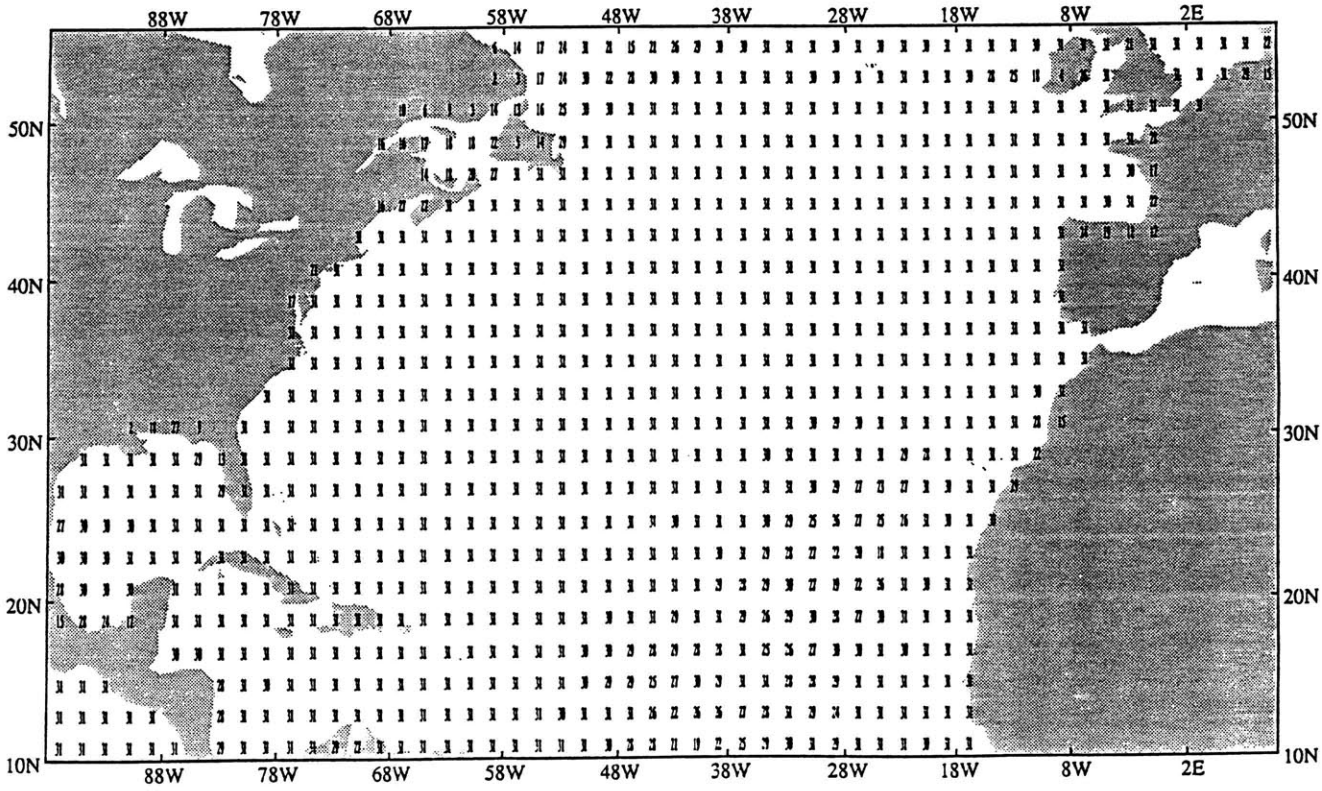

FIGURE 3. (cont.)

Number of years with observation
for January, over the 1854 - 1948 period

SST
Max. Nr. = 95

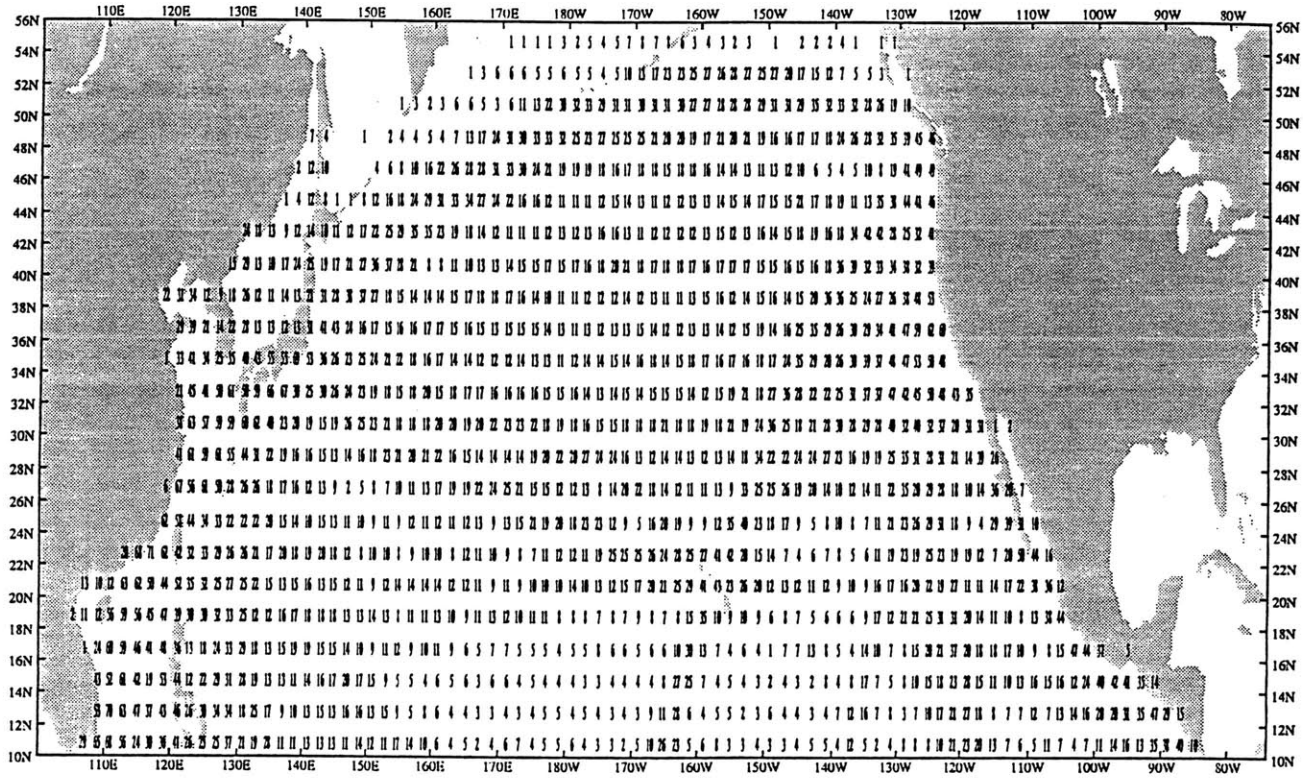

Number of years with observation
for January, over the 1949 - 1979 period

SST
Max. Nr. = 31

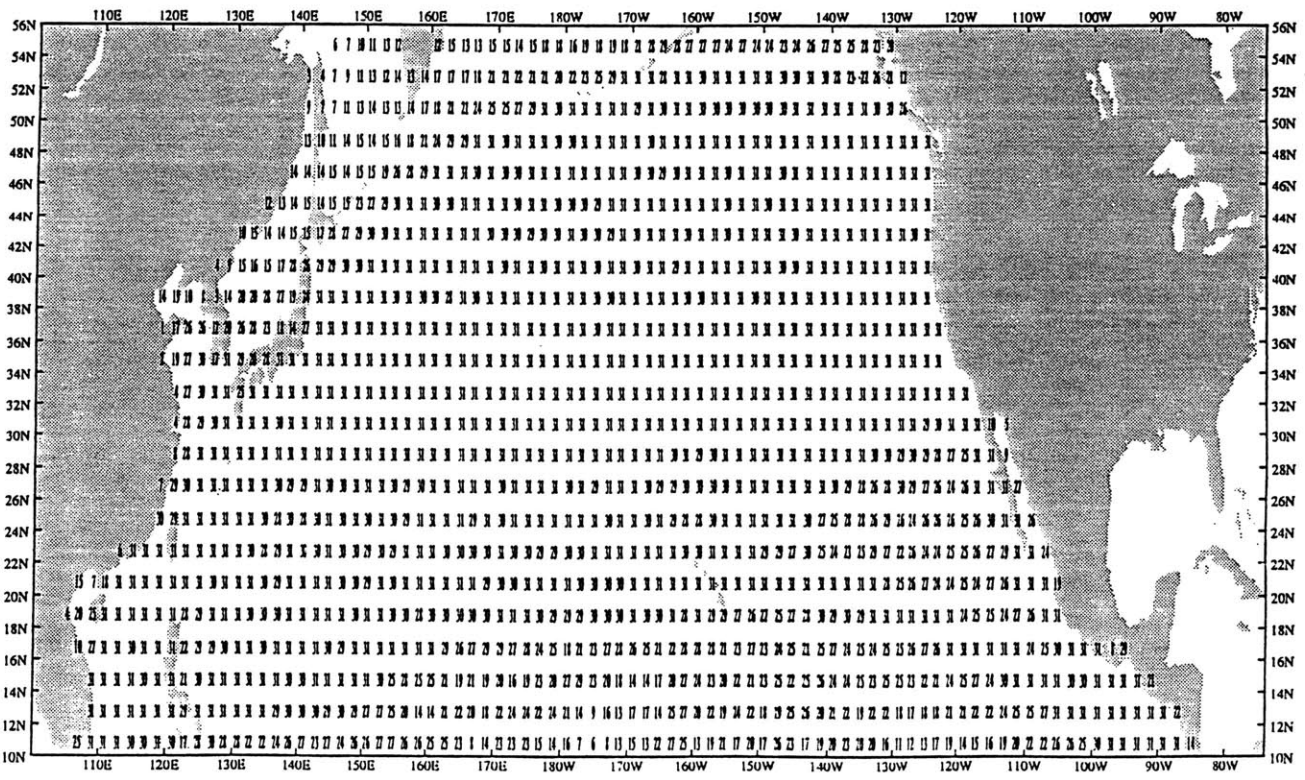

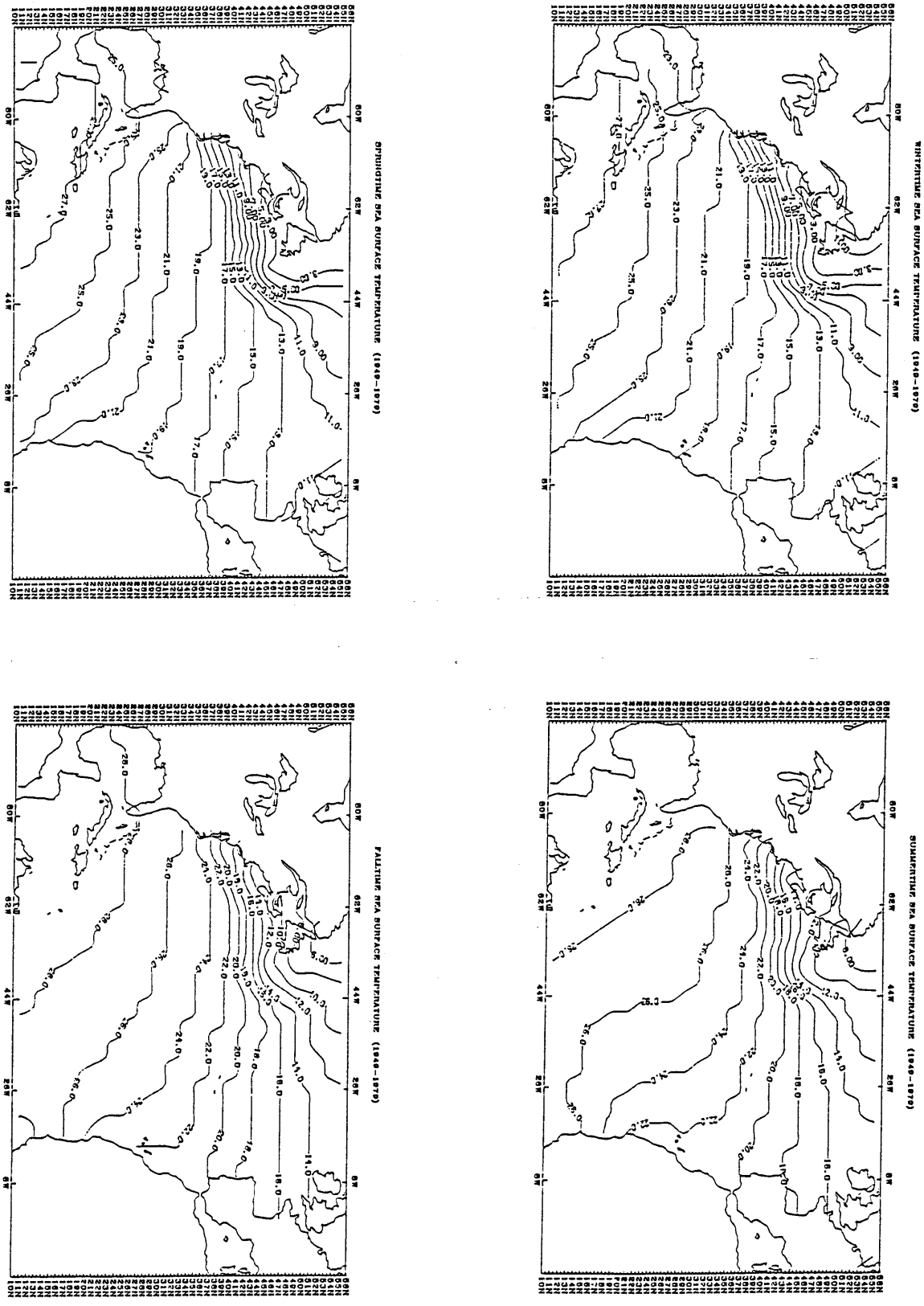
WINTERTIME NEA SURFACE TEMPERATURE (1940-1979)
SPRINGTIME NEA SURFACE TEMPERATURE (1940-1979)
SUMMERTIME NEA SURFACE TEMPERATURE (1940-1979)
FALLTIME NEA SURFACE TEMPERATURE (1940-1979)

FIGURE 4.

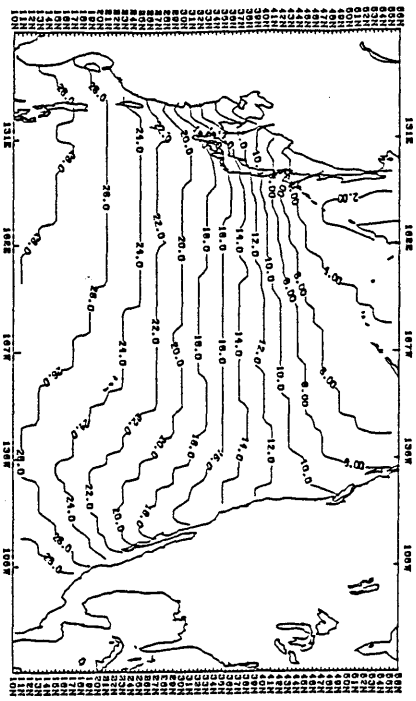
SPRINGTIME SEA SURFACE TEMPERATURE (1949-1979)

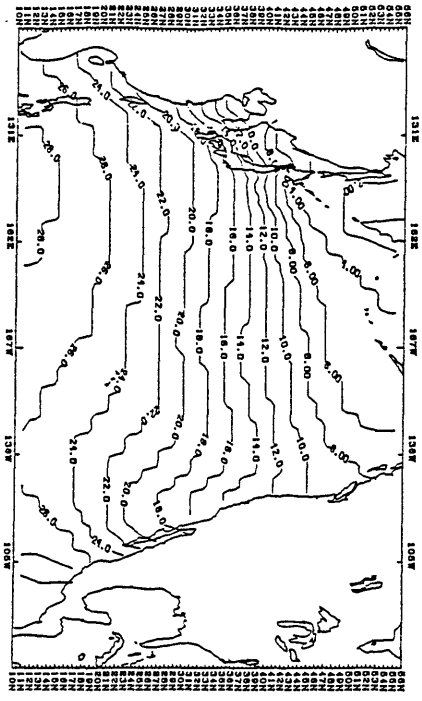
WINTERTIME SEA SURFACE TEMPERATURE (1949-1979)

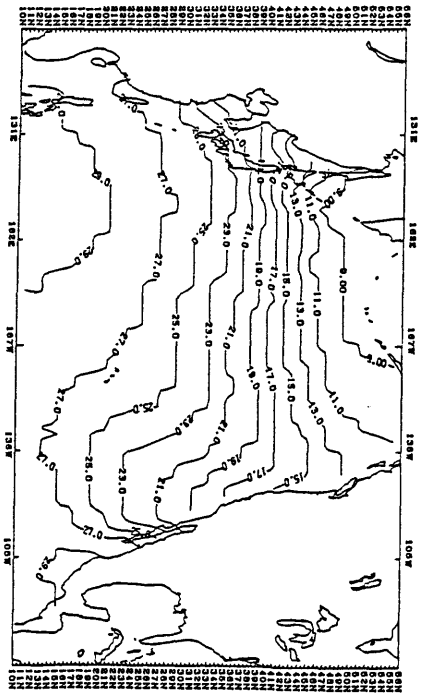
FALLTIME SEA SURFACE TEMPERATURE (1949-1979)

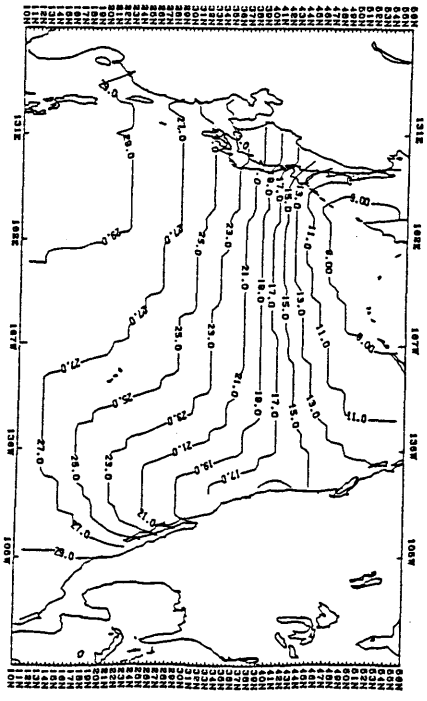
SUMMERTIME SEA SURFACE TEMPERATURE (1949-1979)

FIGURE 5.

FIGURE 6.

AMPLITUDE OF THE SEASONAL CYCLE SST (1949-1979)

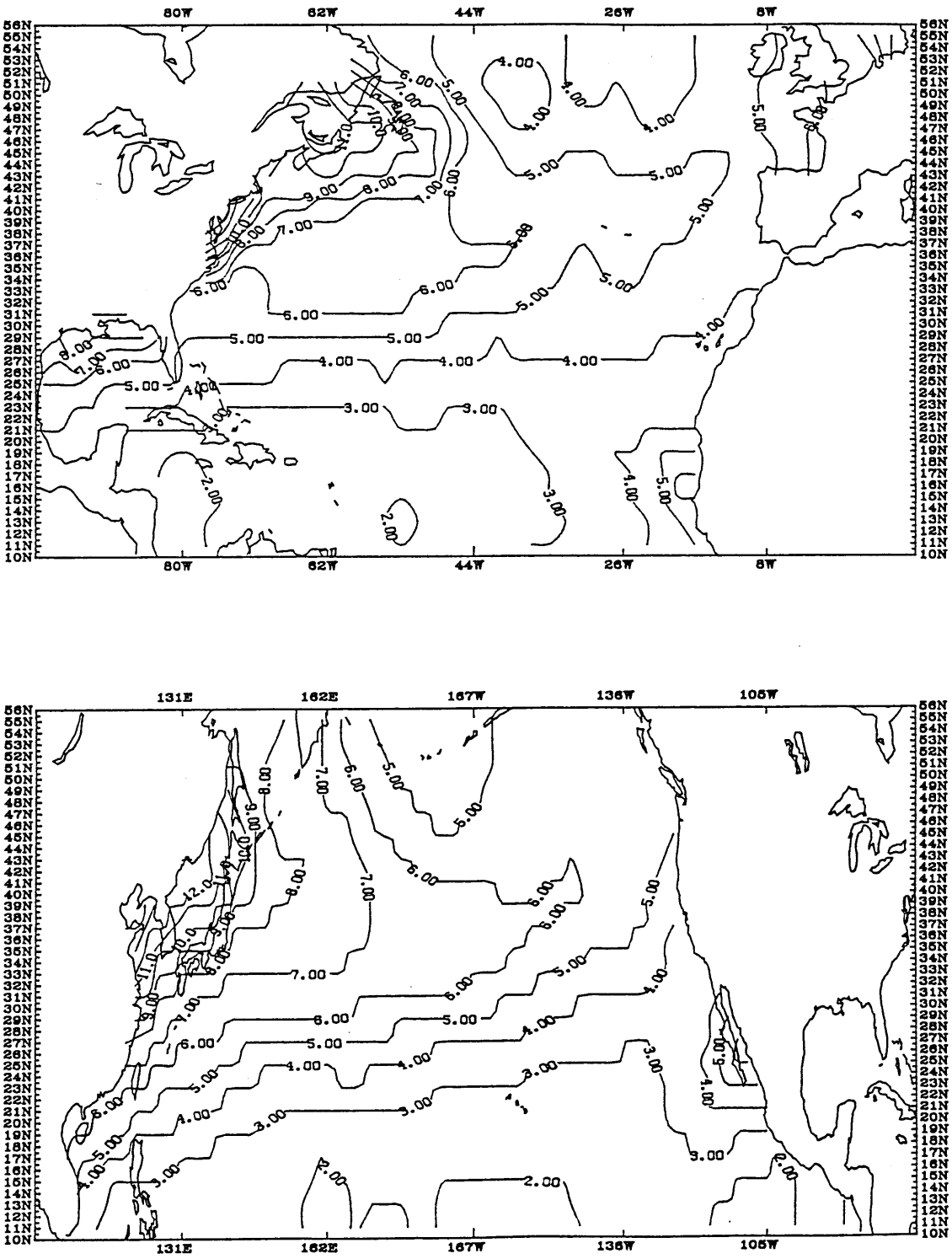

FIGURE 7.

Long term averaged wind
for Winter, 1949 - 1979

Min. Obs. =30(3x31)
Smoothed

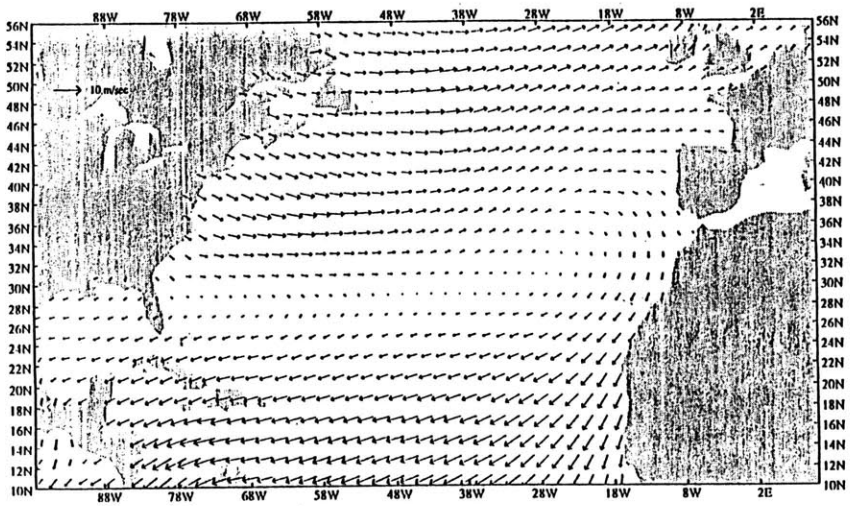

Long term averaged wind
for Summer, 1949 - 1979

Min. Obs. =30(3x31)
Smoothed

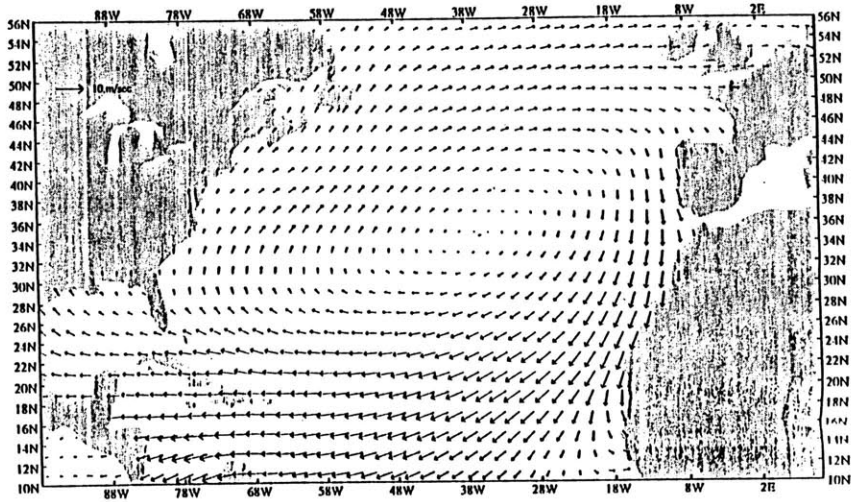

Long term averaged wind
for Spring, 1949 - 1979

Min. Obs. =30(3x31)
Smoothed

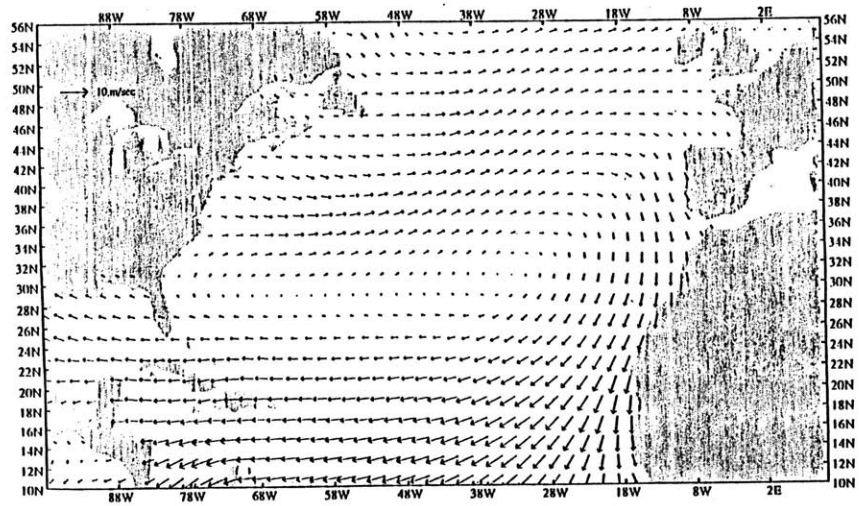

Long term averaged wind
for Fall, 1949 - 1979

Min. Obs. =30(3x31)
Smoothed

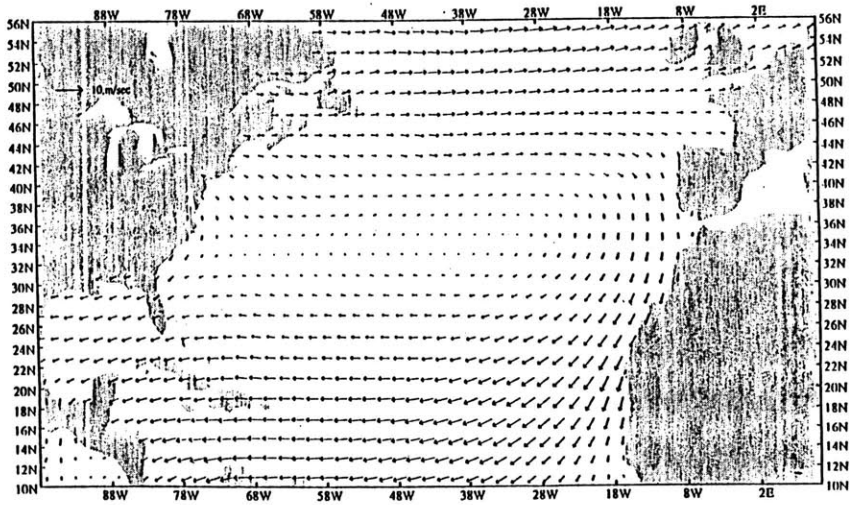

FIGURE 8.

Long term averaged wind
for Winter, 1949 - 1979

Min. Obs. =30(3x31)
Smoothed

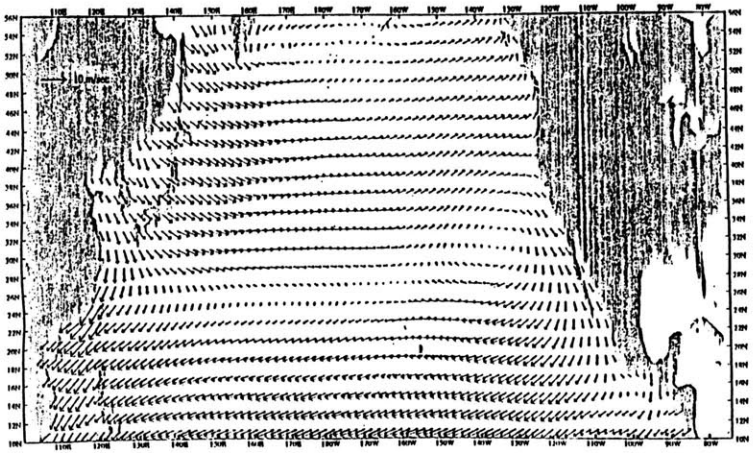

Long term averaged wind
for Summer, 1949 - 1979

Min. Obs. =30(3x31)
Smoothed

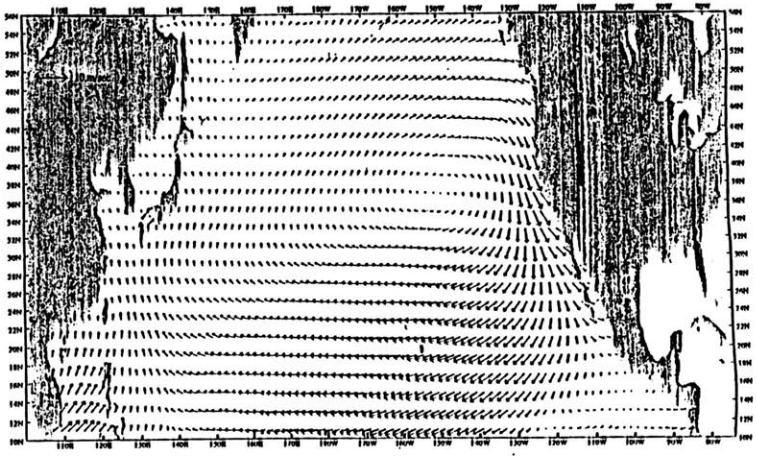

Long term averaged wind
for Spring, 1949 - 1979

Min. Obs. =30(3x31)
Smoothed

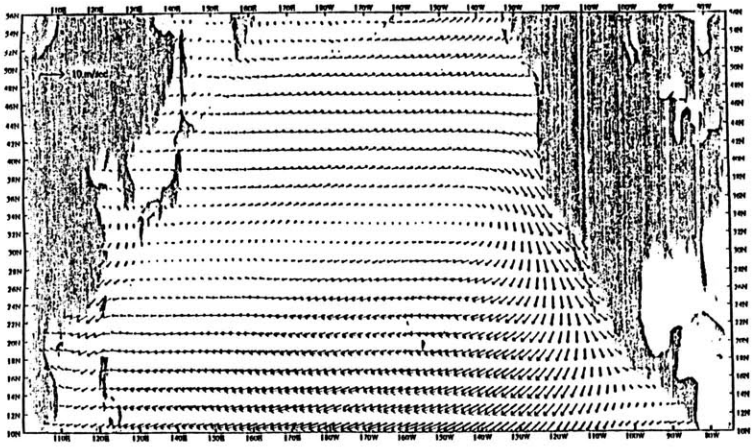

Long term averaged wind
for Fall, 1949 - 1979

Min. Obs. =30(3x31)
Smoothed

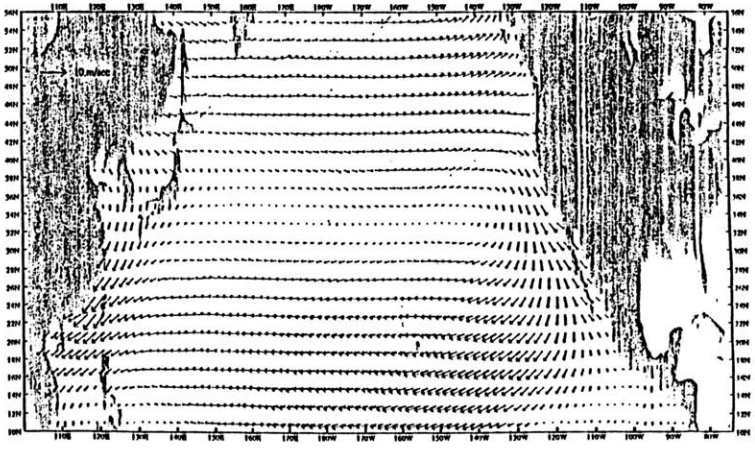

Number of soundings for

January, 1949

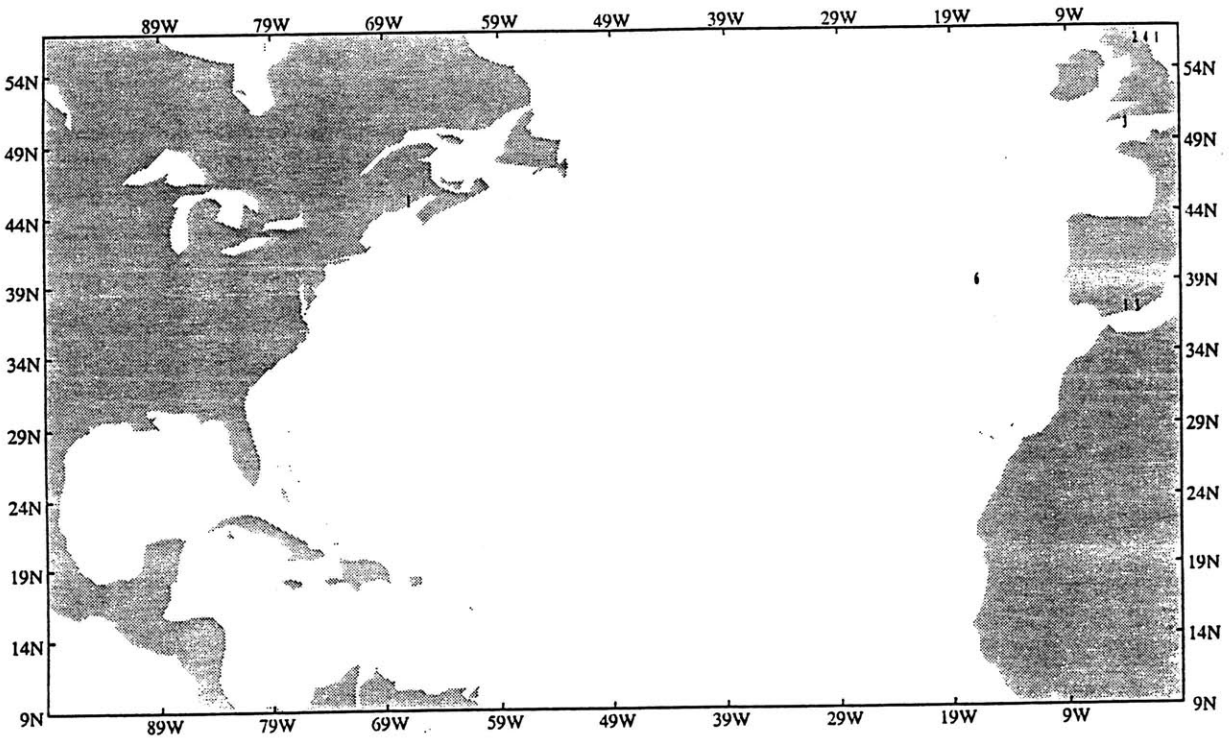

Number of soundings for

July, 1949

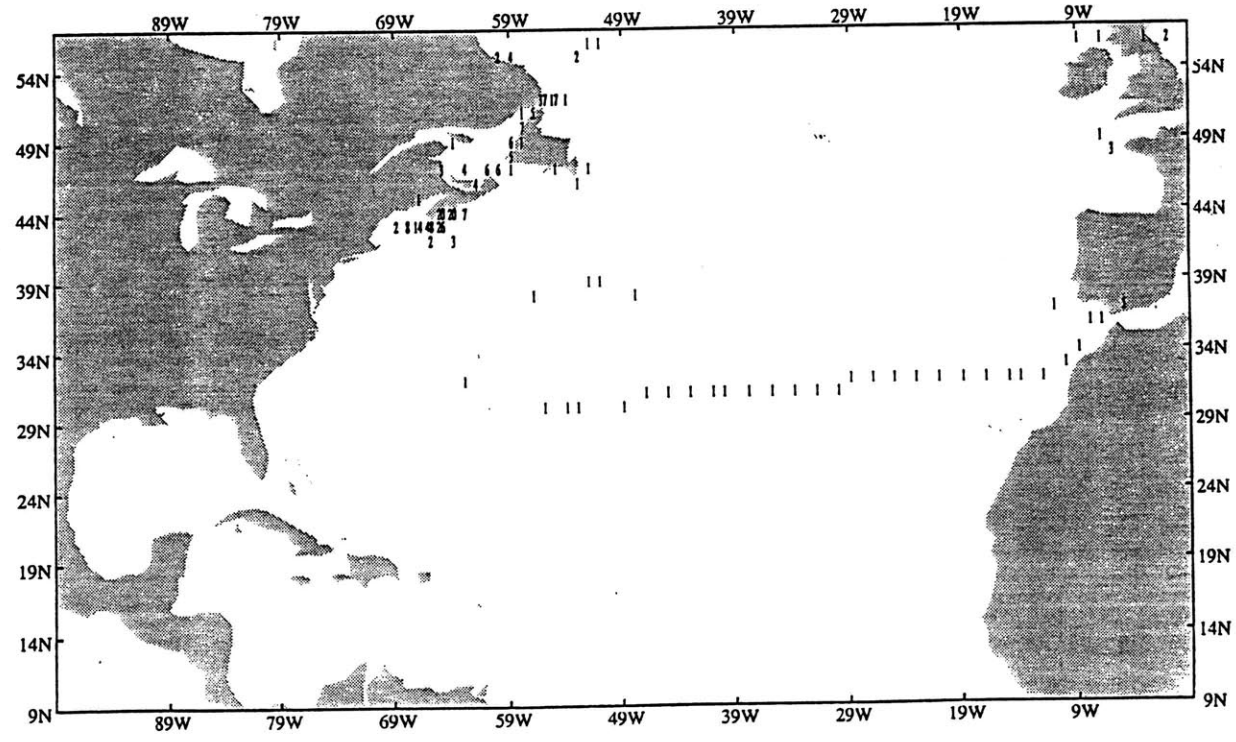

FIGURE 9.

Number of soundings for

January, 1964

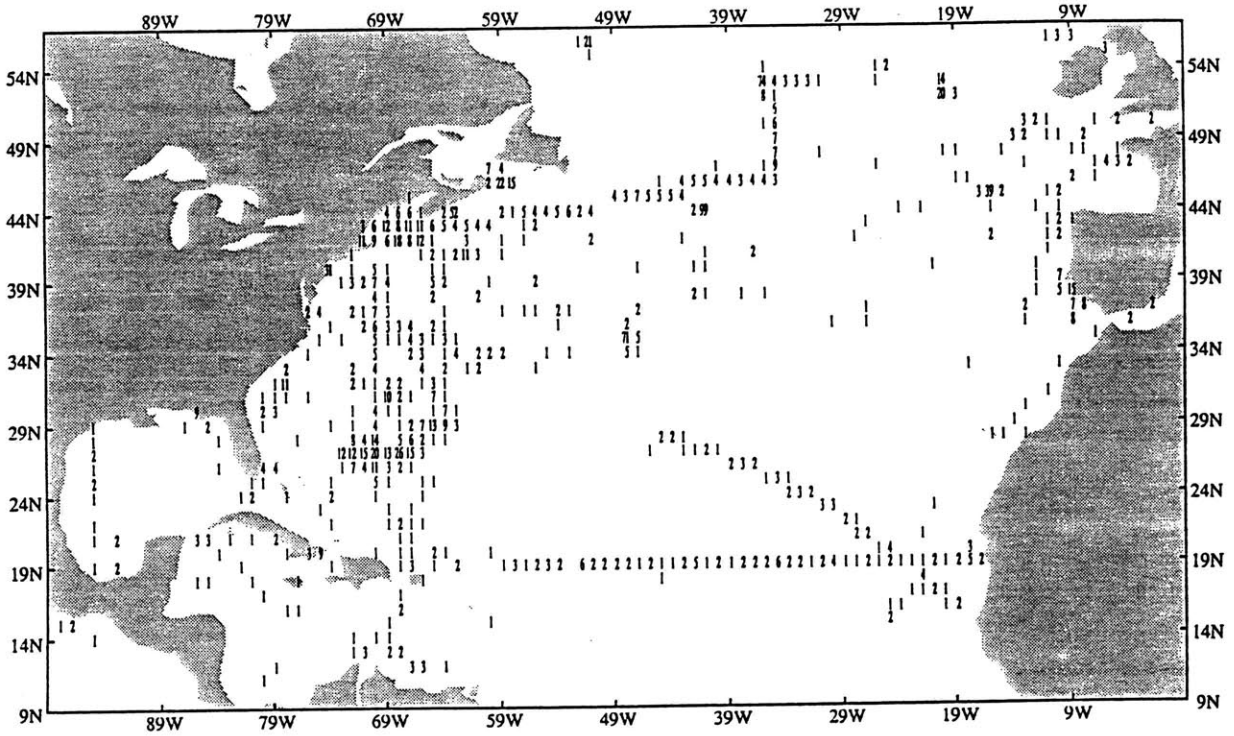

Number of soundings for

July, 1964

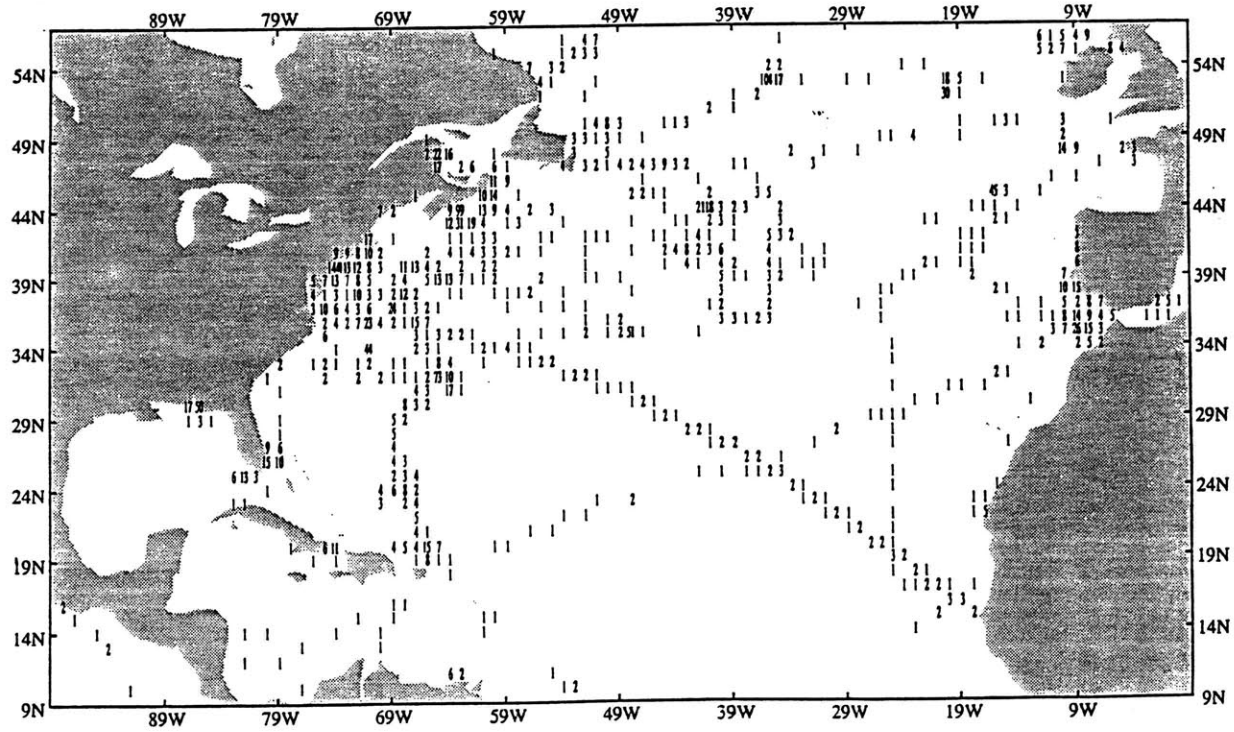

FIGURE 9. (cont.)

Number of soundings for

January, 1973

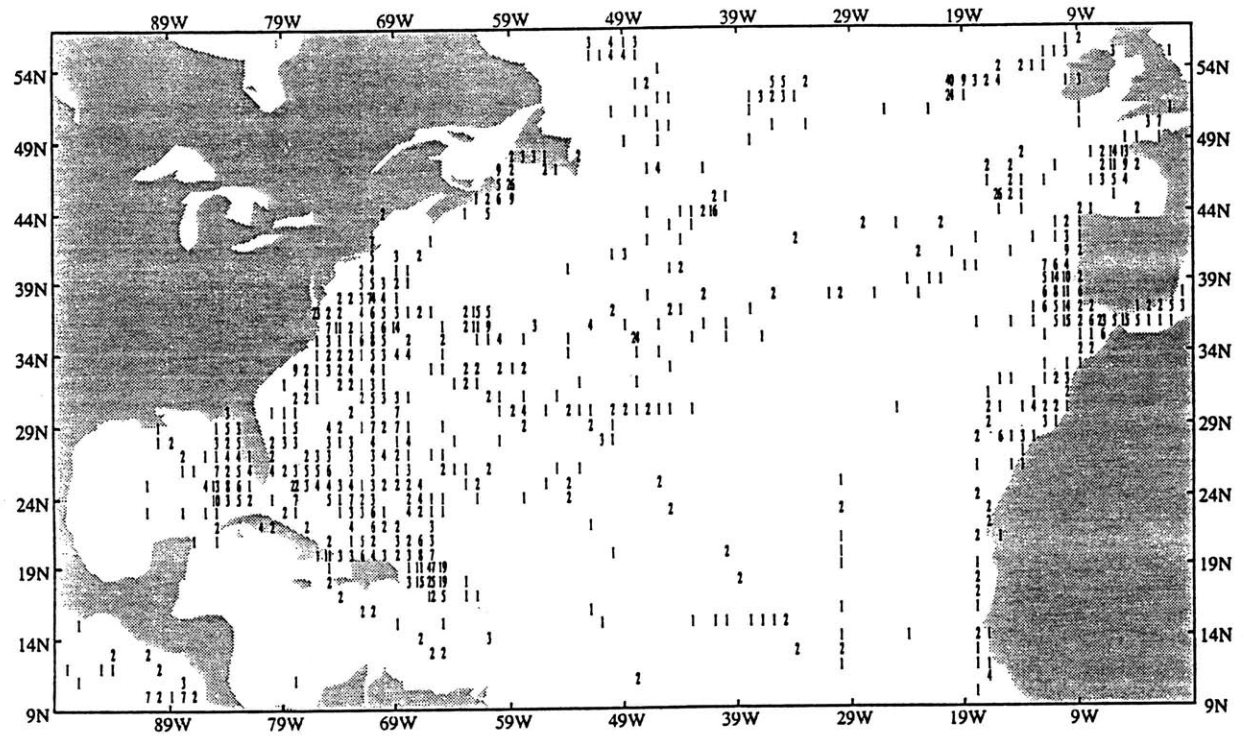

Number of soundings for

July, 1973

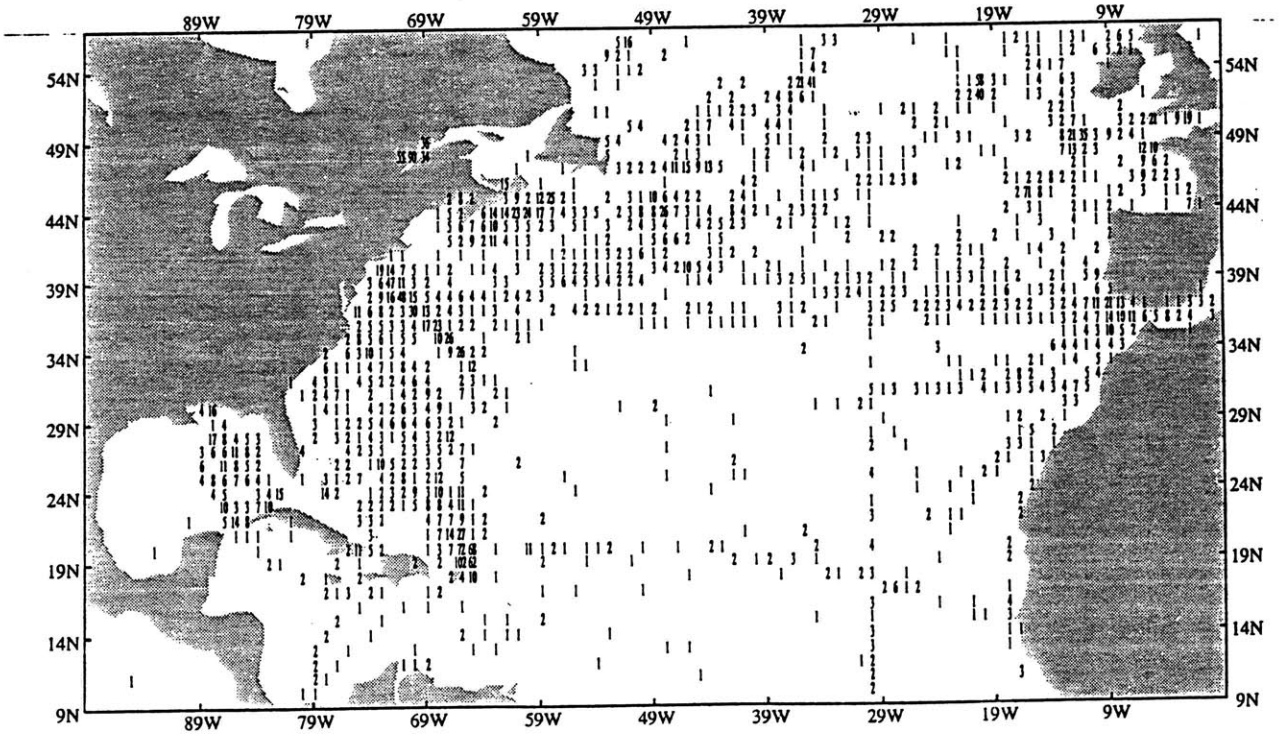

FIGURE 9. (cont.)

FIGURE 10.

Number of soundings for July,1949

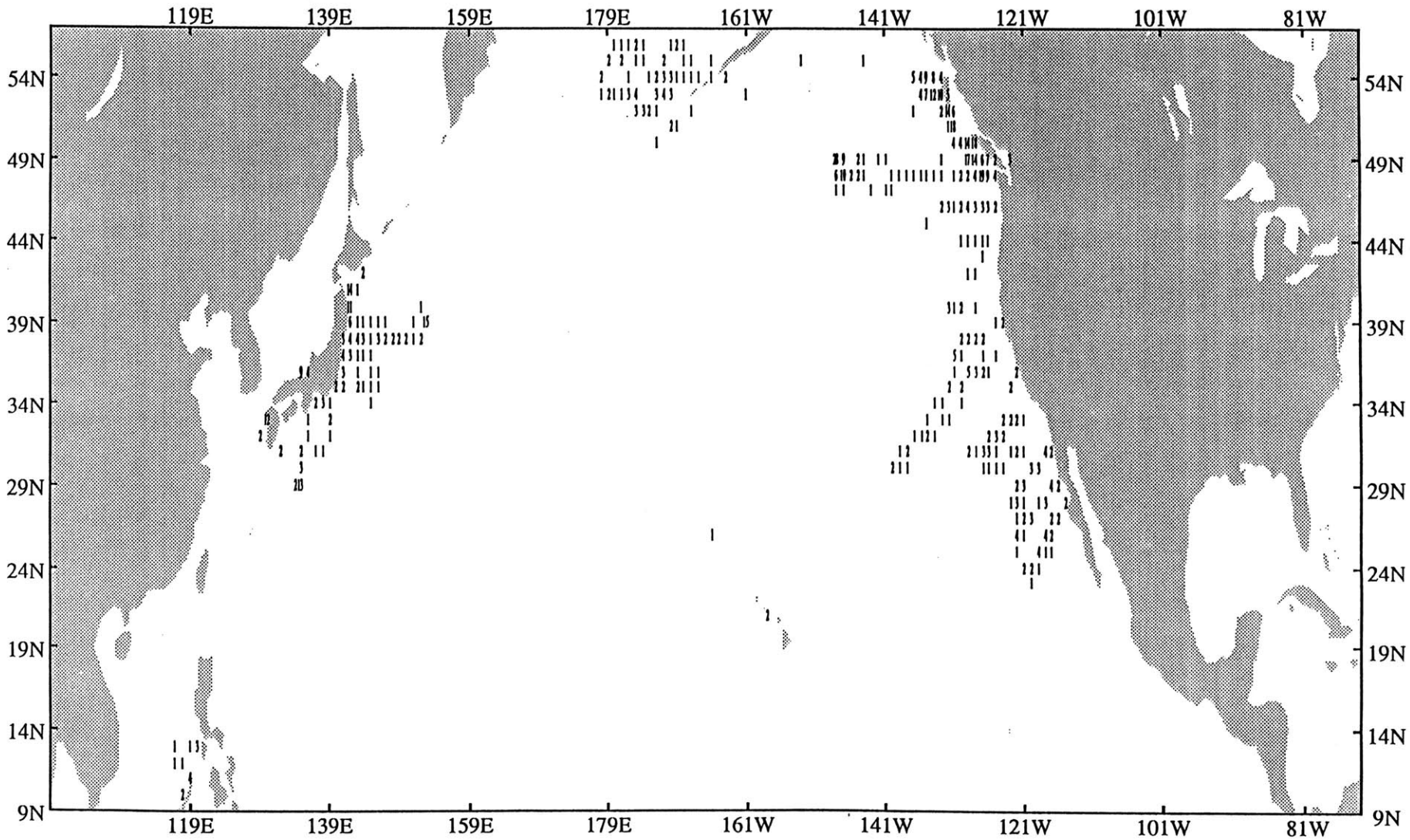

FIGURE 10. (cont.)

Number of soundings for July,1964

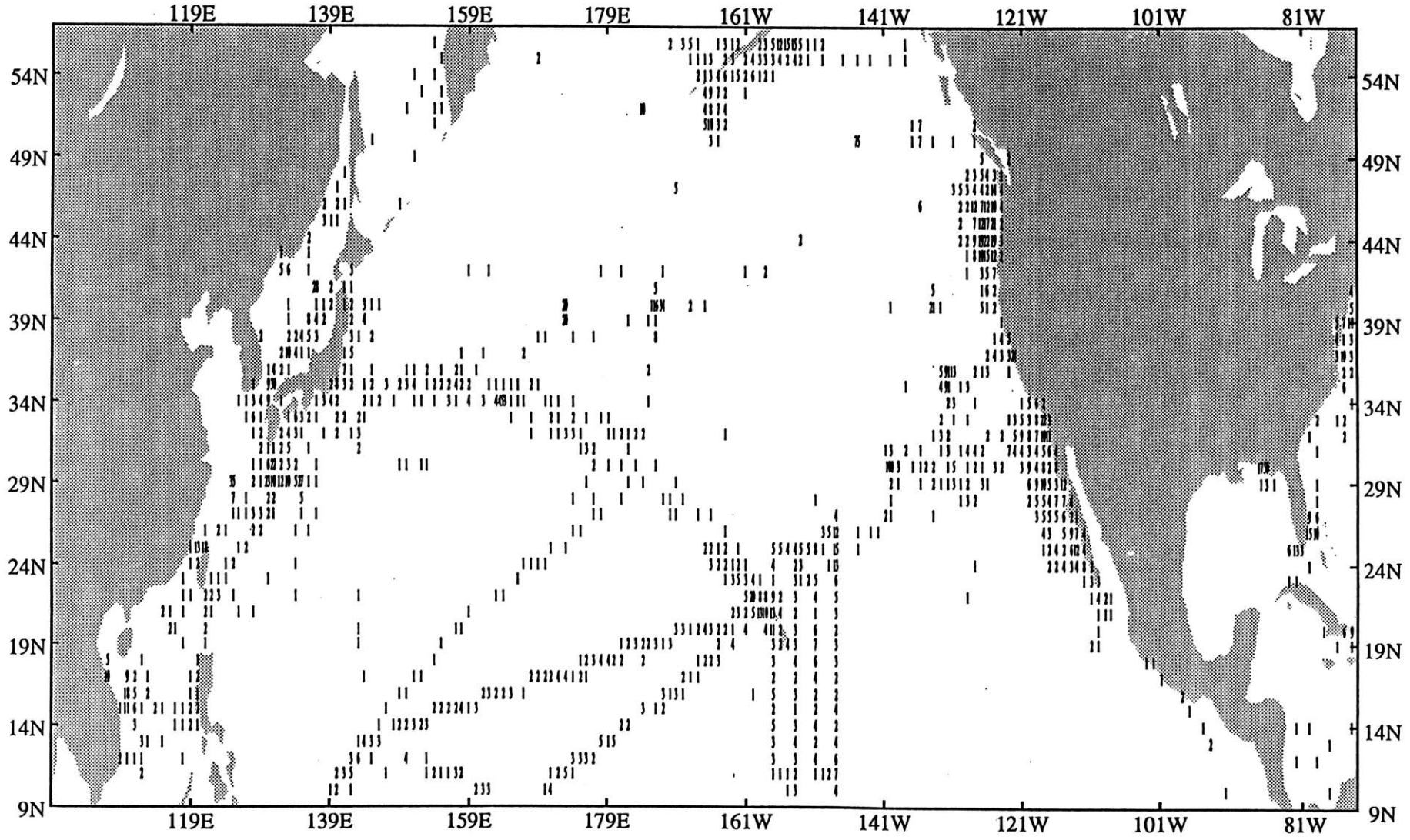

FIGURE 10. (cont.)

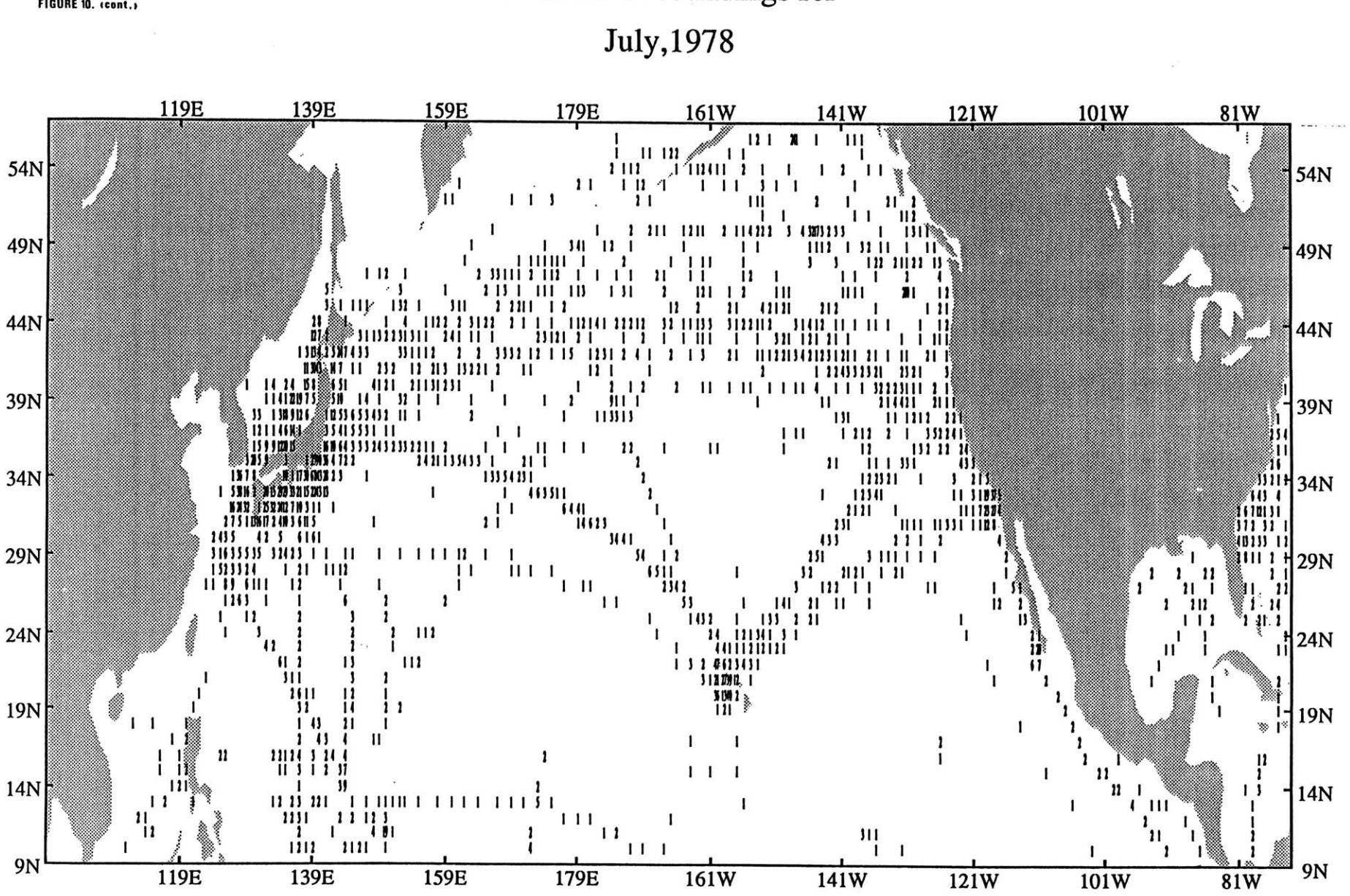

A sampling-based rejection criterion

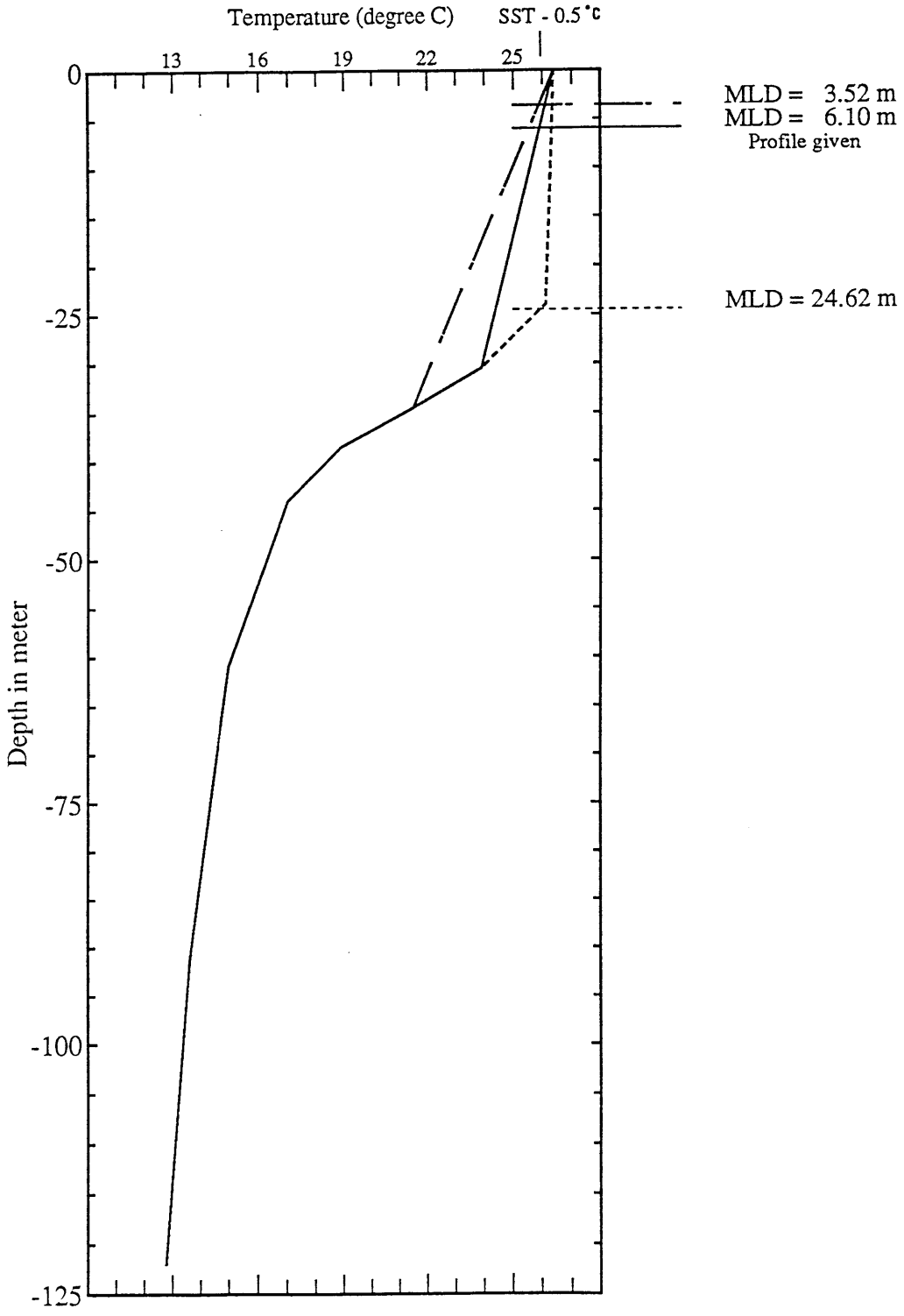

FIGURE 11

FIGURE 12.

WINTERTIME MIXED LAYER DEPTH (1949–1979)

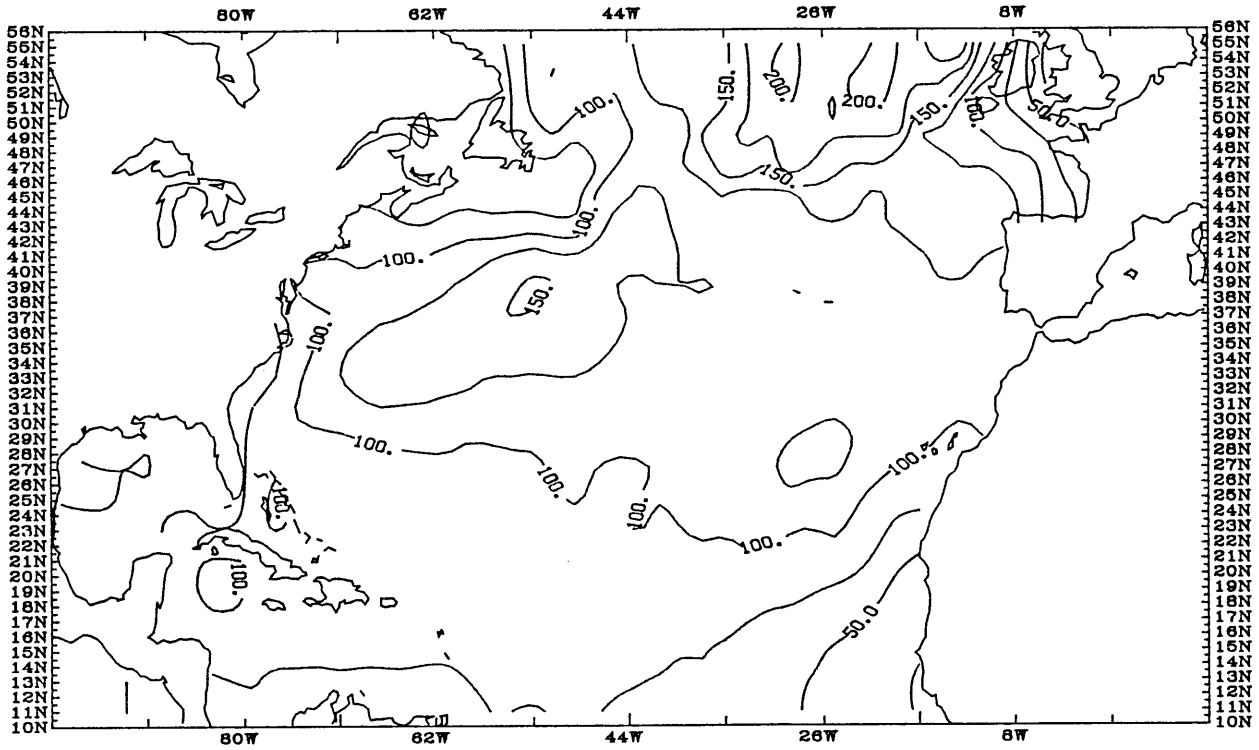

SPRINGTIME MIXED LAYER DEPTH (1949–1979)

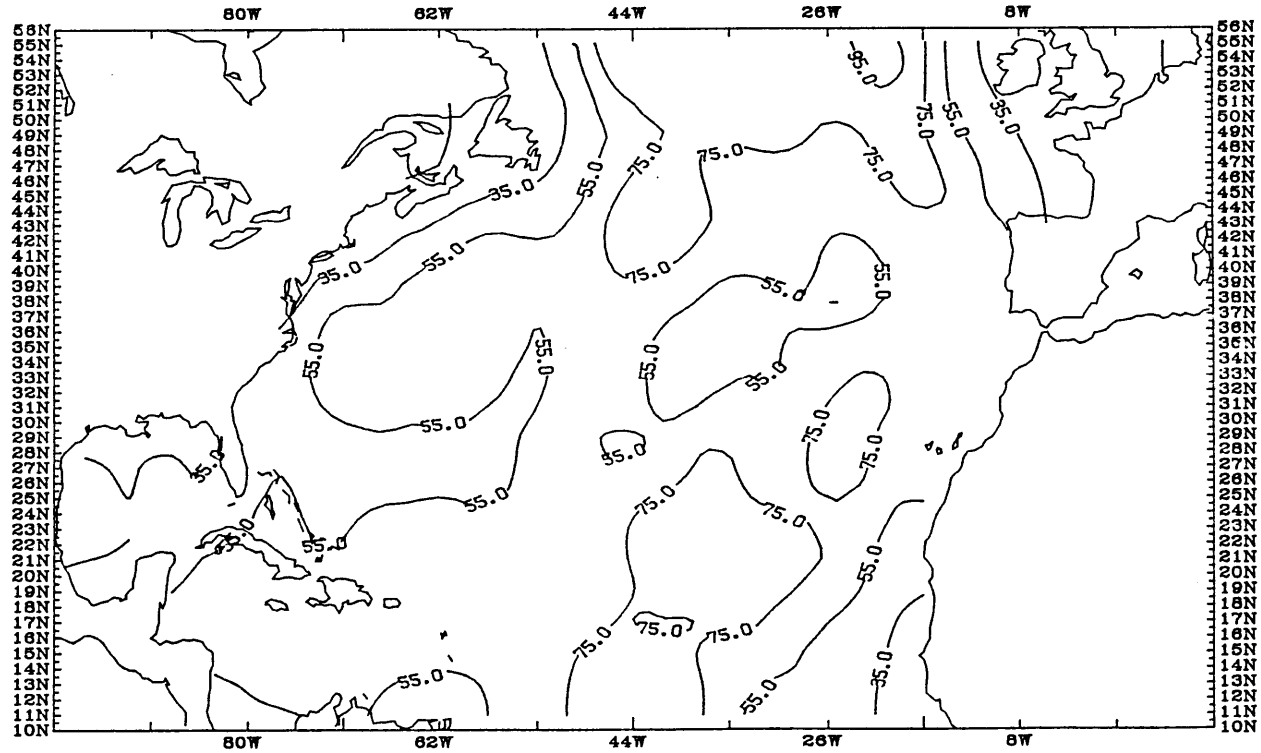

FIGURE12 (cont.)

SUMMERTIME MIXED LAYER DEPTH (1949–1979)

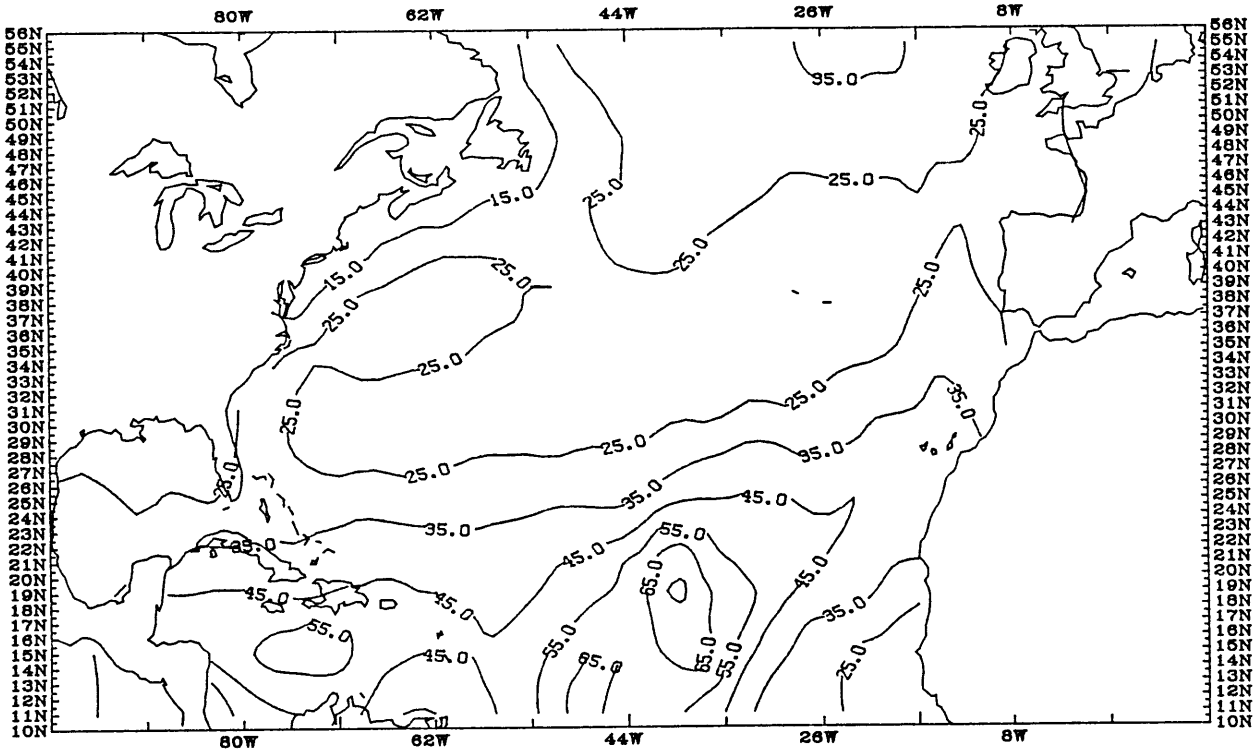

FALLTIME MIXED LAYER DEPTH (1949–1979)

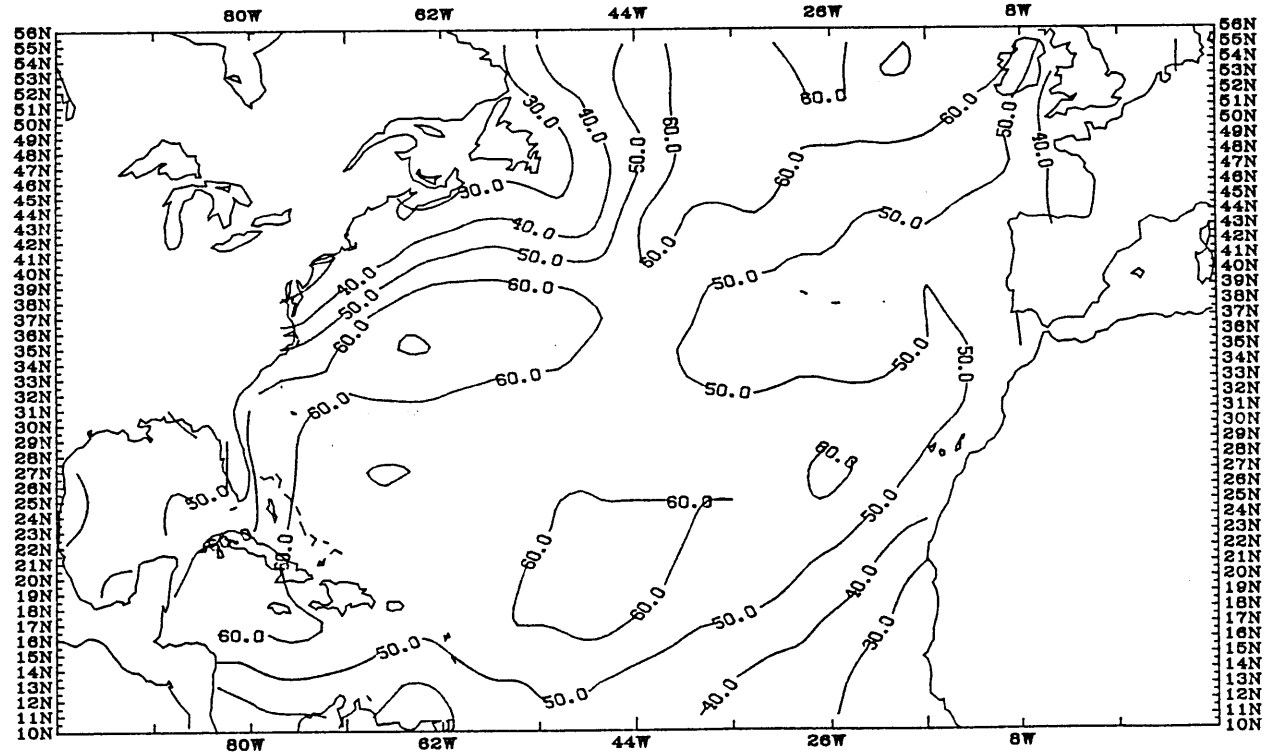

FIGURE13 .

WINTERTIME MIXED LAYER DEPTH (1949–1979)

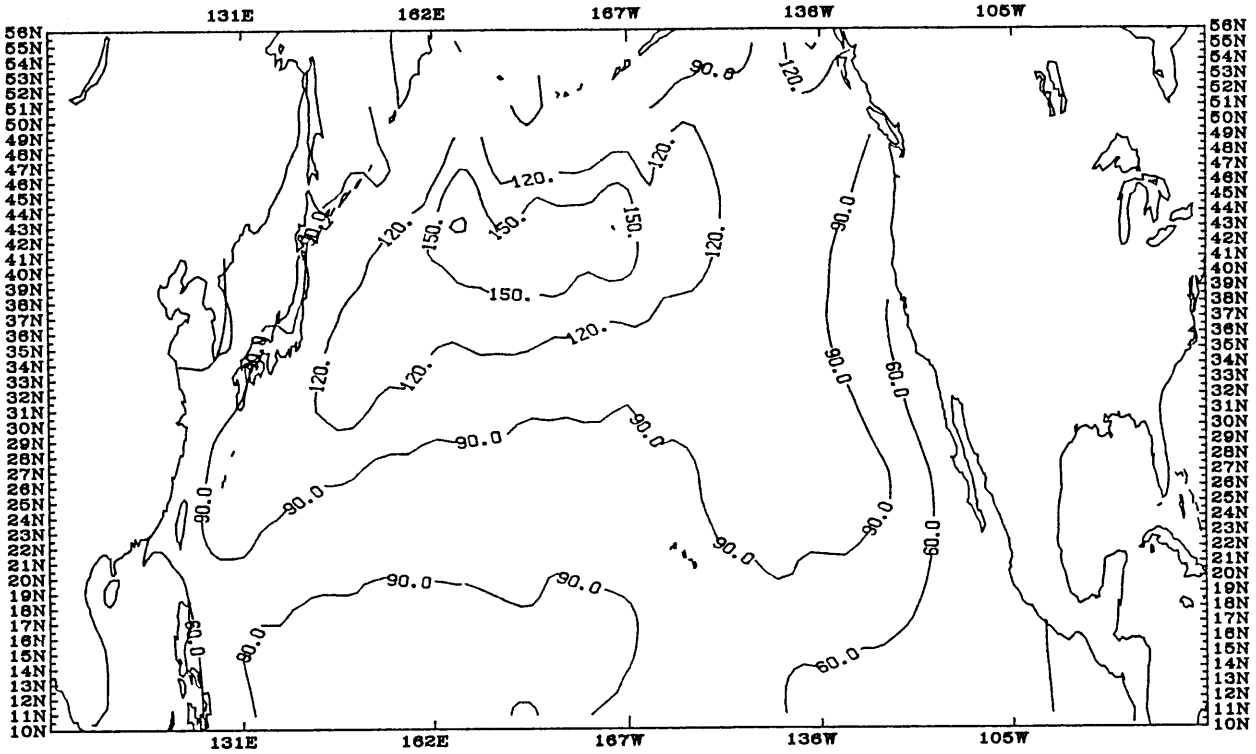

SPRINGTIME MIXED LAYER DEPTH (1949–1979)

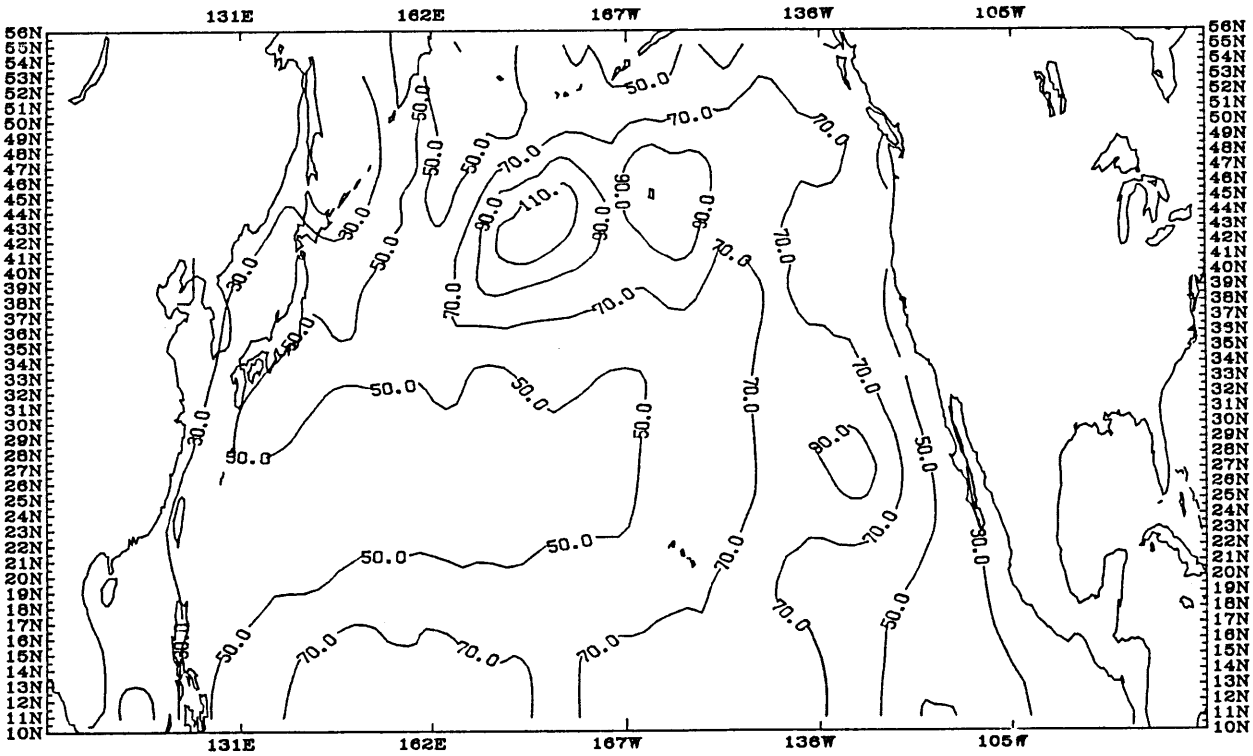

FIGURE 13. (cont.)

SUMMERTIME MIXED LAYER DEPTH (1949–1979)

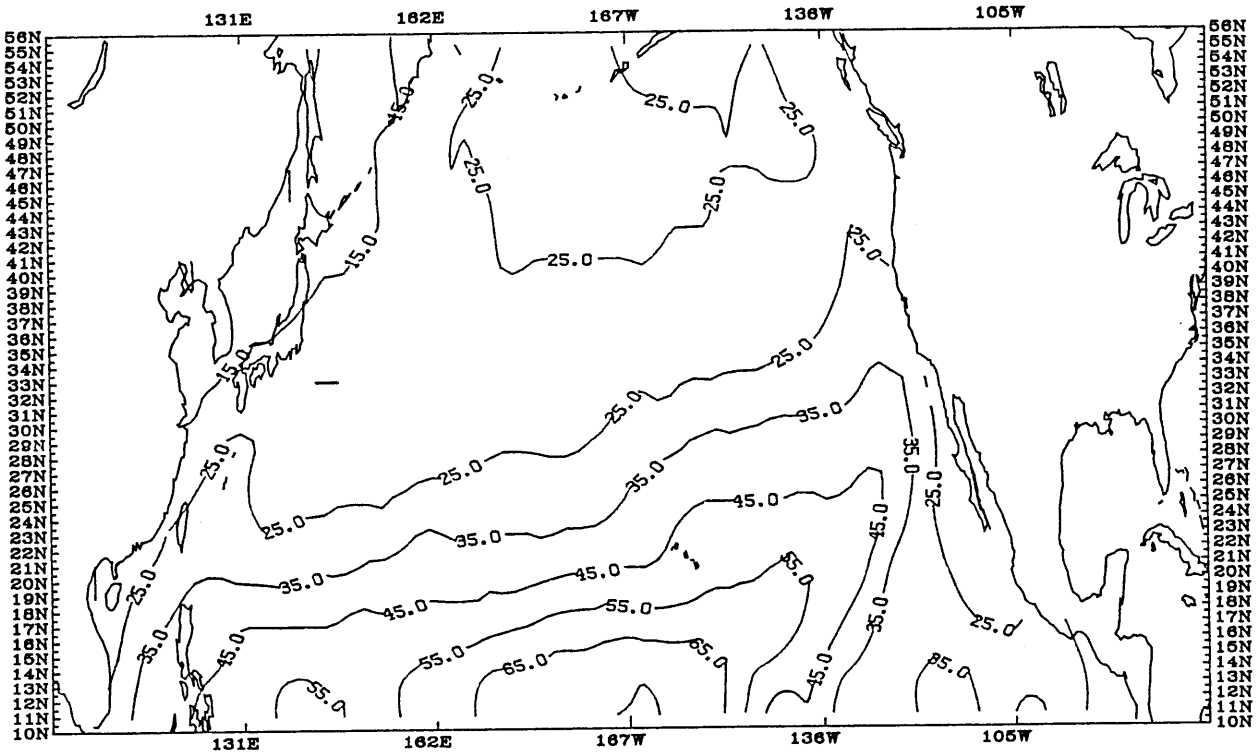

FALLTIME MIXED LAYER DEPTH (1949–1979)

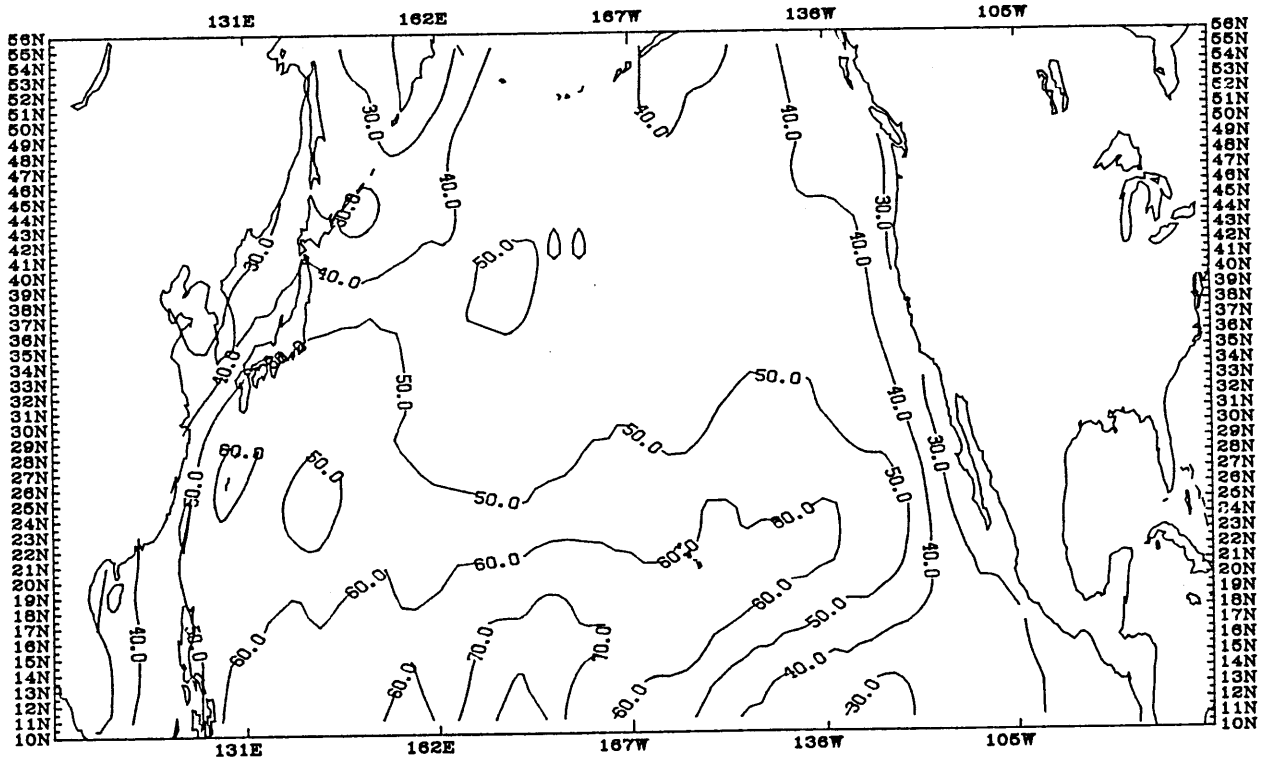

FIGURE 14.

AMPLITUDE OF THE SEASONAL CYCLE MLD (1949–1979)

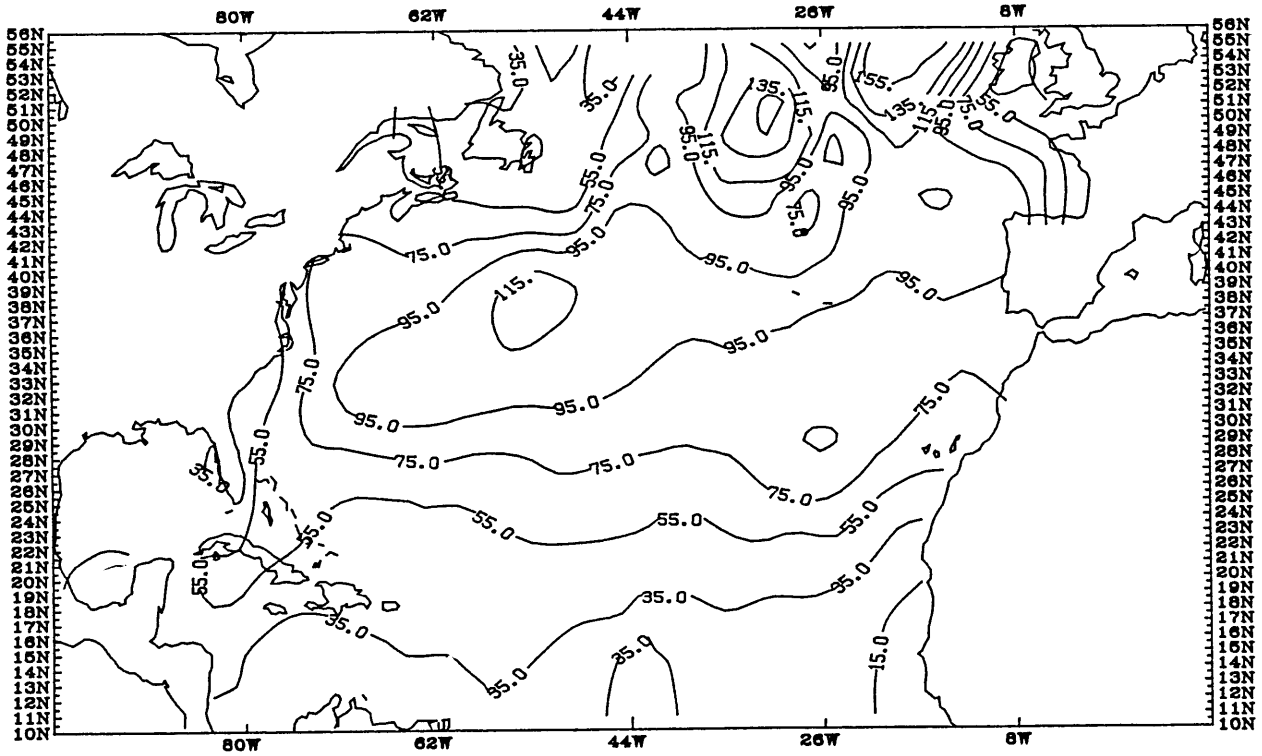

ATLANTIC OCEAN

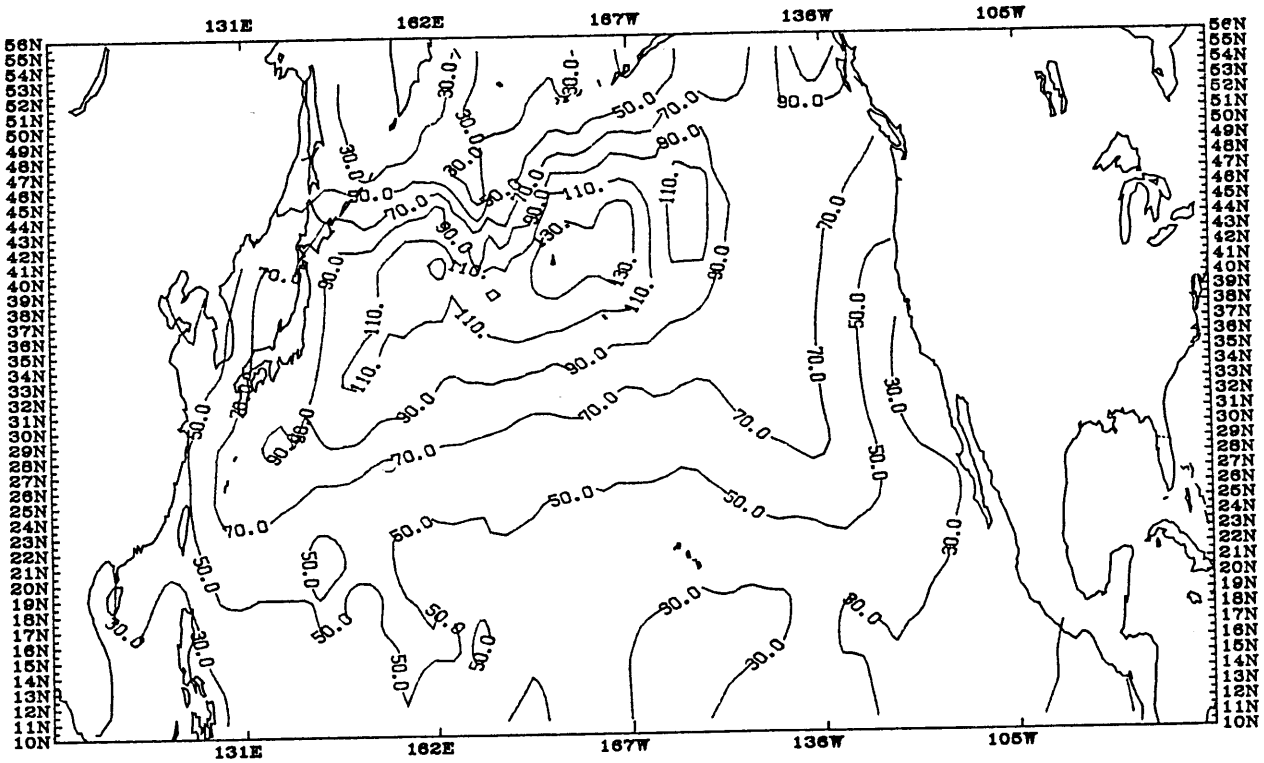

PACIFIC OCEAN

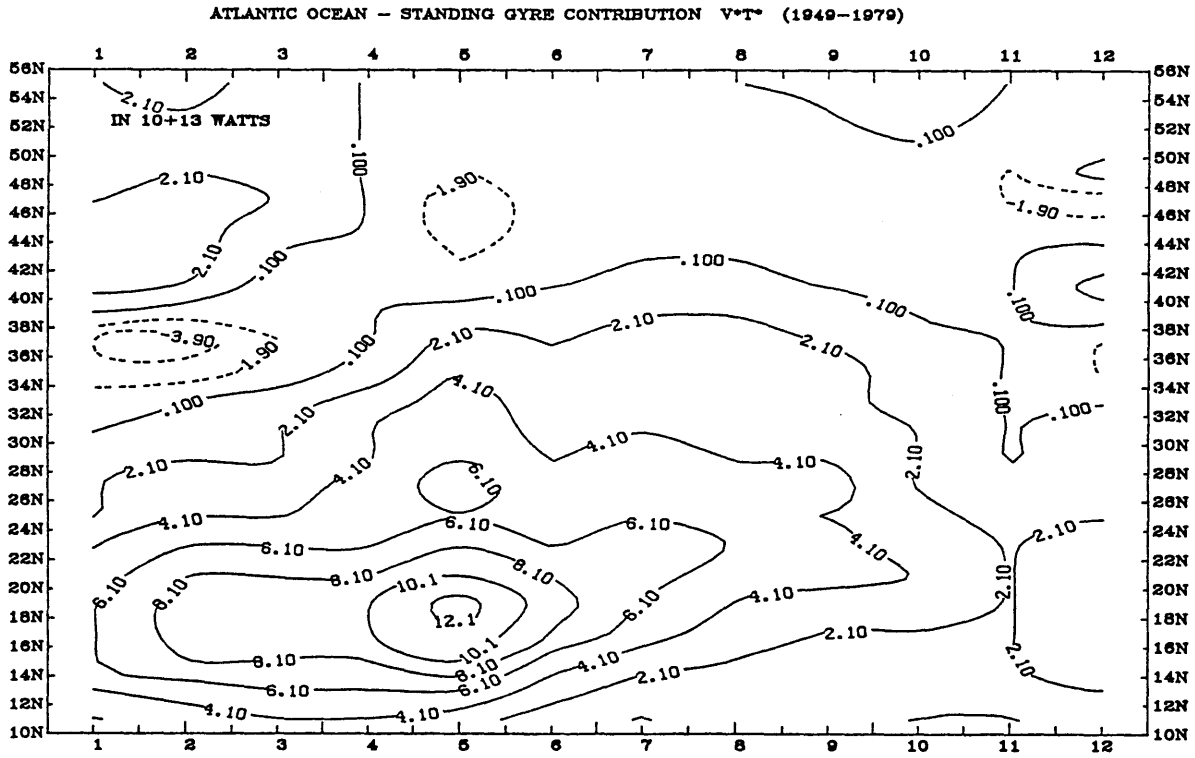
ATLANTIC OCEAN – STANDING GYRE CONTRIBUTION V*T* (1949–1979)
IN 10+13 WATTS

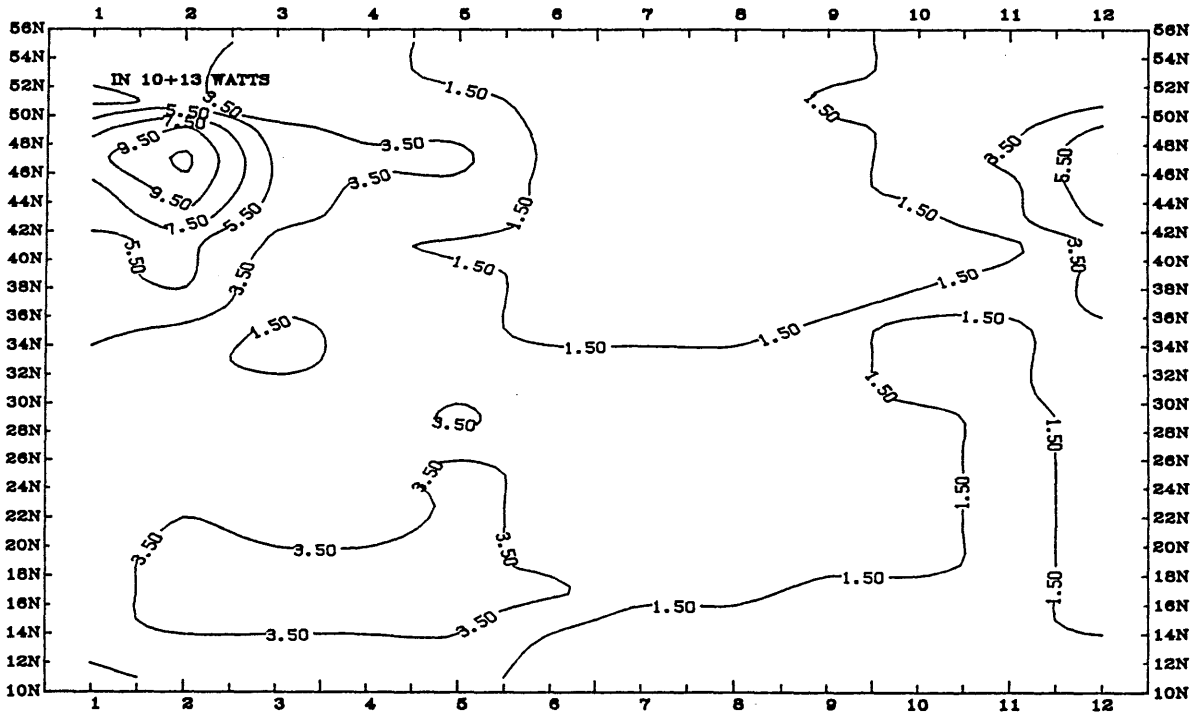
ATLANTIC OCEAN – STANDING GYRE CONTRIBUTION STD(V*T*) (1949–1979)
IN 10+13 WATTS

FIGURE 15.

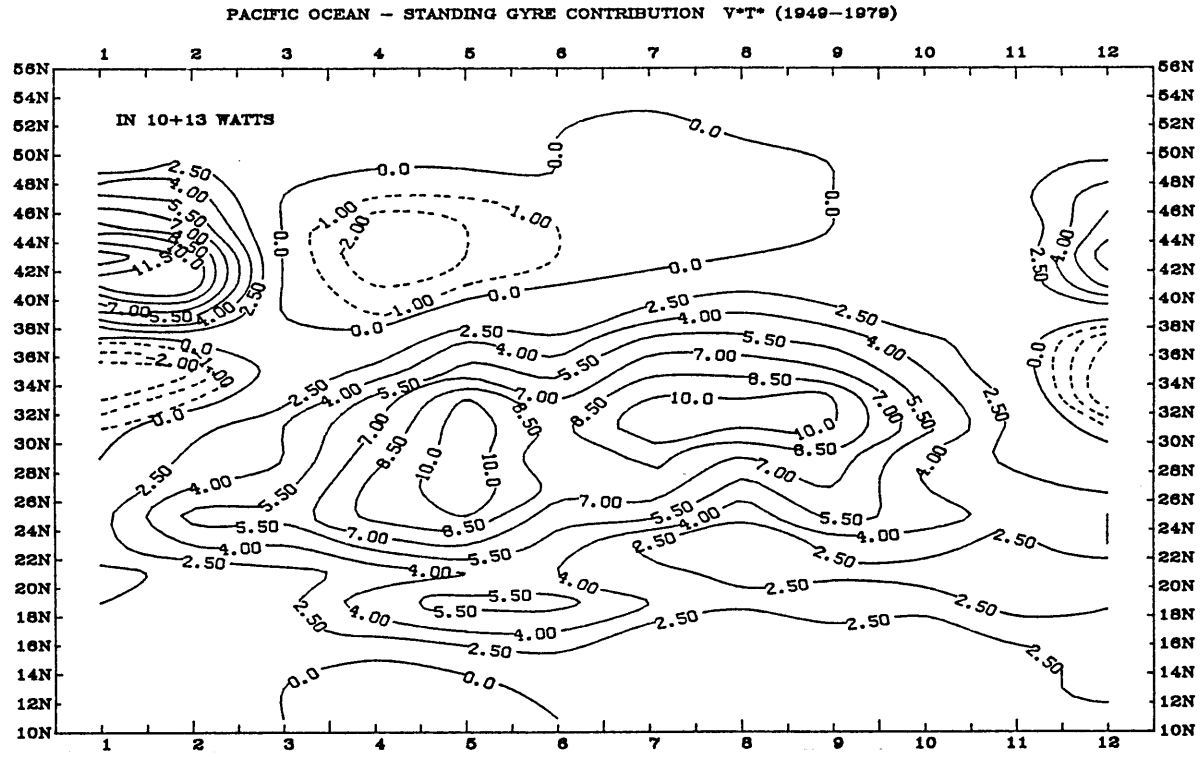
PACIFIC OCEAN – STANDING GYRE CONTRIBUTION V*T* (1949–1979)
IN 10+13 WATTS

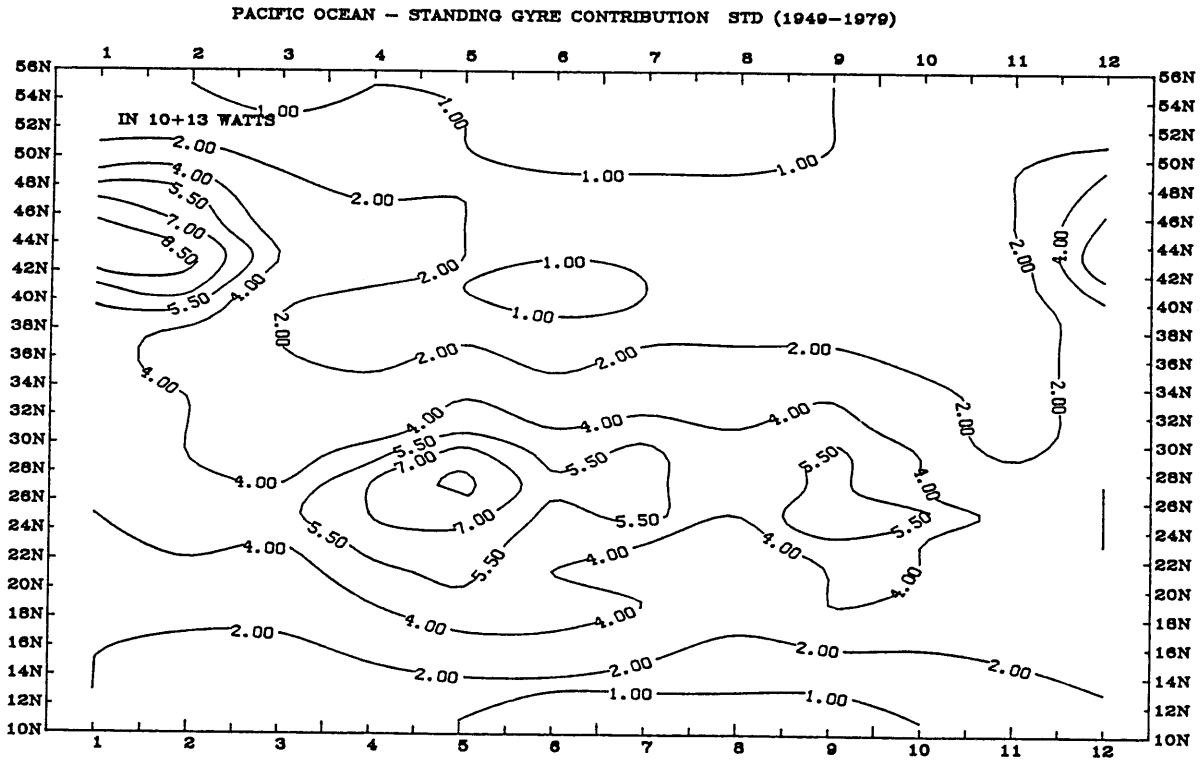
PACIFIC OCEAN – STANDING GYRE CONTRIBUTION STD (1949–1979)
IN 10+13 WATTS

FIGURE 16.

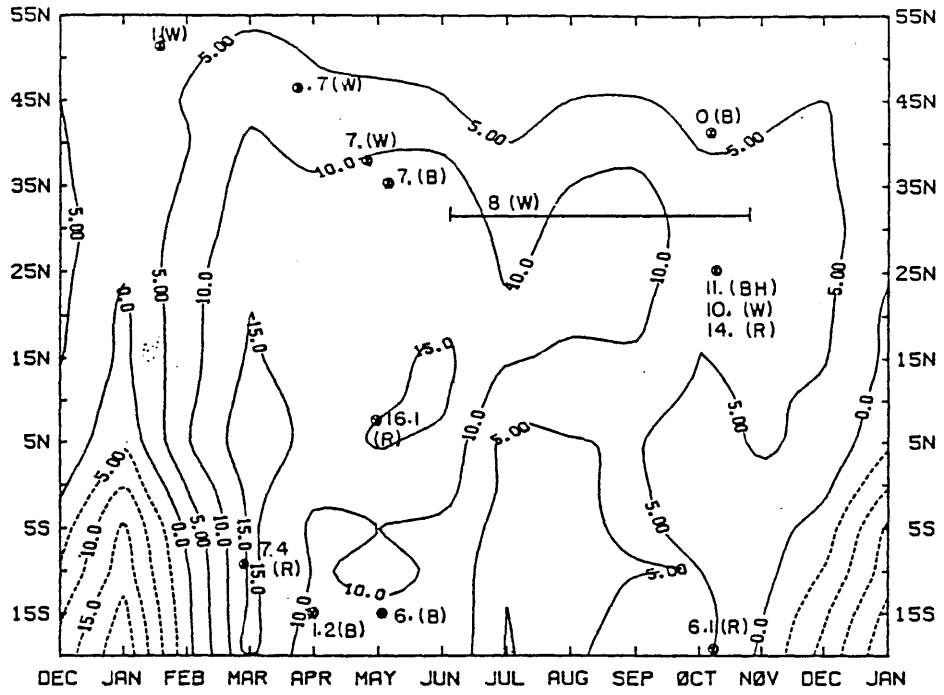

Zonal averages of meridional transport, 0–300 m, 10^{14} W, for the Atlantic Ocean. Positive values denote northward transport. Estimates from direct observations are shown with letters representing authors: B = Bryan (1962); BH = Bryden and Hall (1980), Hall and Bryden (1982); R = Roemmich (1983); W = Wunsch (1980).

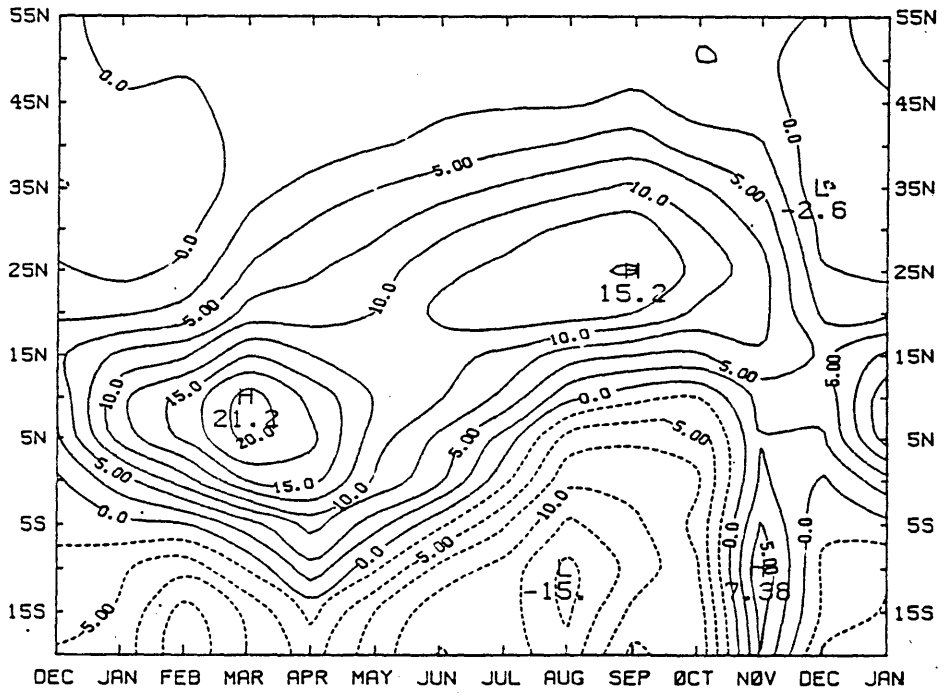

for the Pacific Ocean.

FIGURE 17.

From HSIUNG et al 1988

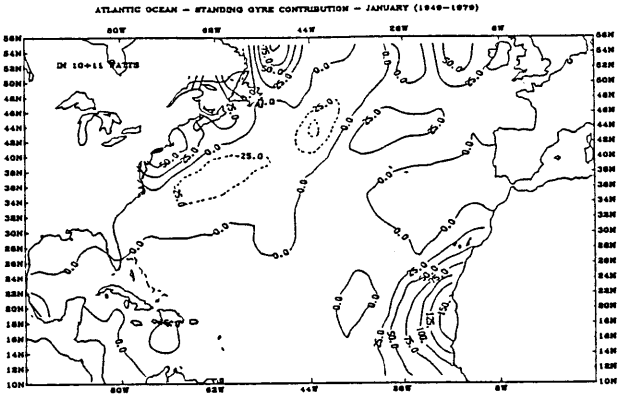
ATLANTIC OCEAN - STANDING GYRE CONTRIBUTION - JANUARY (1948-1978)
IN 10+11 WATTS

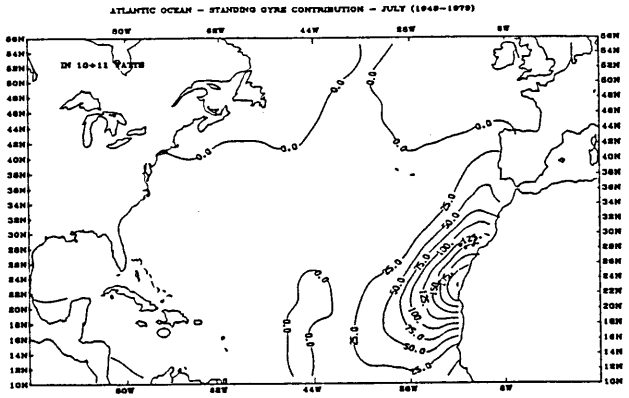
ATLANTIC OCEAN - STANDING GYRE CONTRIBUTION - JULY (1948-1978)
IN 10+11 WATTS

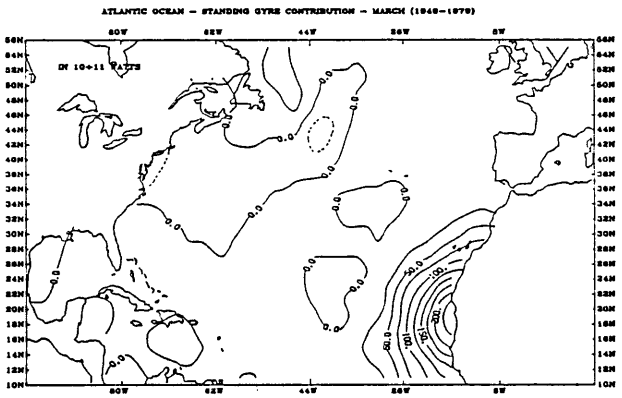
ATLANTIC OCEAN - STANDING GYRE CONTRIBUTION - MARCH (1948-1978)
IN 10+11 WATTS

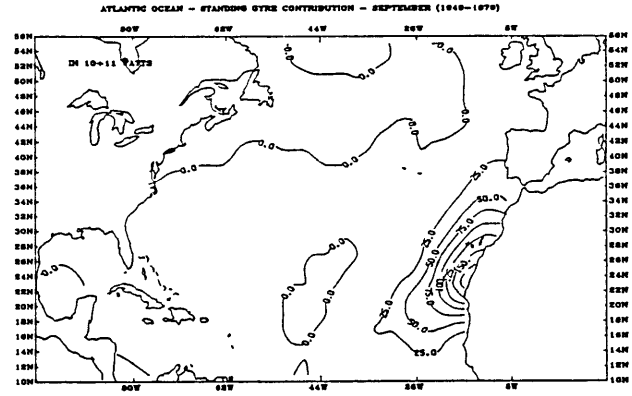
ATLANTIC OCEAN - STANDING GYRE CONTRIBUTION - SEPTEMBER (1948-1978)
IN 10+11 WATTS

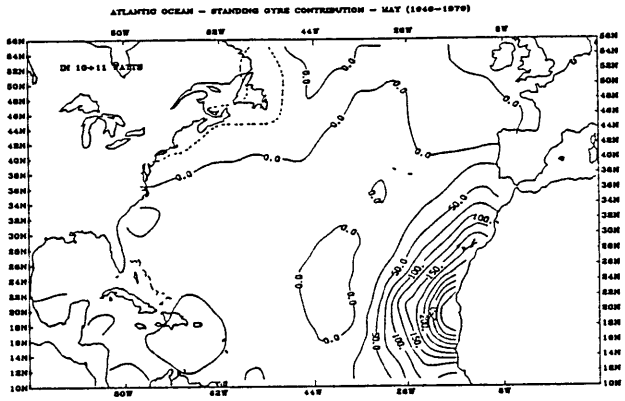
ATLANTIC OCEAN - STANDING GYRE CONTRIBUTION - MAY (1948-1978)
IN 10+11 WATTS

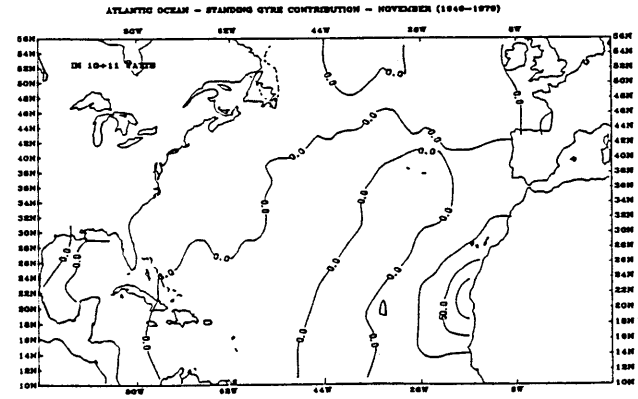
ATLANTIC OCEAN - STANDING GYRE CONTRIBUTION - NOVEMBER (1948-1978)
IN 10+11 WATTS

FIGURE 18.

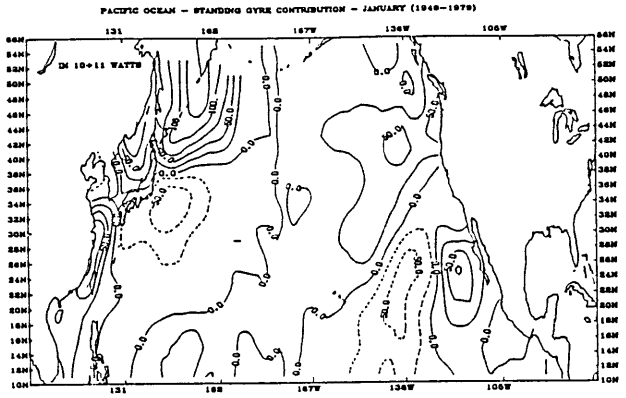
PACIFIC OCEAN – STANDING GYRE CONTRIBUTION – JANUARY (1949–1979)
IN 10**11 WATTS

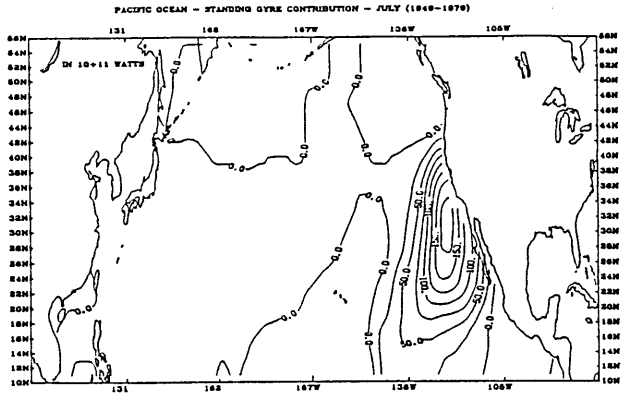
PACIFIC OCEAN – STANDING GYRE CONTRIBUTION – JULY (1949–1979)
IN 10**11 WATTS

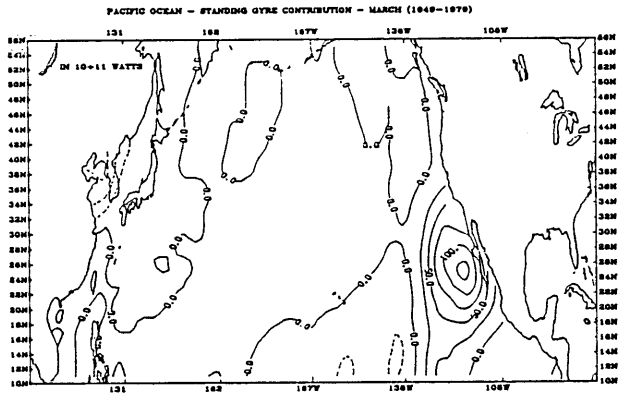
PACIFIC OCEAN – STANDING GYRE CONTRIBUTION – MARCH (1949–1979)
IN 10**11 WATTS

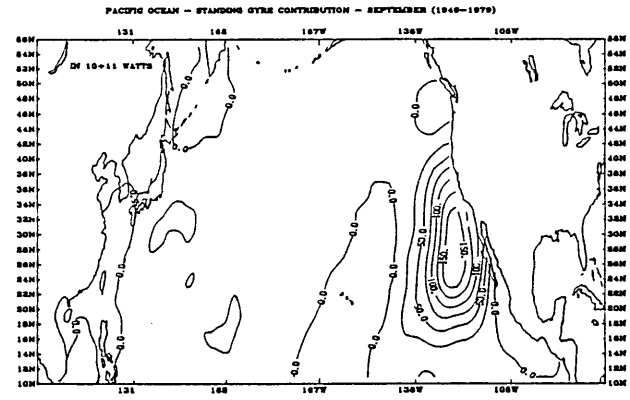
PACIFIC OCEAN – STANDING GYRE CONTRIBUTION – SEPTEMBER (1949–1979)
IN 10**11 WATTS

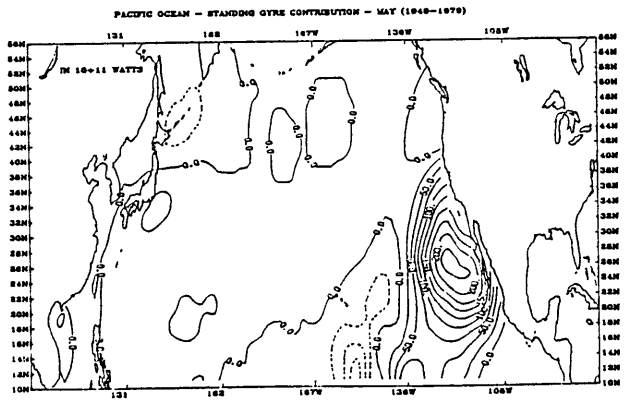
PACIFIC OCEAN – STANDING GYRE CONTRIBUTION – MAY (1949–1979)
IN 10**11 WATTS

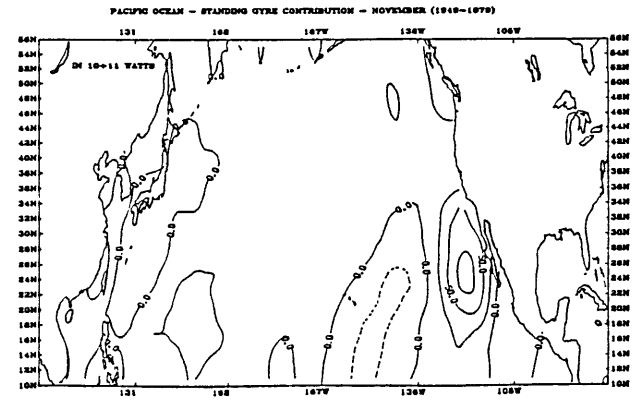
PACIFIC OCEAN – STANDING GYRE CONTRIBUTION – NOVEMBER (1949–1979)
IN 10**11 WATTS

FIGURE 19.

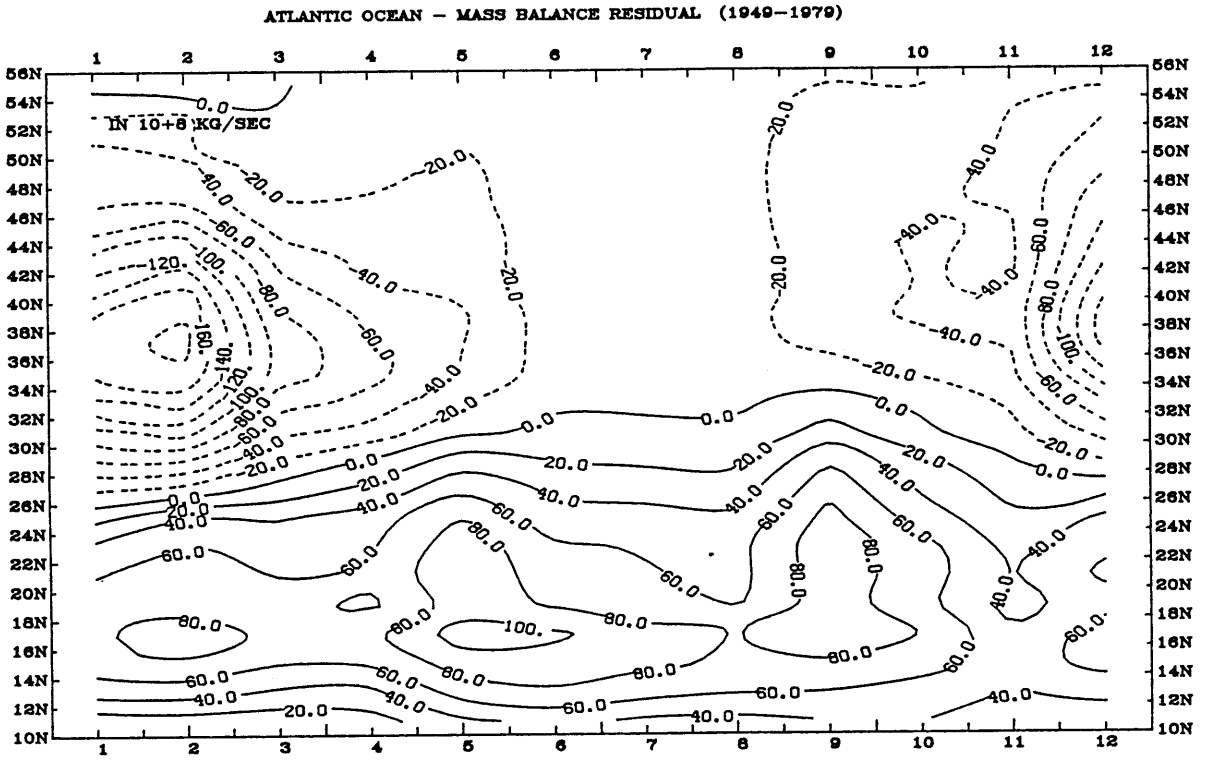
ATLANTIC OCEAN – MASS BALANCE RESIDUAL (1949–1979)
IN 10+8 KG/SEC

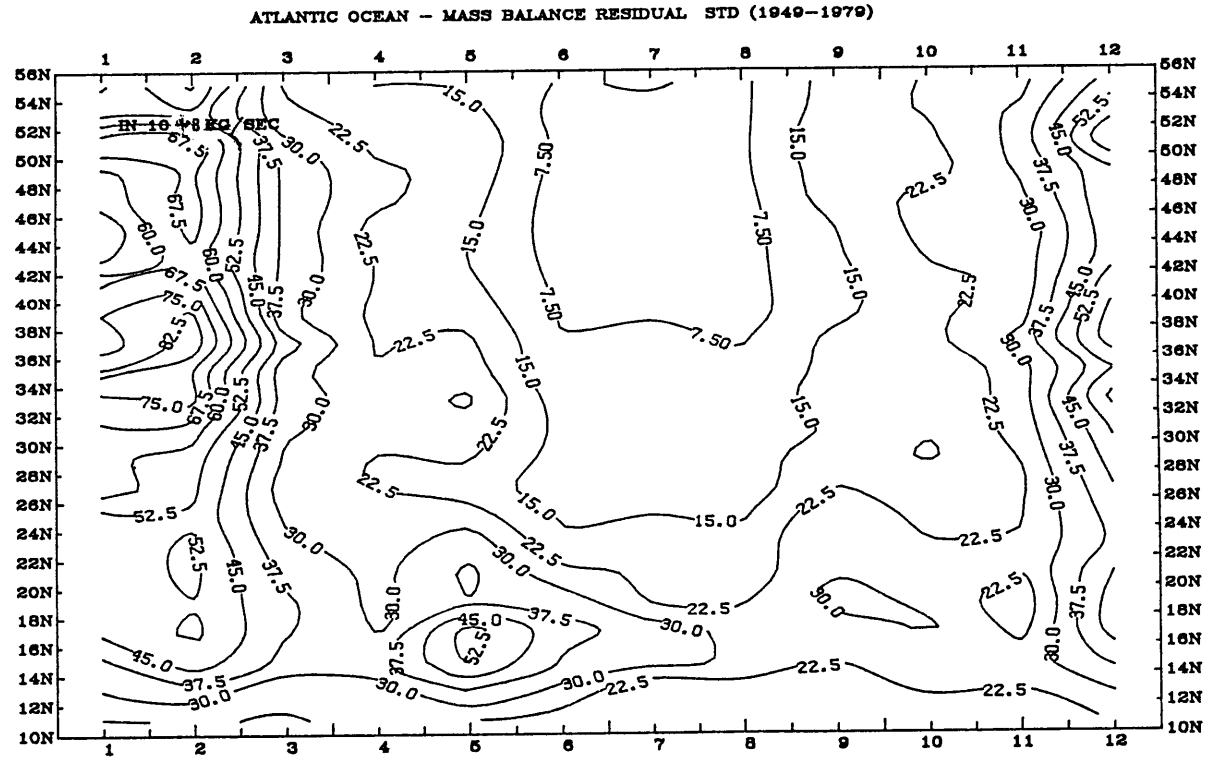
ATLANTIC OCEAN – MASS BALANCE RESIDUAL STD (1949–1979)
IN 10+8 KG/SEC

FIGURE 21.

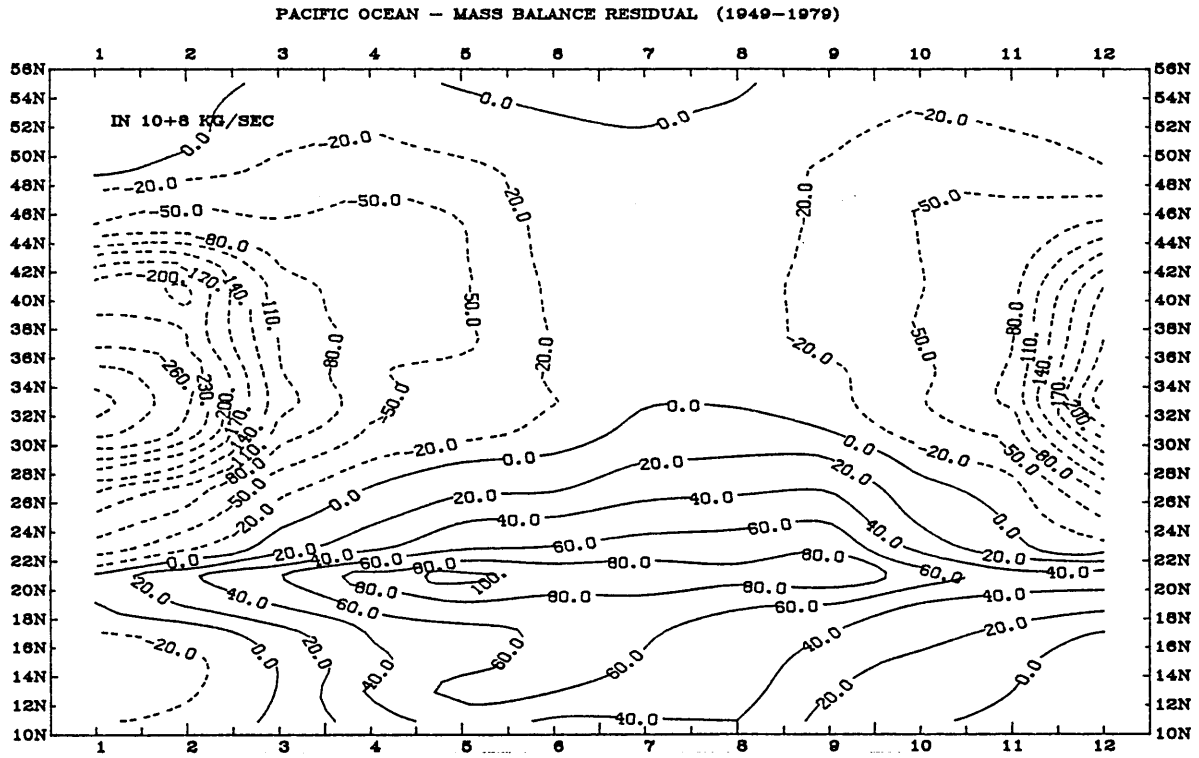
PACIFIC OCEAN – MASS BALANCE RESIDUAL (1949–1979)
IN 10+8 KG/SEC

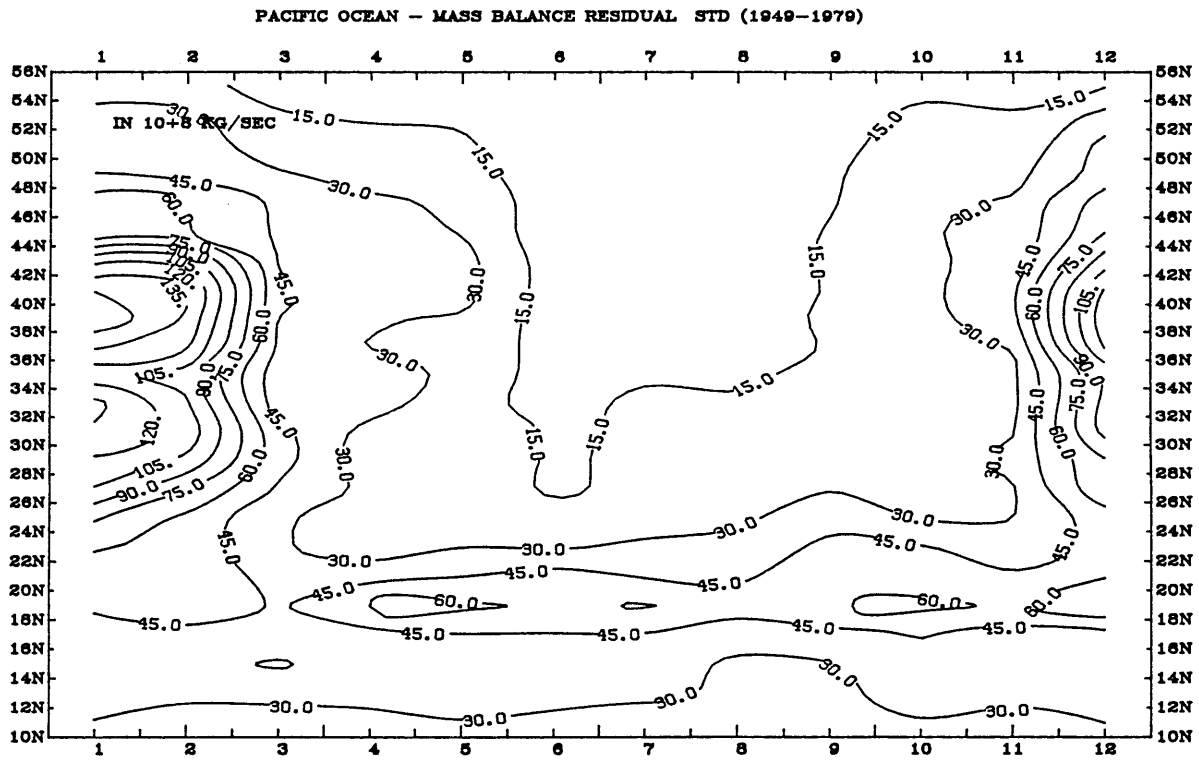
PACIFIC OCEAN – MASS BALANCE RESIDUAL STD (1949–1979)
IN 10+8 KG/SEC

FIGURE 22.

FIGURE 23.

MAIN PATH OF THE KUROSHIO AND GULF-STREAM SYSTEMS

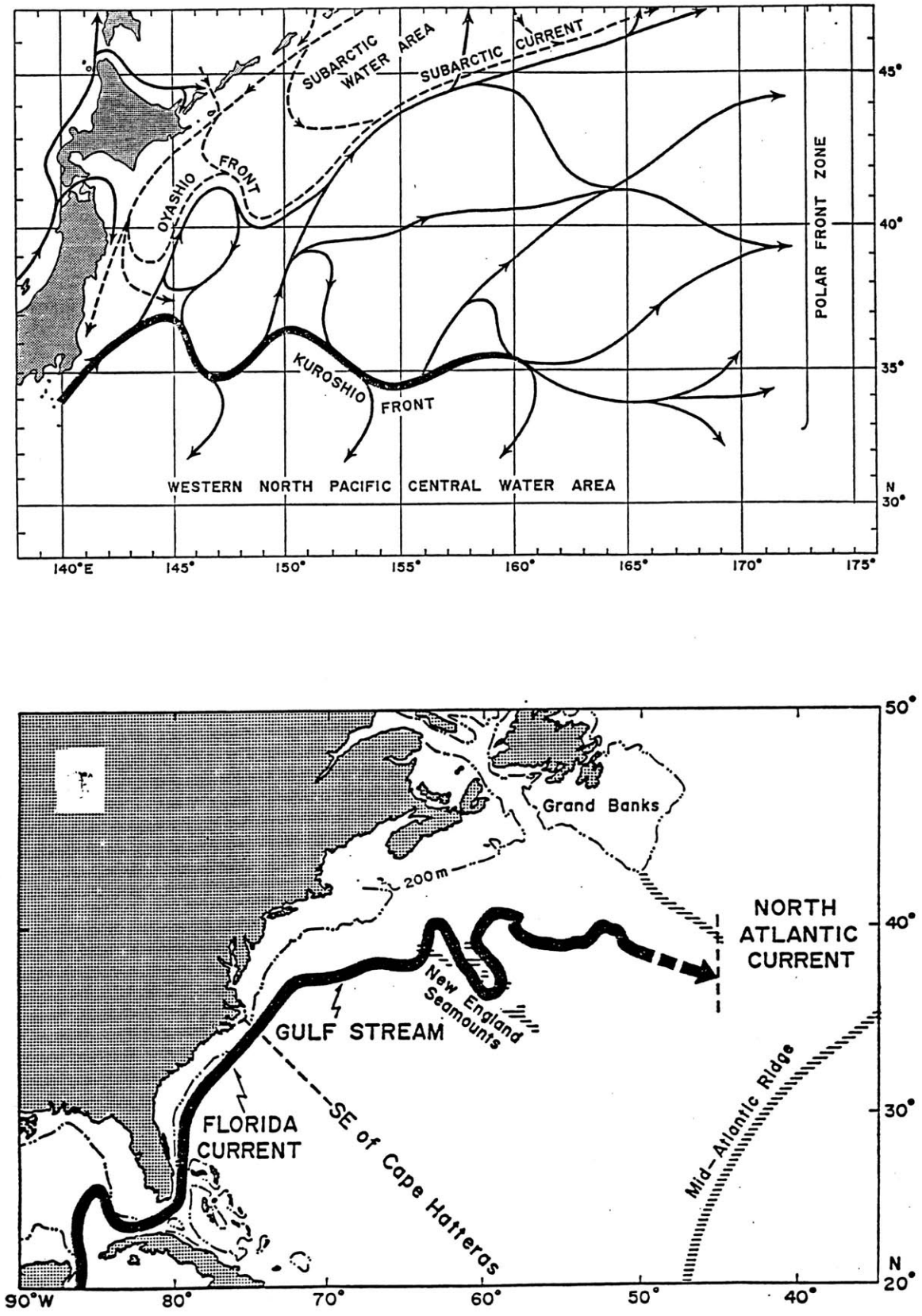

From Hideo Kawai 1972

BOUNDARY CURRENT AND OTHER ZONES USED FOR MASS BALANCE CORRECTION

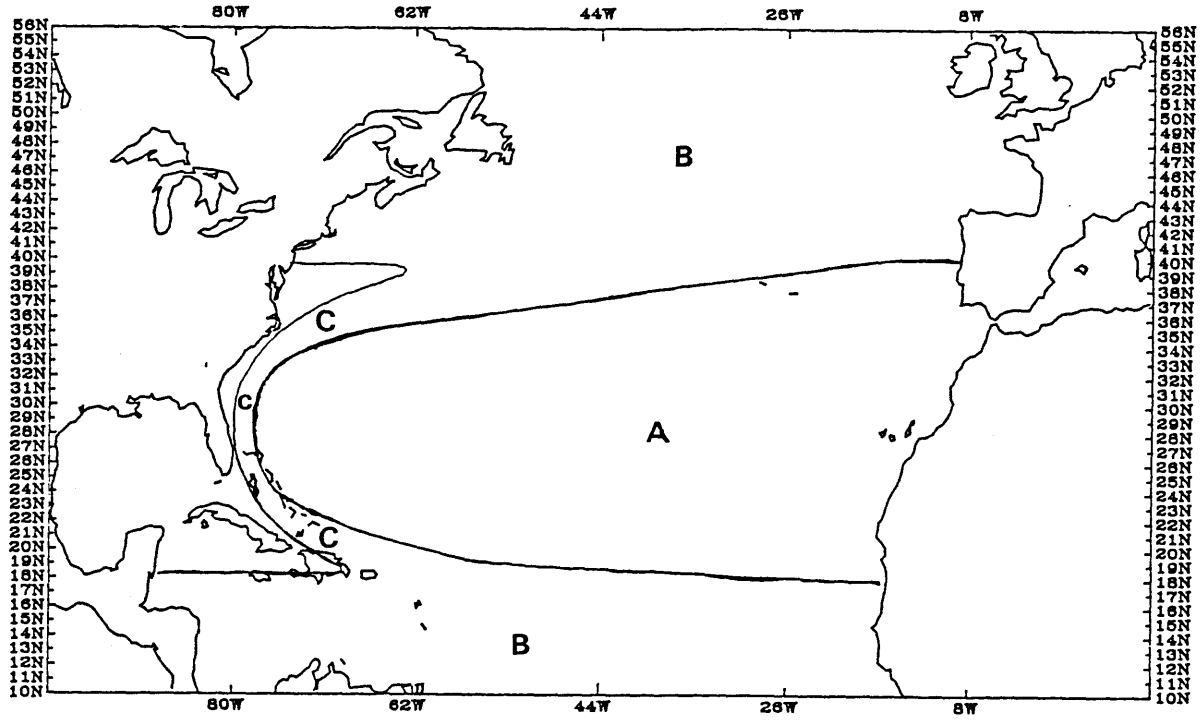

BOUNDARY CURRENT AND OTHER ZONES USED FOR MASS BALANCE CORRECTION

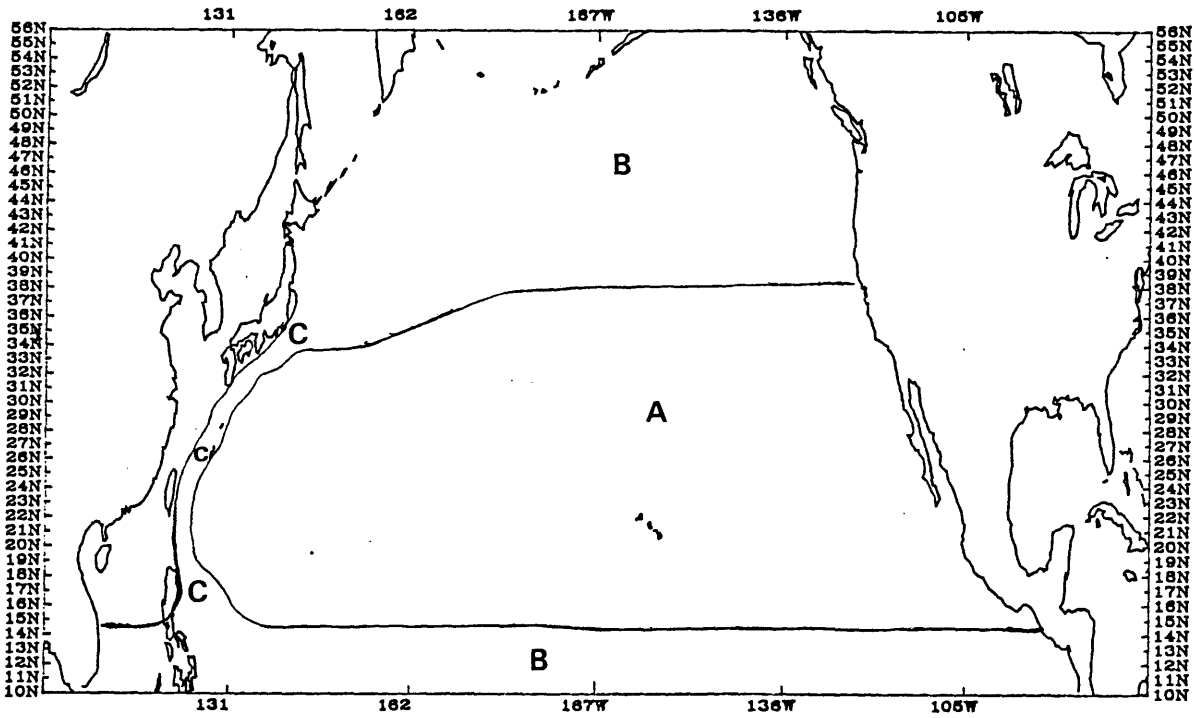

ATLANTIC OCEAN – ADJUSTED STANDING GYRE CONTRIBUTION V*T* (1949–1979)

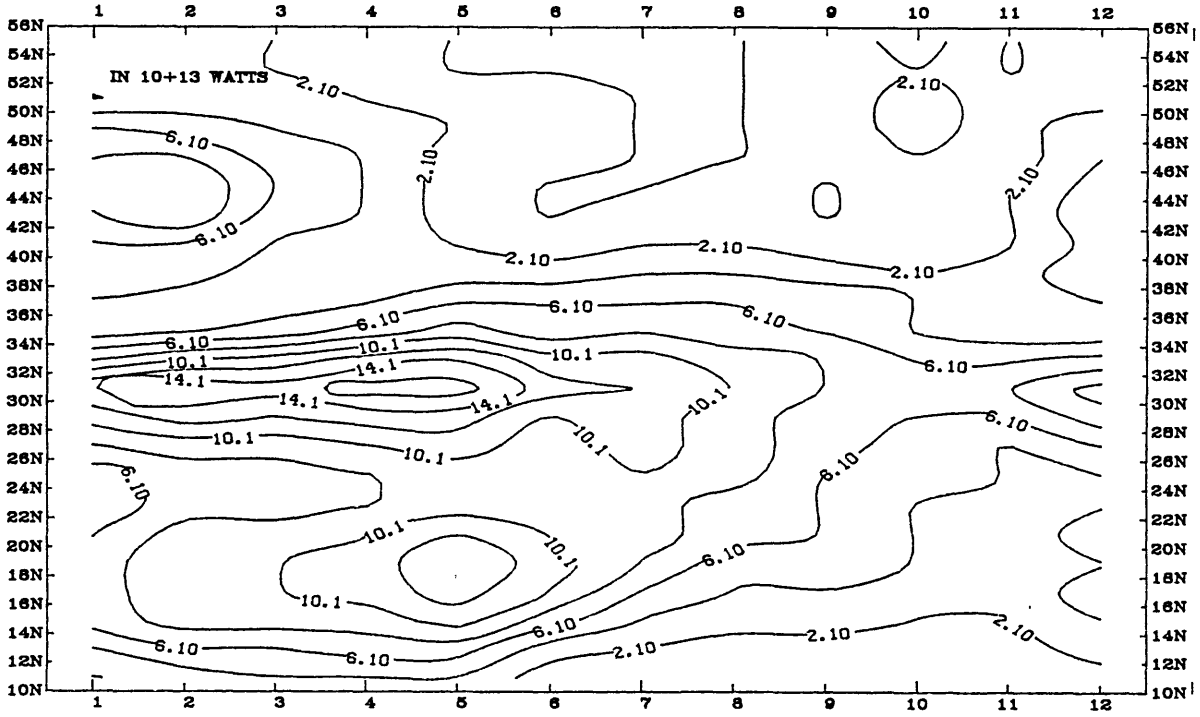

ATLANTIC OCEAN – ADJUSTED STANDING GYRE CONTRIBUTION STD (1949–1979)

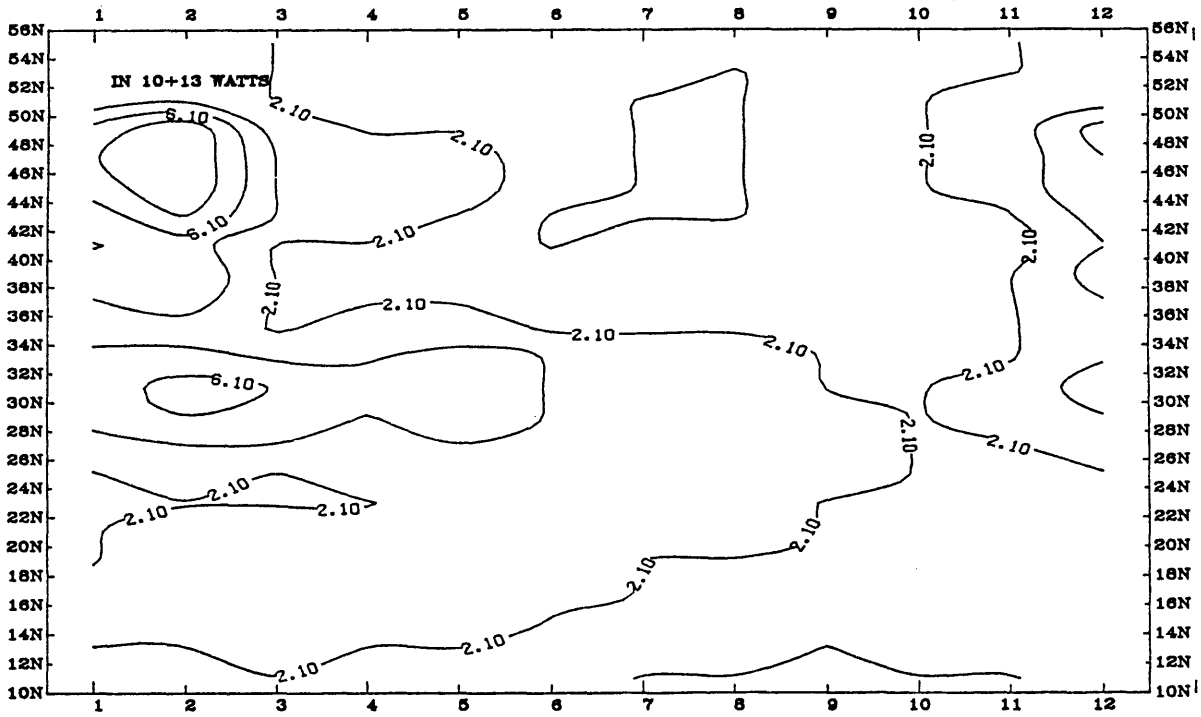

FIGURE 25

PACIFIC OCEAN — ADJUSTED STANDING GYRE CONTRIBUTION V*T* (1949–1979)

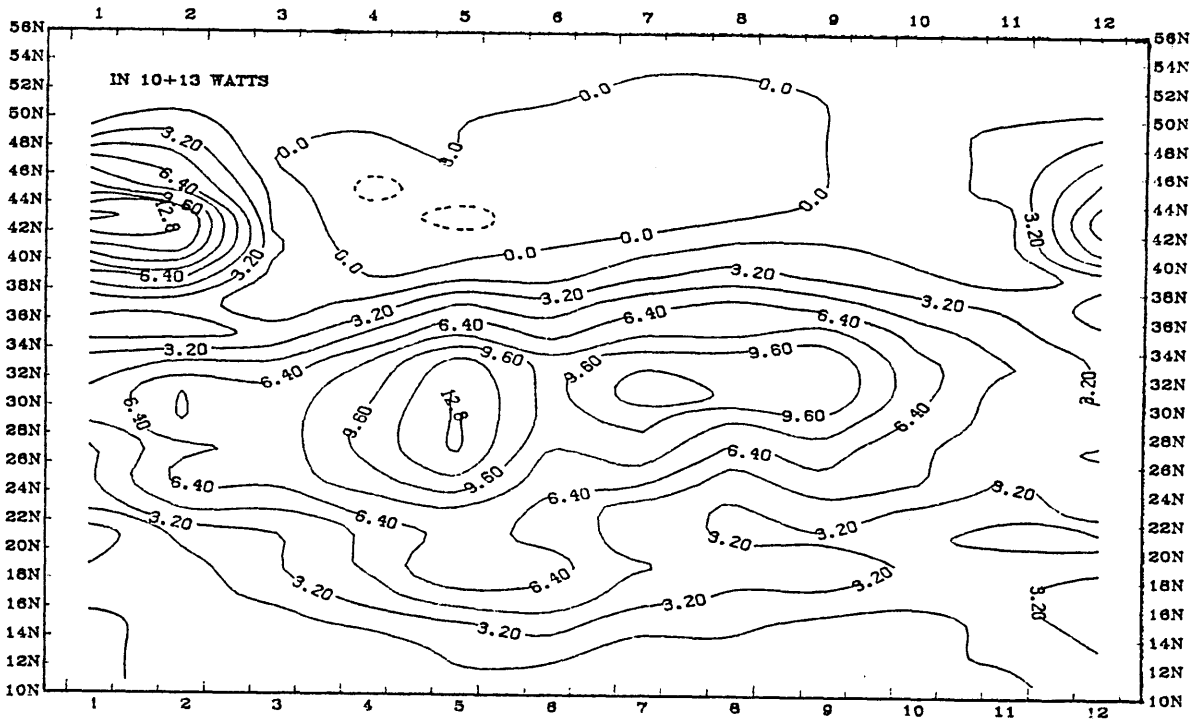

PACIFIC OCEAN — ADJUSTED STANDING GYRE CONTRIBUTION STD (1949–1979)

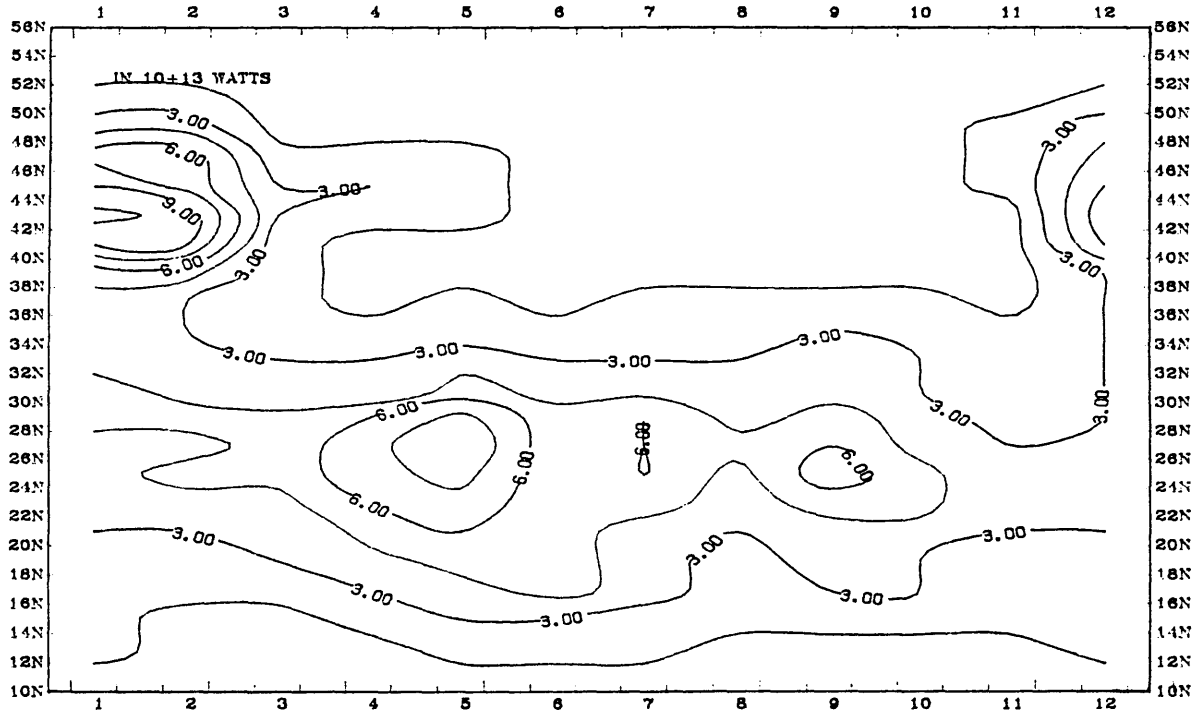

FIGURE 26

ATLANTIC OCEAN – T* IN THE BOUNDARY CURRENT AREA (1949–1979)

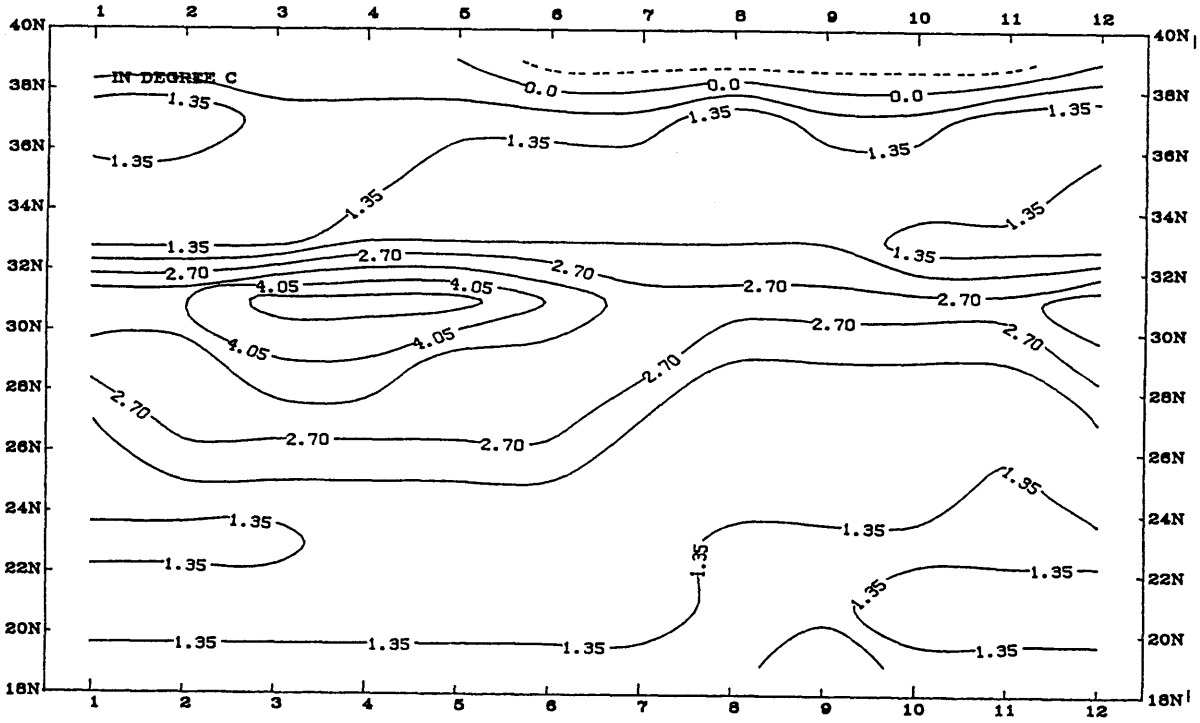

PACIFIC OCEAN – T* IN THE BOUNDARY CURRENT AREA (1949–1979)

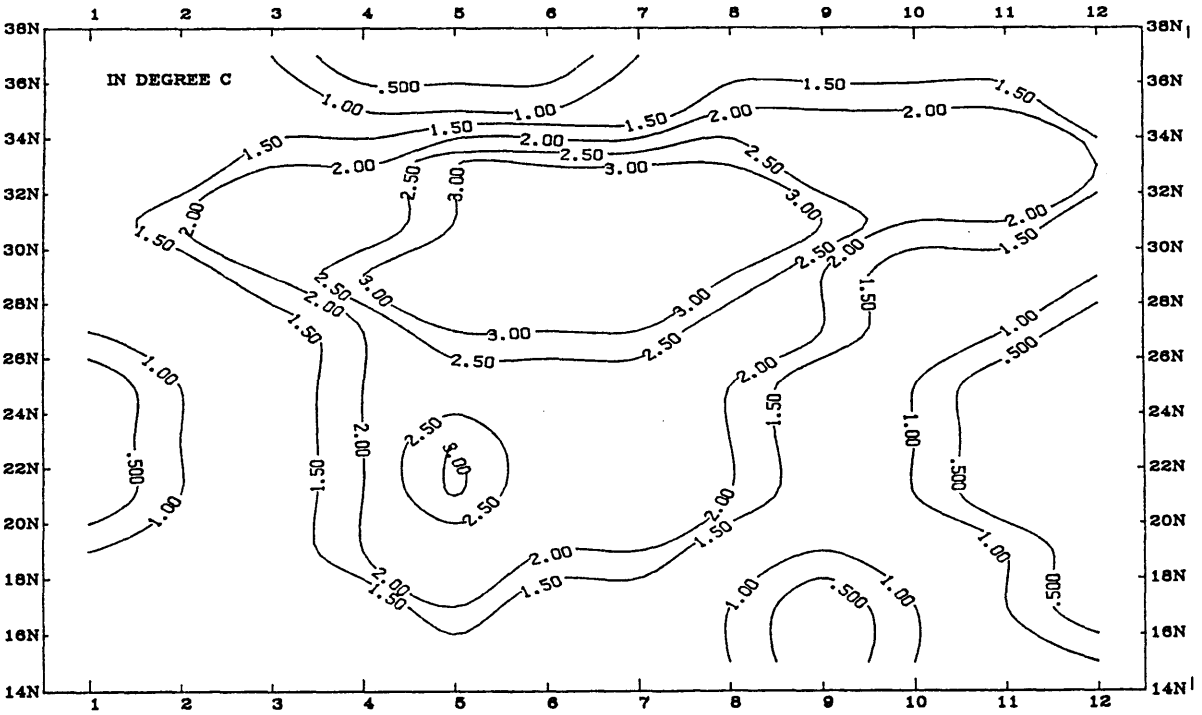

FIGURE 27

References :

Bauer R. (1982)
Functional description of the Master Oceanographic Observation Data Set (MOODS).
Compass Systems, Inc., San Diego, CA.

Bortkovskii R. S. (1968)
Quantitative relations between water, heat and salt transport in the ocean.
Problems in Dynamical Oceanography
A. I. Fel'zenbaum Editor, Akademiya Nauk SSSR.

Budyko M. I. (1963)
Atlas of the heat balance of the Earth.
Moscow, Globnaia Geofiz. Observ., 69 pp

J. Dana Thompson and W. J. Schmitz, jr (1989)
A Limited-Area Model of the Gulf-Stream : Design, Initial Experiments, and Model-Data Intercomparison.
J. Phys. Oceanog., 19 (6), 791 - 814.

De Szoeke, Levine M. D. (1981)
The advective flux of heat by mean geostrophic motions in the southern ocean.
Deep Sea Research 28A 10, 1057-1085.

Fuglister F. C. (1951)
Annual variations in current speeds in the Gulf Stream system.
Journal of Marine Research 10, 119 - 127.

Halpern David (1980)
Variability of near-surface currents in the Atlantic North Equatorial countercurrent during GATE.
J. Phys. Oceanog., 10, 1213 - 1220.

Hall M. M. and Bryden H. L. (1982)
Direct estimates and mechanisms of ocean heat transport.
Deep Sea Research, Vol. 29, No 3A, 339-359.

Hideo Kawai (1972)
Kuroshio : its physical aspects. Henry Stommel and Kozo Yoshida Editors. University of Tokyo press.
235 - 352.

Rui Xin Huang (1984)
The thermocline and current structure in subtropical/subpolar basins.
Ph. D. thesis MIT.

Hsiung J. C. (1983)
Large scale sea-air energy fluxes and global sea surface temperature fluctuations.
Ph. D. thesis MIT.

Hsiung J. C. (1986)
Mean surface energy fluxes over the global ocean.
J. Geophys. Res., 91, 10,585 - 10,606.

Hsiung J, Newell R. E., Houghtby T. (1989)
The annual cycle of oceanic heat storage and oceanic meridional heat transport.
Quart. J. Roy. Meteor. Soc 115, 1-28.

Kraus E. B. (1987)
Les couches melangees : energetique, modelisation, et role dans le ssysteme ocean-atmosphere.
La Meteorologie, Vol 17.

Levitus S. (1987)
Meridional Ekman Fluxes for the World Ocean and Individual Ocean Basins.
J. Phys. Oceanog., 17, 1484 - 1492

Niiler P. P. (1977)
One dimensional models of the seasonal thermocline. The Sea,
E. D. Goldberg, I. N. Mc Cave, J. J. O'Brien and J. H. Steele Eds.
Wiley, 97 - 115.

Oort A. H. and T. H. Vonder Haar (1976)
On the observed annual cycle in the ocean-atmosphere heat balance over the Northern Hemisphere.
J. Phys. Oceanog., 6, 781-800

Riser S. C., Freeland H. and Rossby H. T. (1978)
Mesoscale motions near the deep western boundary current of the North Atlantic circulation.
Deep Sea Research 25, 1179 - 1191.

Schopf P. S. and Cane M. A.(1983)
On Equatorial Dynamics Mixed-Layer Physics and SST.
J. Phys. Oceanog., 13, 917 - 935.

Slutz R. J. and seven others (1985)
COADS, Comprehensive Ocean - Atmosphere Data Set
Release 1, CIRES-ERL-NCAR-NCDC, Boulder, CO, 39 pp.

Worthington L. V. (1976)
On the North Atlantic Circulation.
The John Hopkins Oceanographic Studies 6.
John Hopkins University Press, 110 pp.

Annexe I : Acronyms

MBT : Mechanical Bathythermograph

XBT : Expendable Bathythermograph

AXBT : Aircraft dropped XBT

STD : Salinity temperature density probe

Annexe II :

1) Total number of soundings at each grid square integrated into the computation of the seasonal climatology of the mixed-layer depth. Results are shown for each season. Atlantic Ocean.

2) Number of years with observation at each grid square for the mixed-layer depth seasonal climatology. Atlantic Ocean.

3) Standard deviation for the mixed-layer depth seasonal climatology. Atlantic Ocean.

4) Same as 1,2,3 but for the Pacific Ocean.

Total number of soundings at each grid square integrated into the MLD computation for Fall, 1949 - 1979

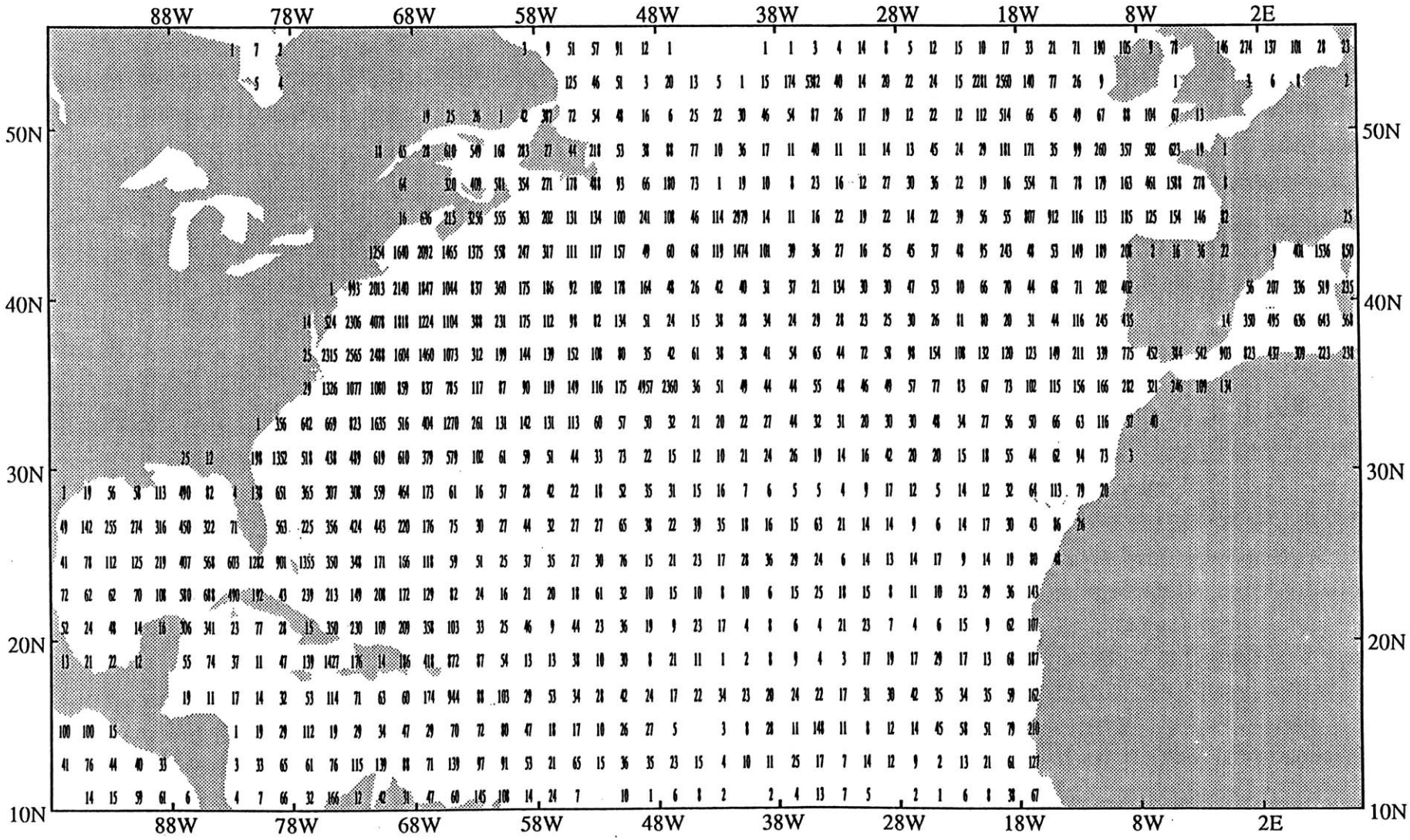

Total number of soundings at each grid square integrated into the MLD computation for Summer, 1949 - 1979

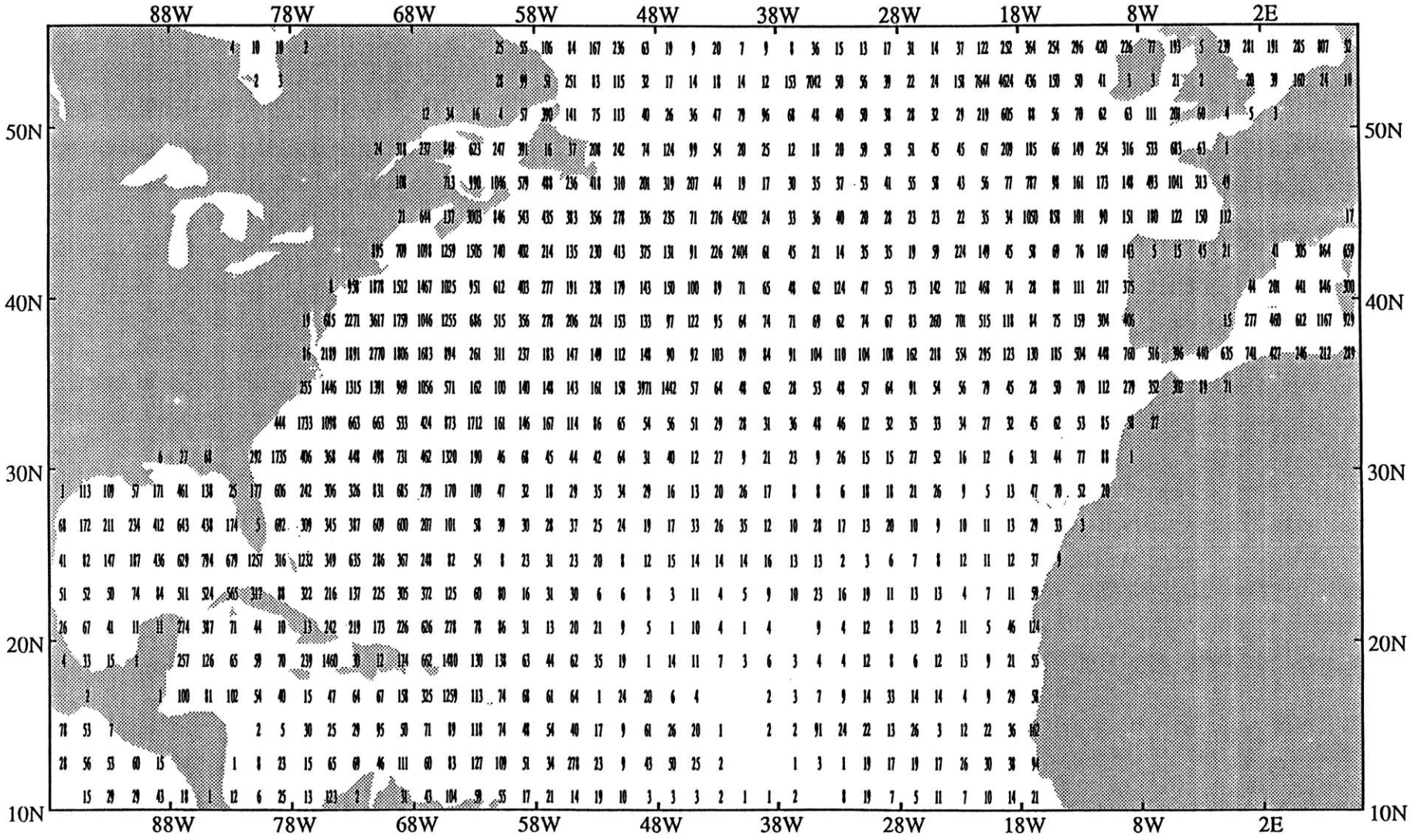

Total number of soundings at each grid square integrated into the MLD computation for Spring, 1949 - 1979

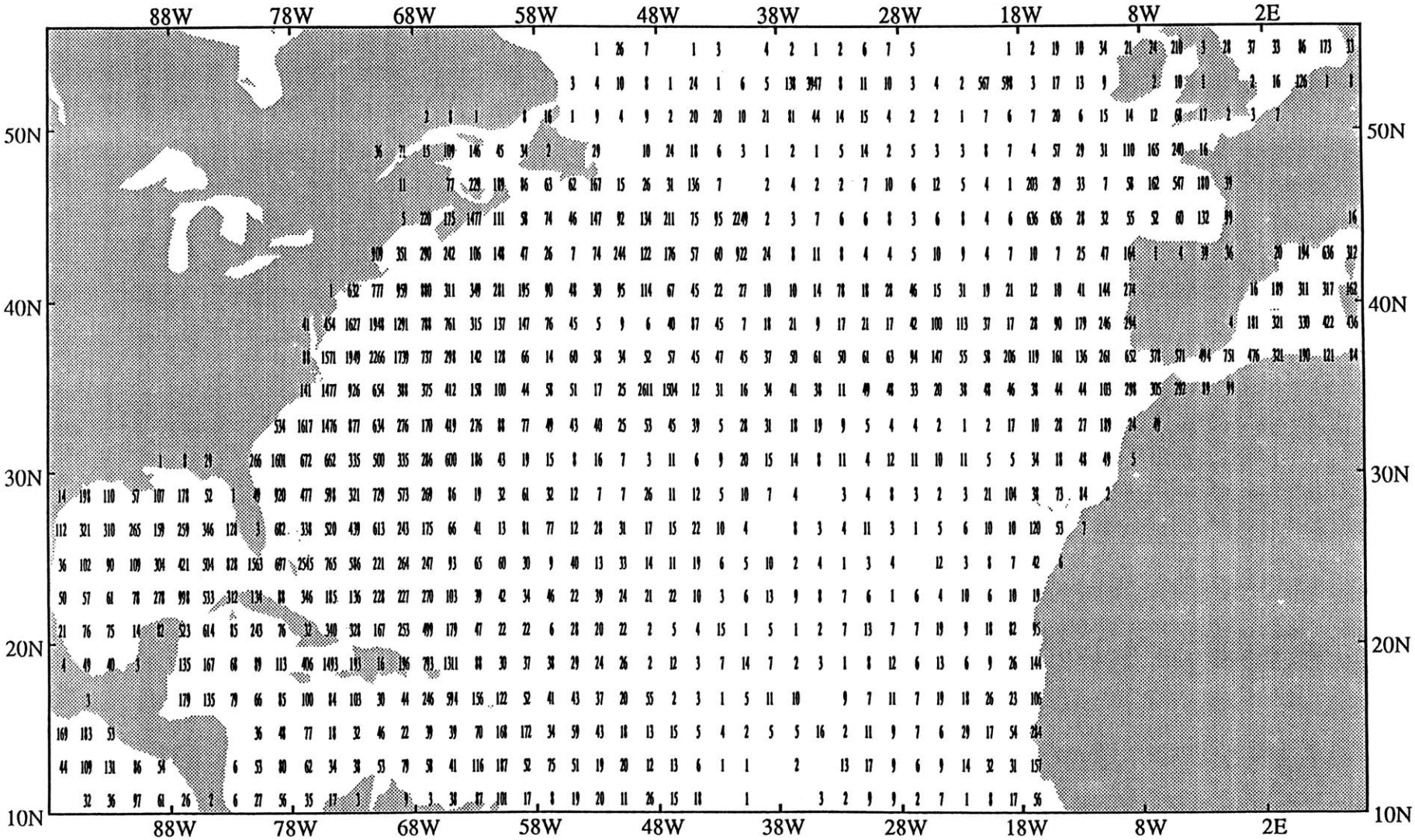

Total number of soundings at each grid square integrated into the MLD computation for Winter, 1949 - 1979

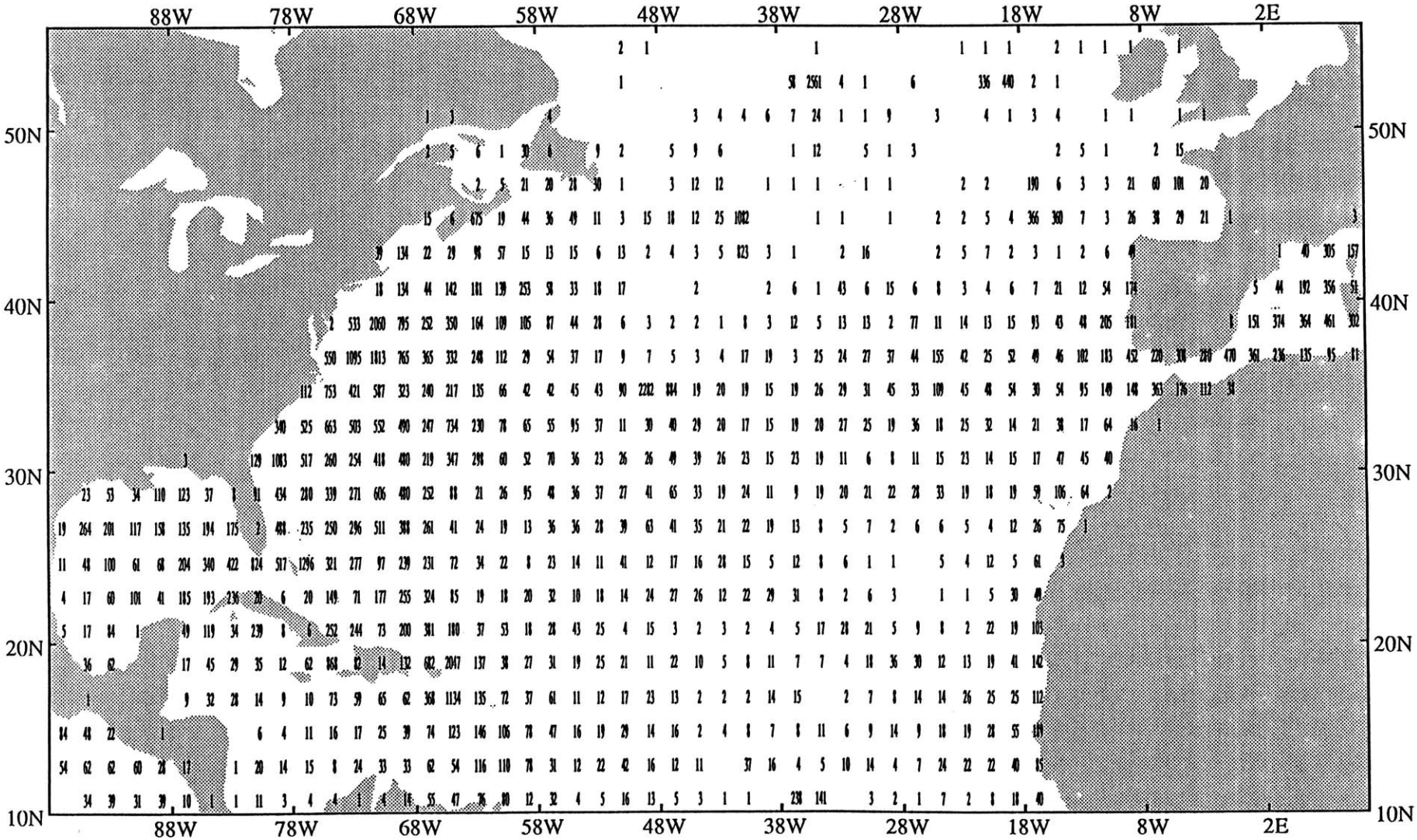

MLD
Max. Nr. = 31

Number of years with observation at each grid square for Fall, 1949 - 1979

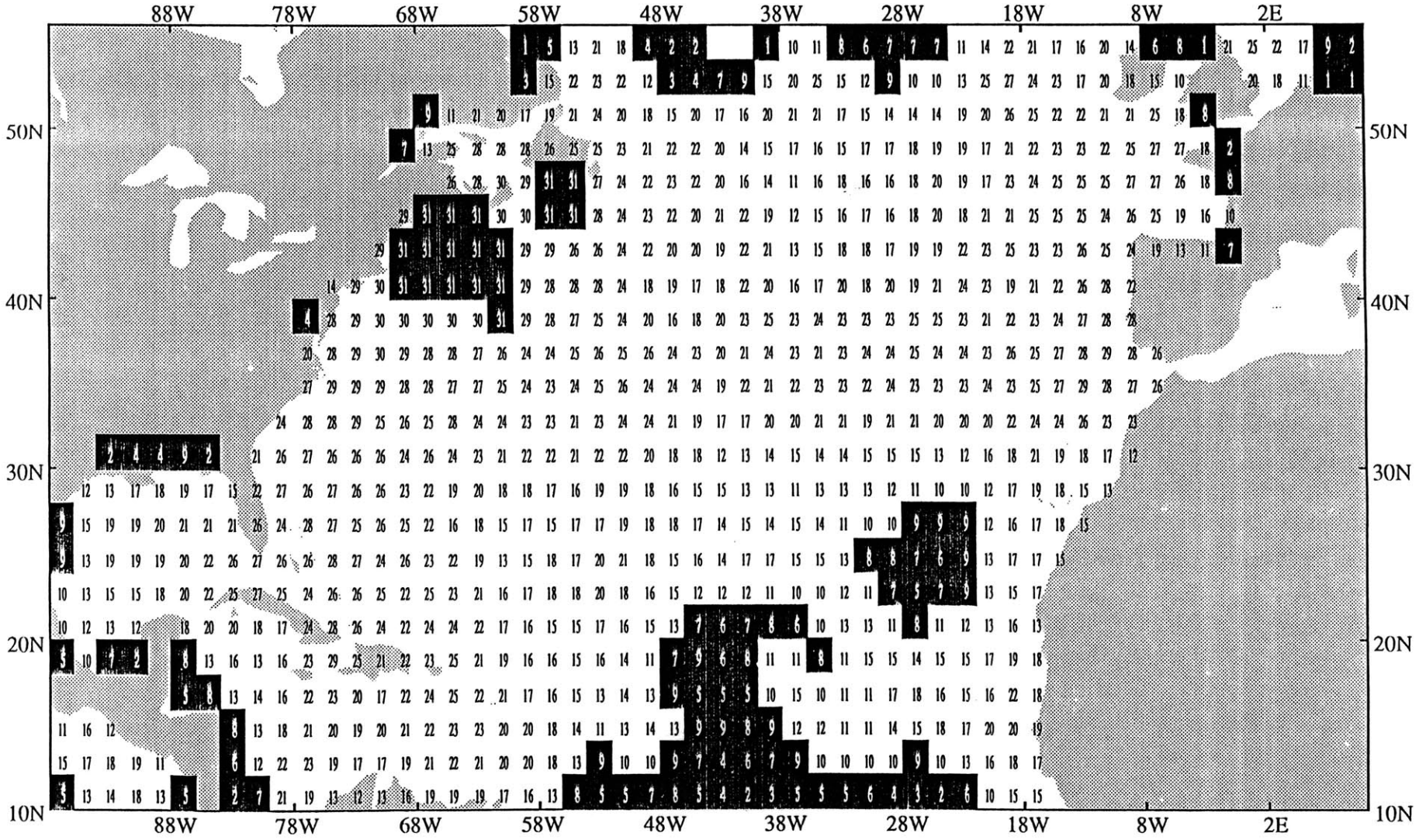

MLD
Max. Nr. = 31

Number of years with observation at each grid square

for Summer, 1949 - 1979

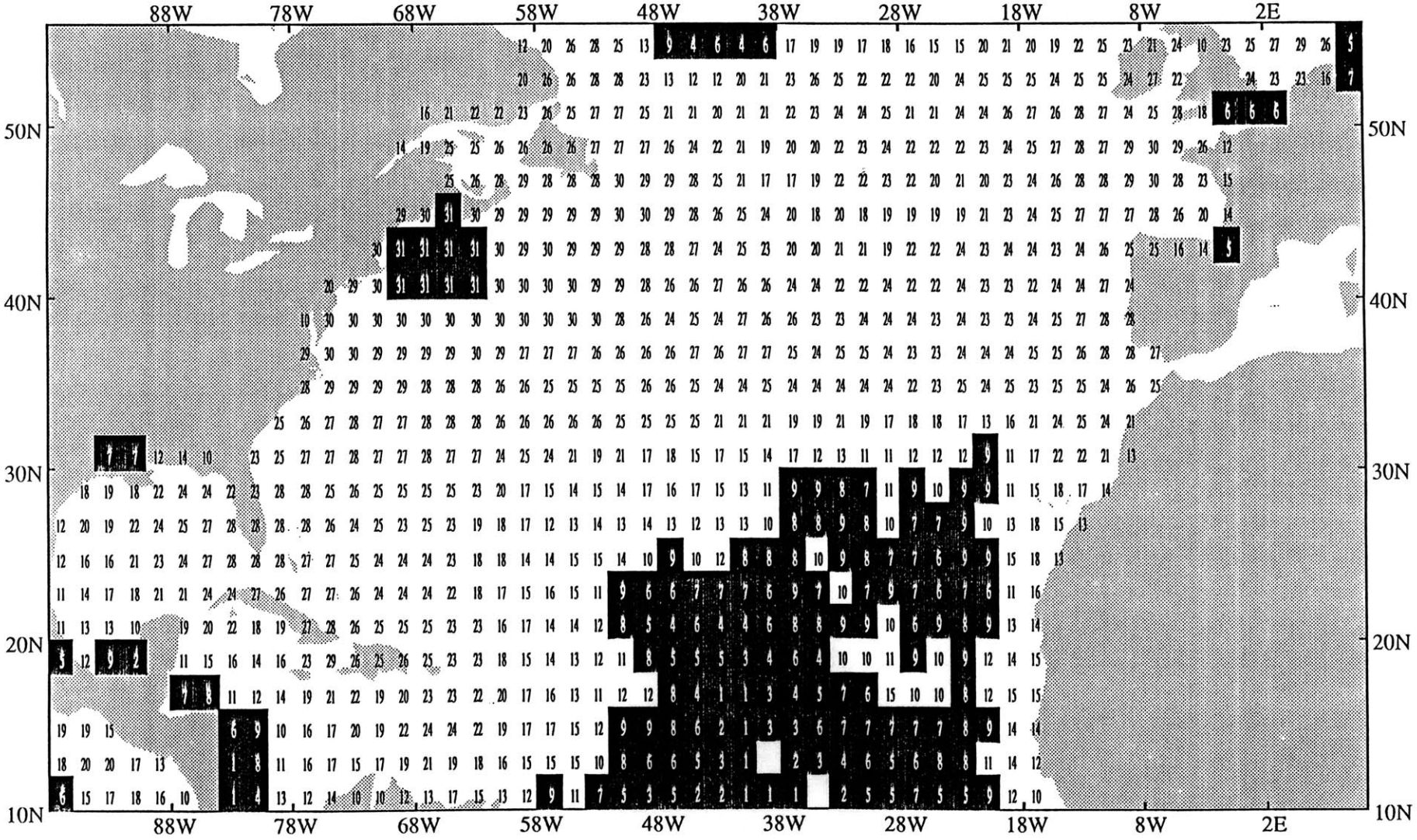

MLD

Max. Nr. = 31

Number of years with observation at each grid square for Spring, 1949 - 1979

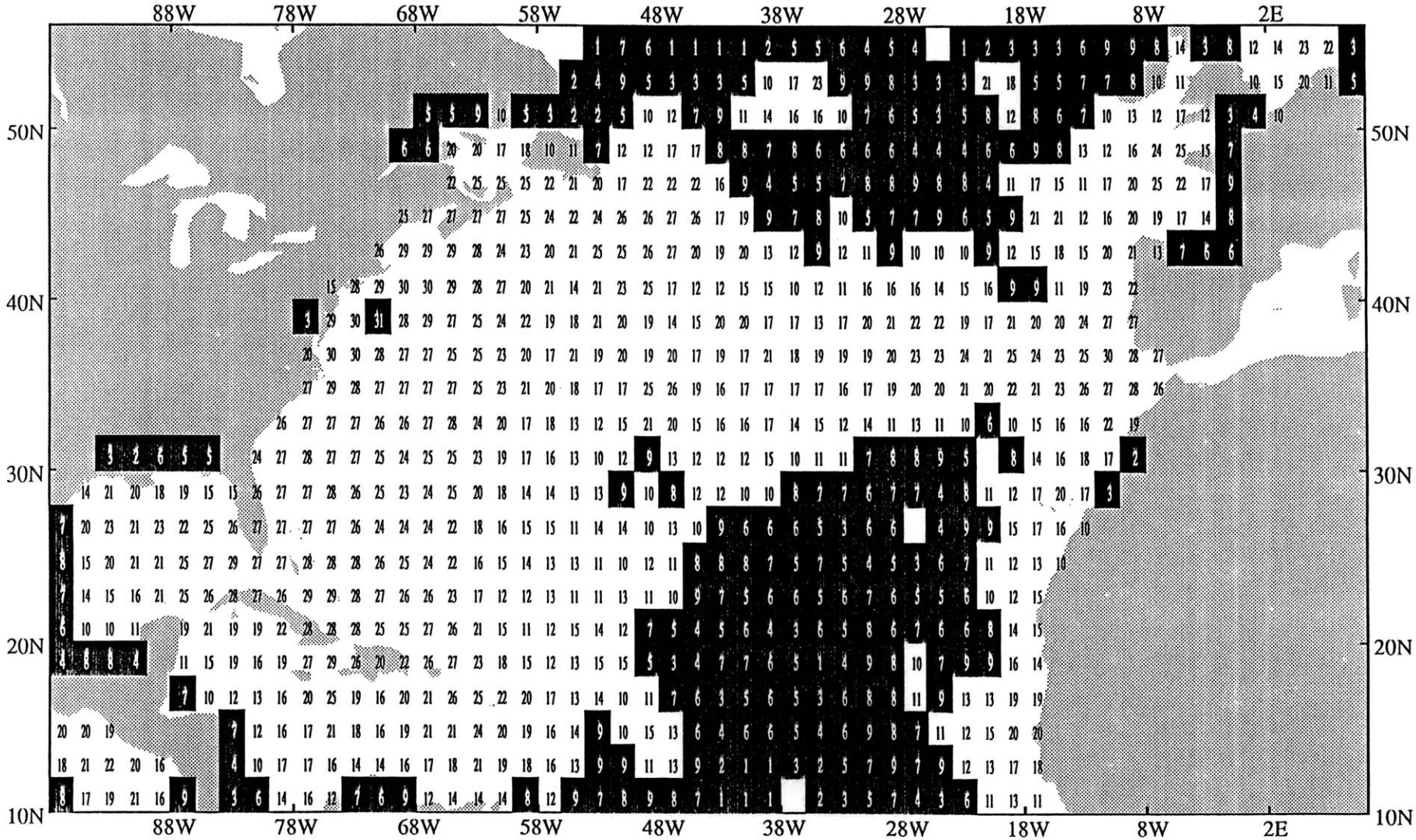

MLD
Max. Nr. = 31

Number of years with observation at each grid square for Winter, 1949 - 1979

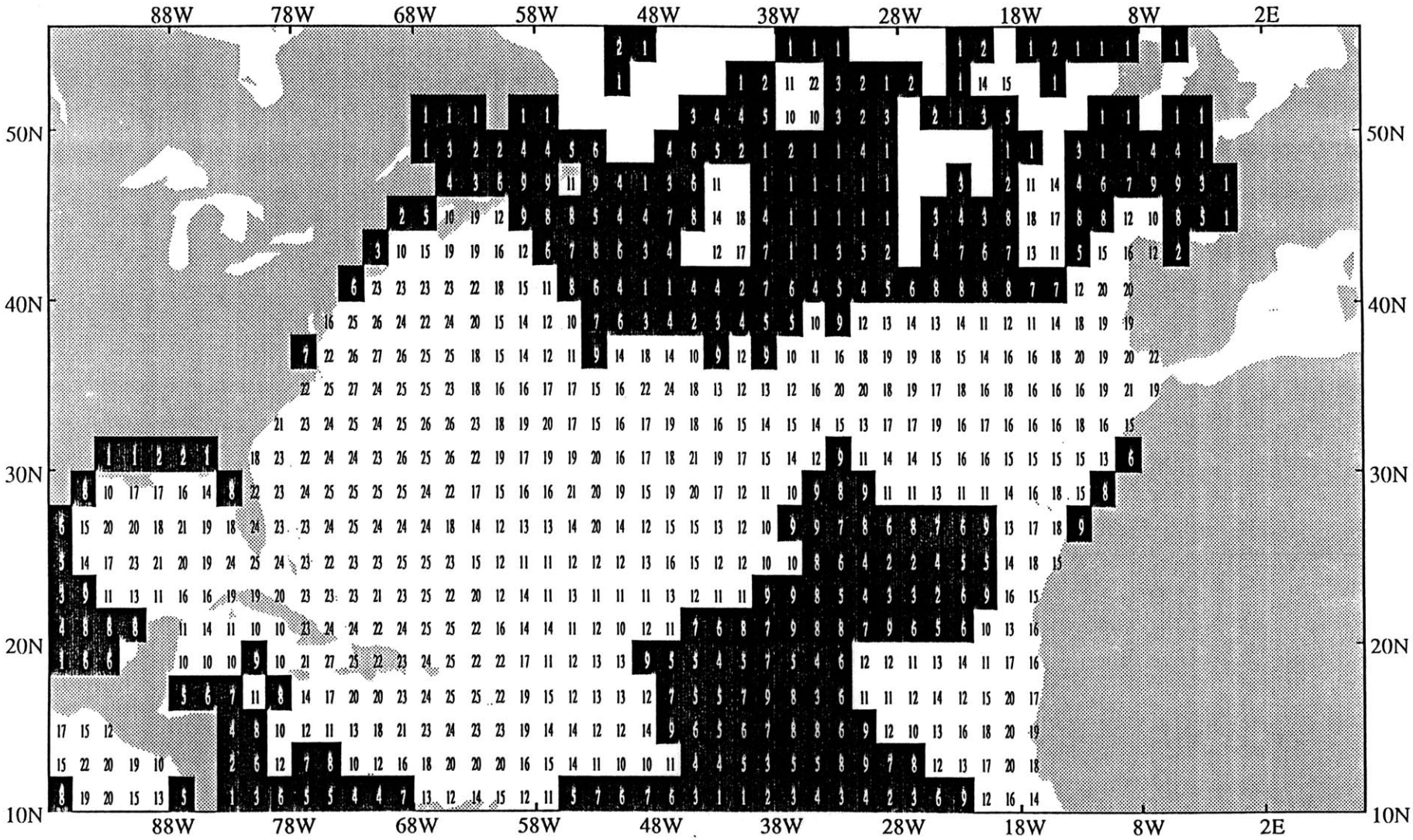

Standard deviation at each grid square
for Fall, 1949 - 1979

MLD
In meter

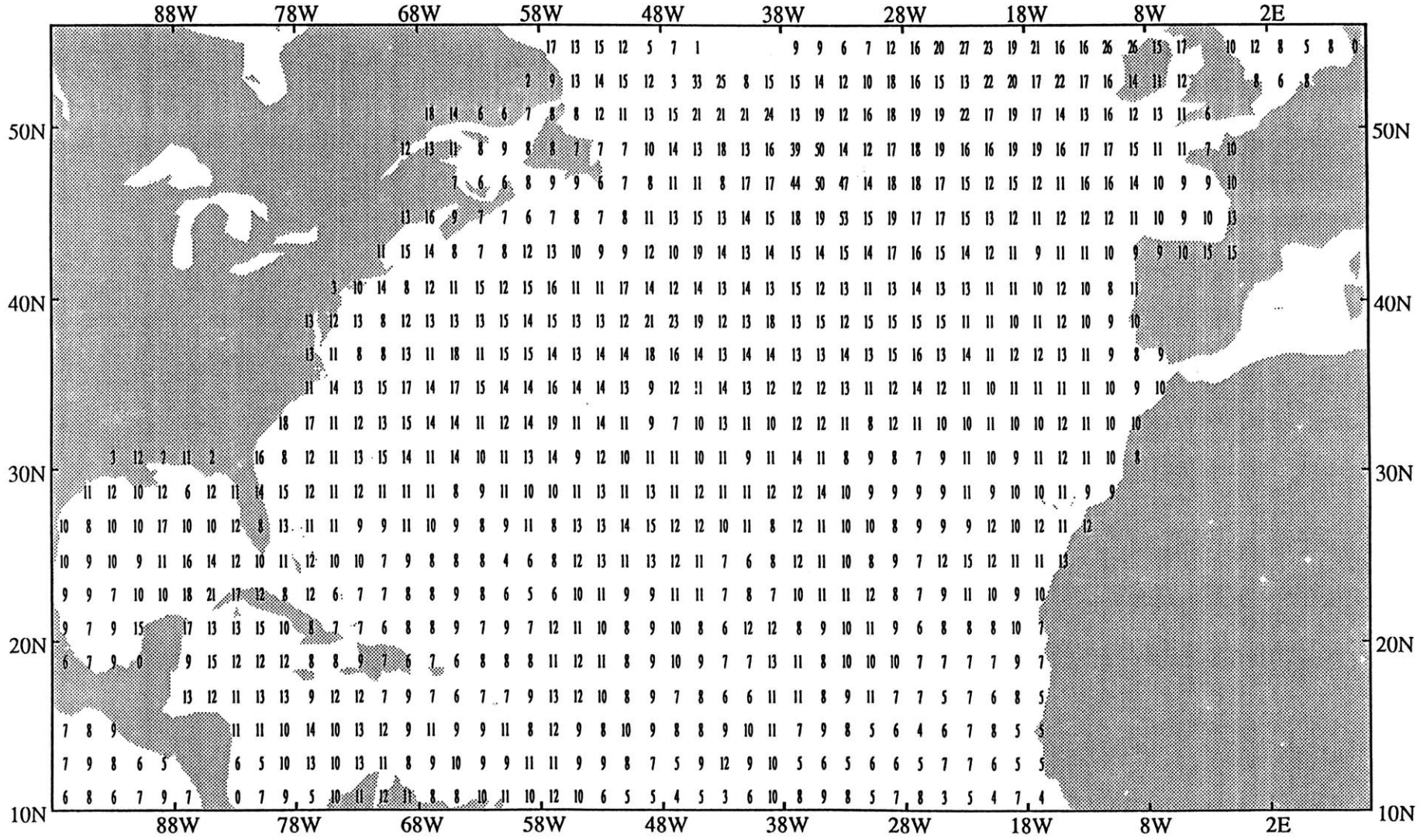

Standard deviation at each grid square
for Summer, 1949 - 1979

MLD
In meter

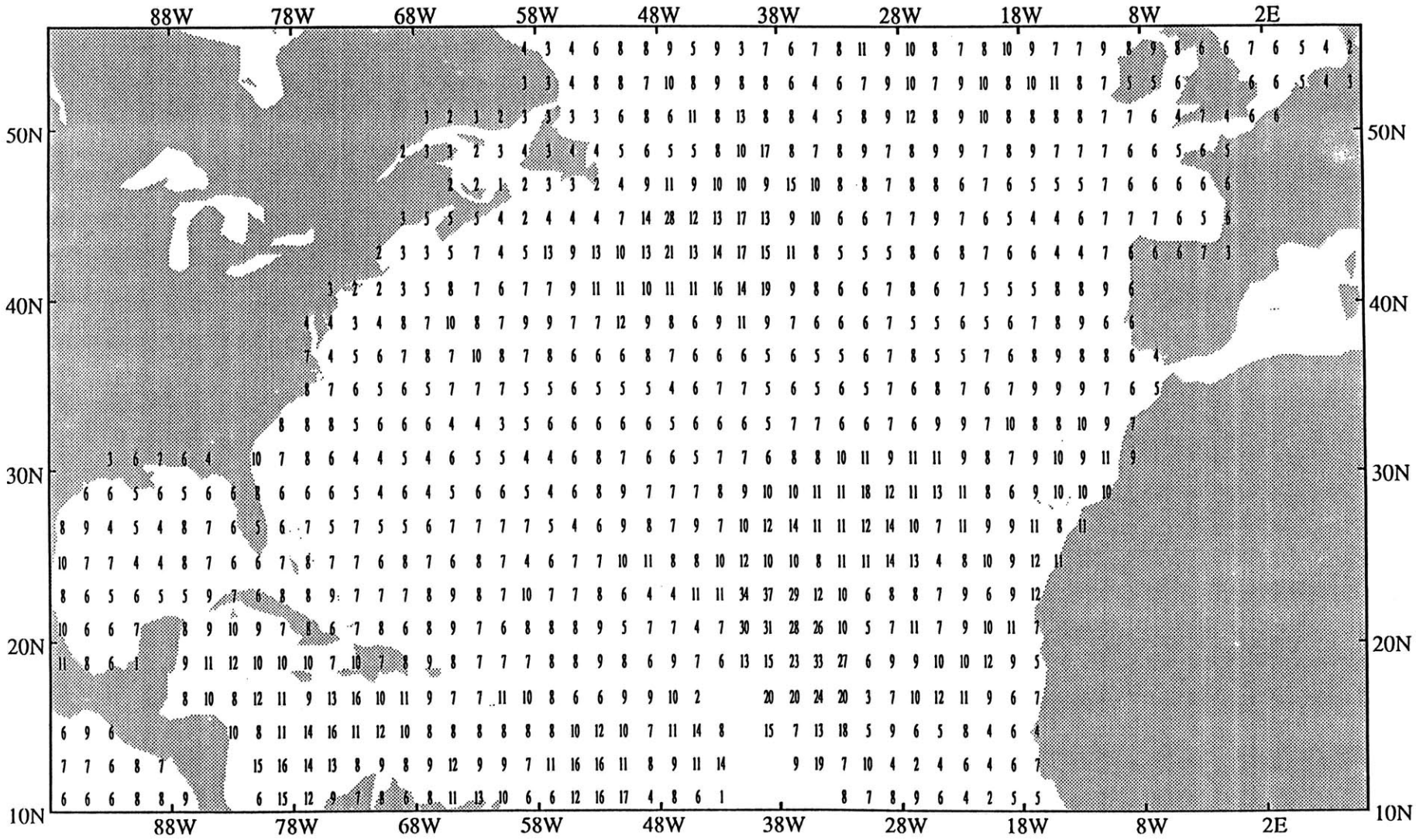

Standard deviation at each grid square
for Spring, 1949 - 1979

MLD
In meter

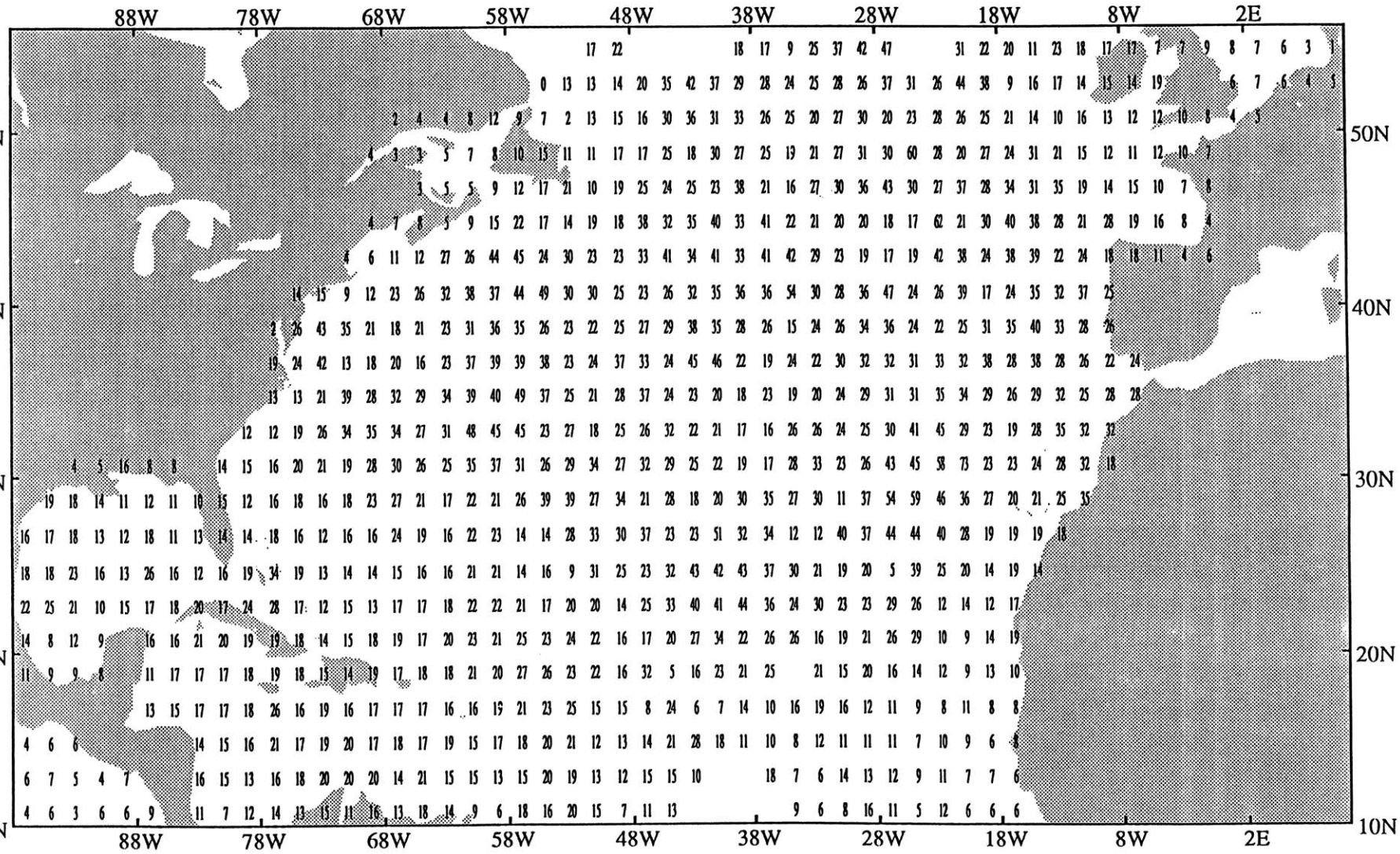

Standard deviation at each grid square
for Winter, 1949 - 1979

MLD
In meter

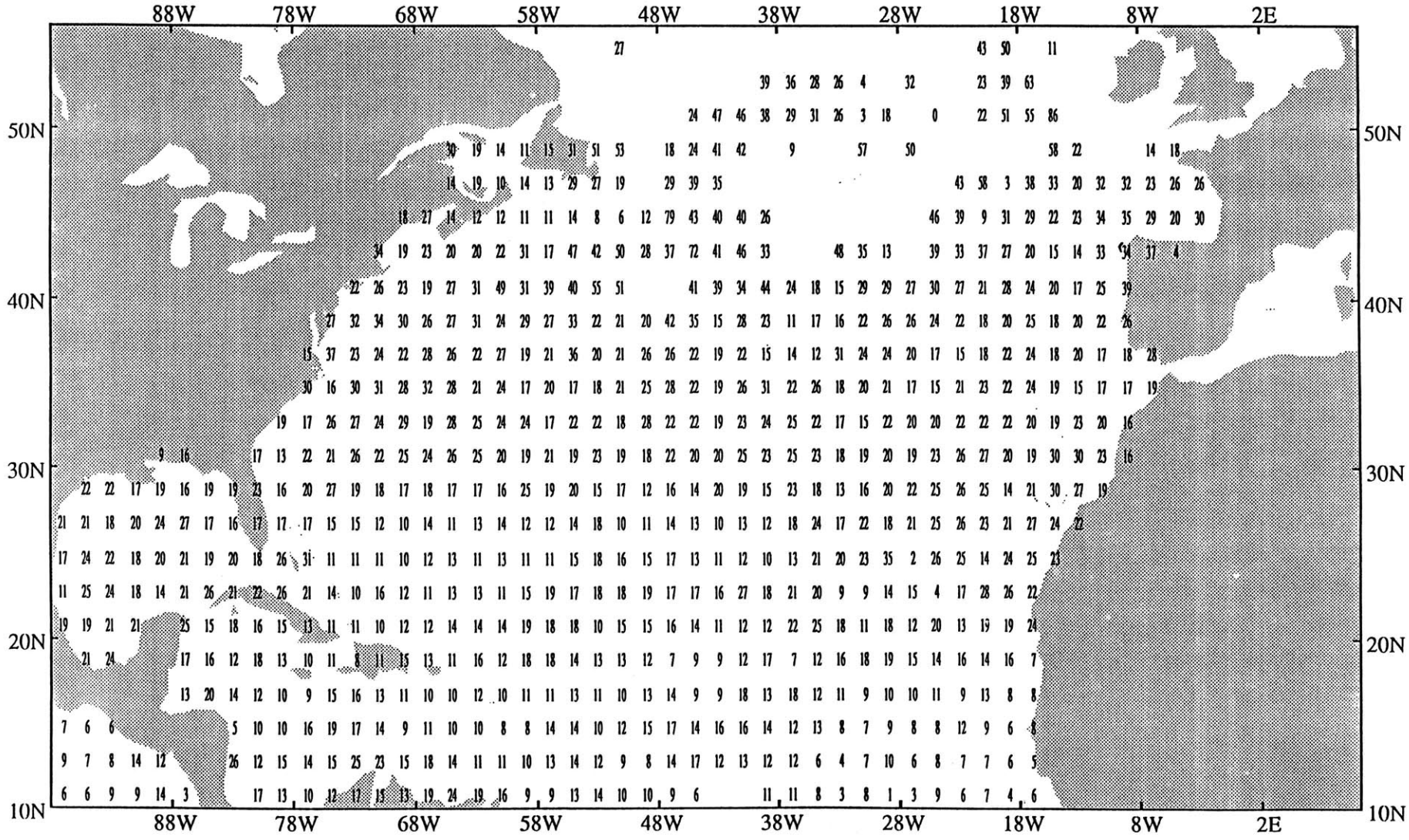

Total number of soundings at each grid square integrated into the MLD computation for Fall, 1949 - 1979

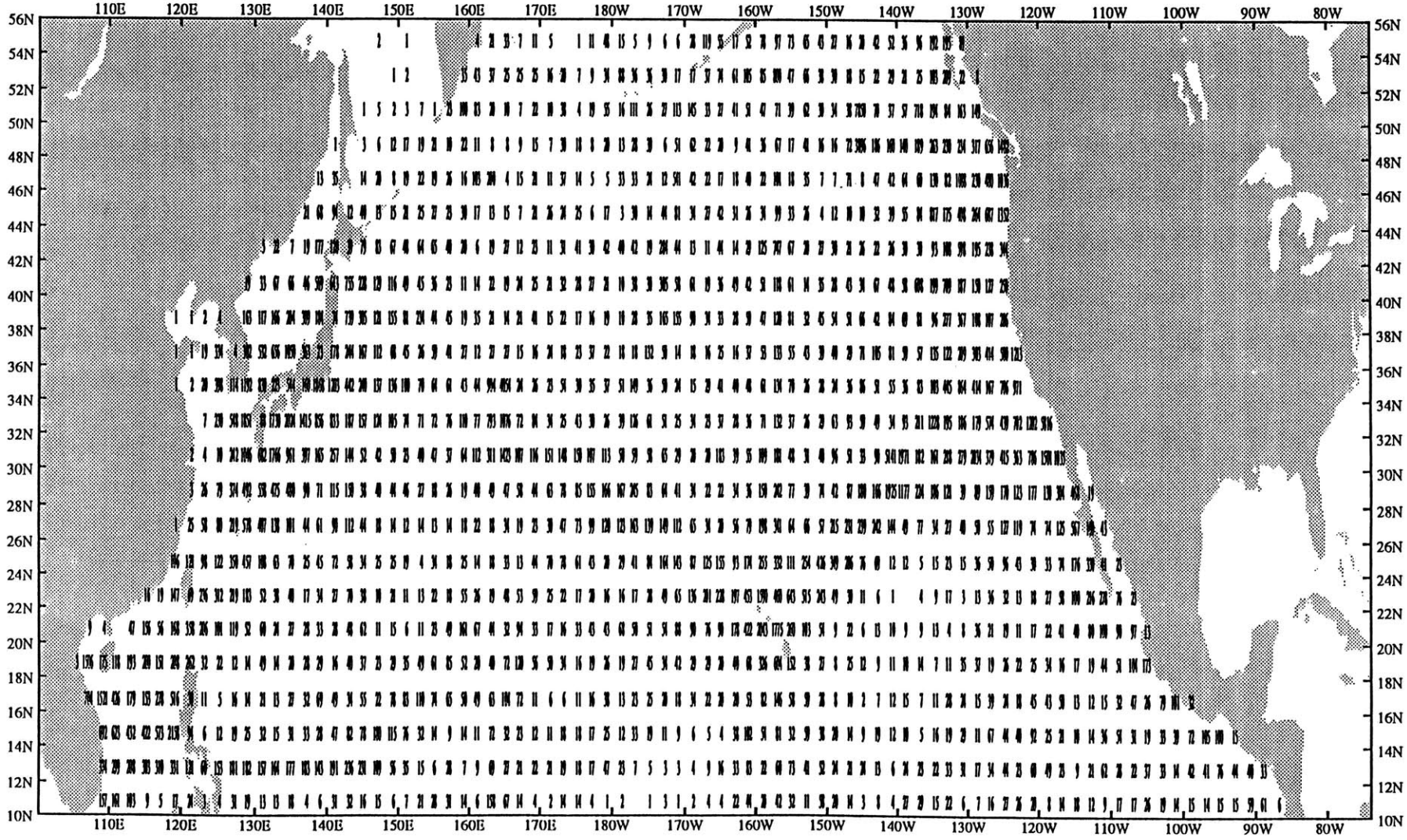

Total number of soundings at each grid square integrated into the MLD computation for Summer, 1949 - 1979

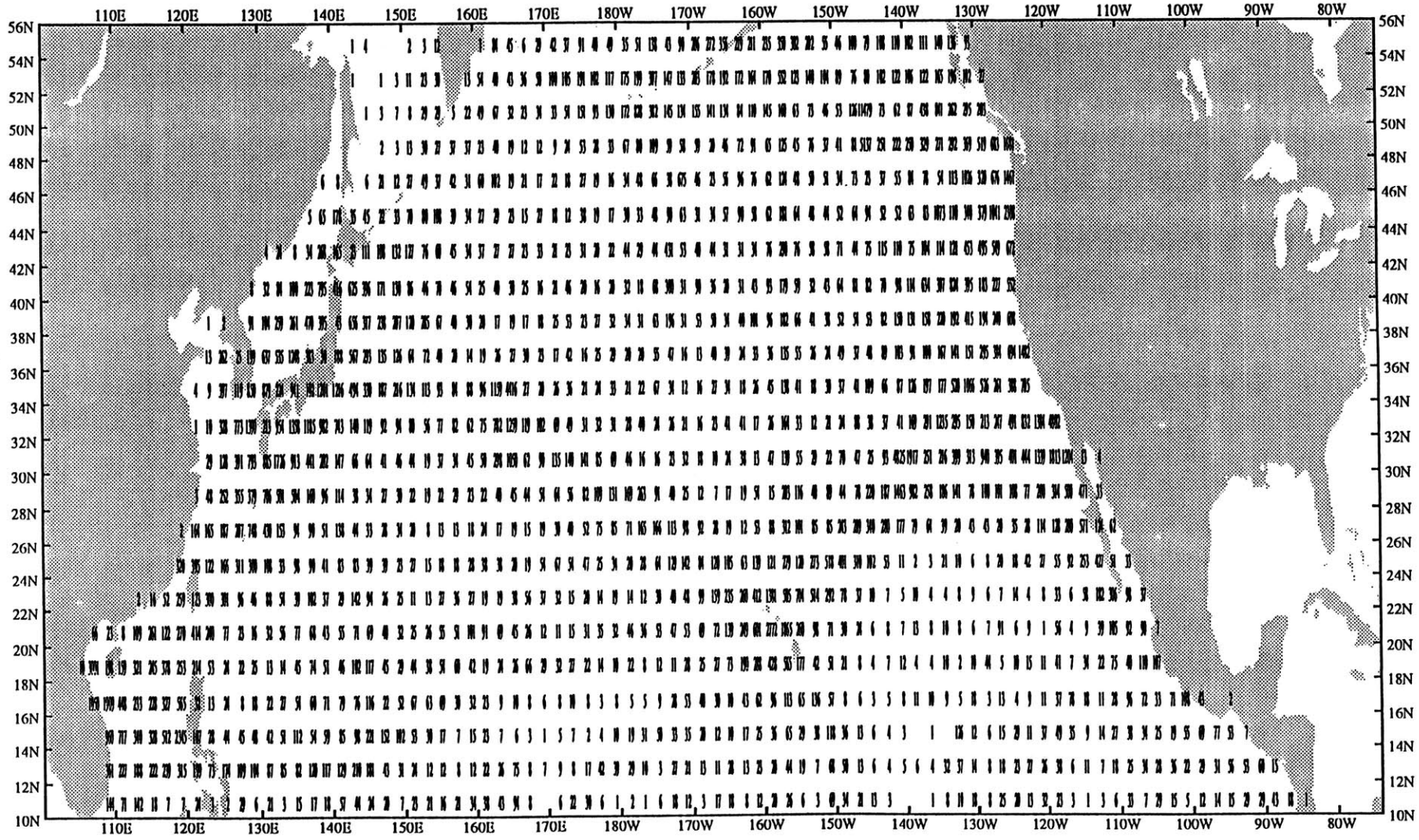

Total number of soundings at each grid square integrated into the MLD computation for Spring, 1949 - 1979

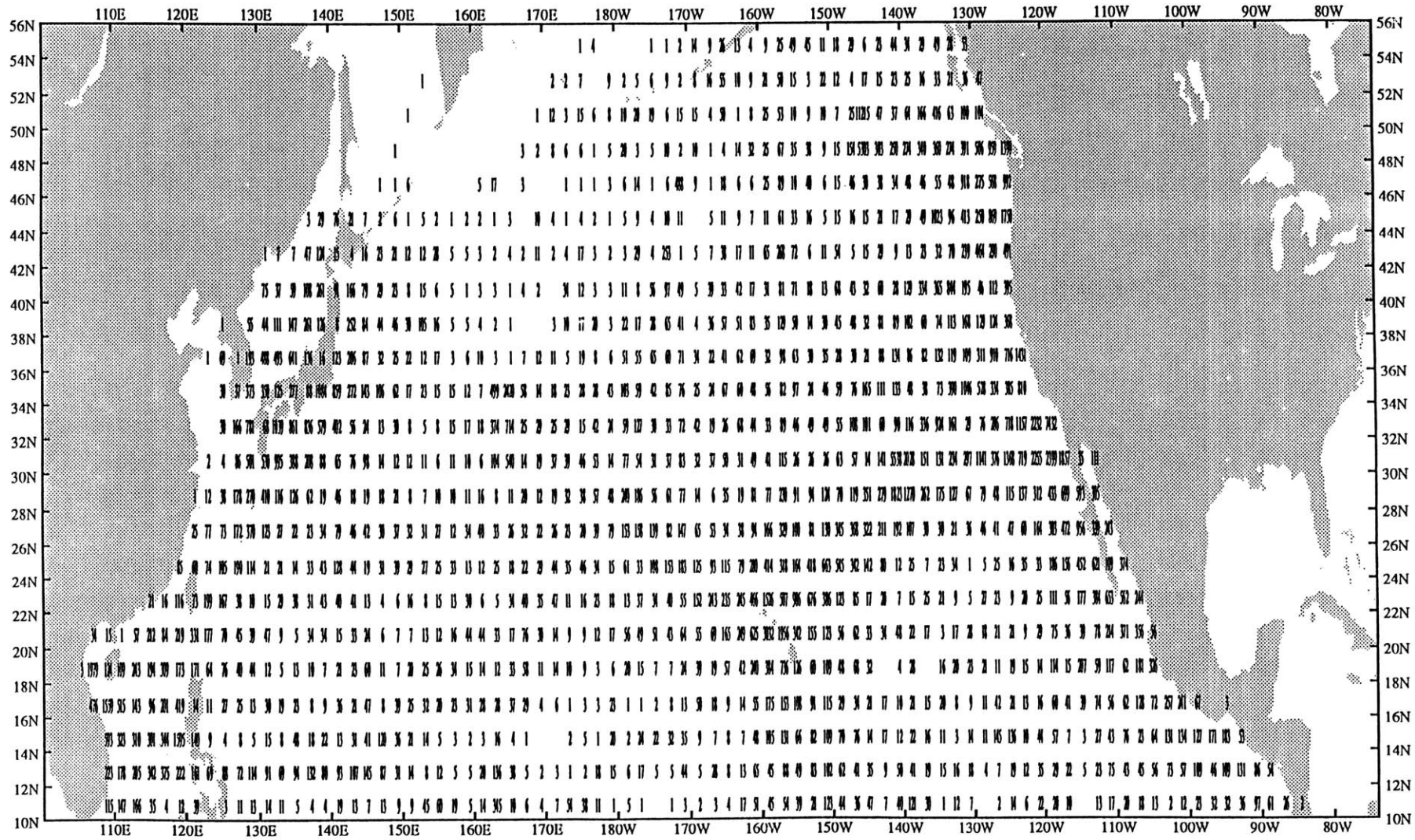

Total number of soundings at each grid square integrated into the MLD computation for Winter, 1949 - 1979

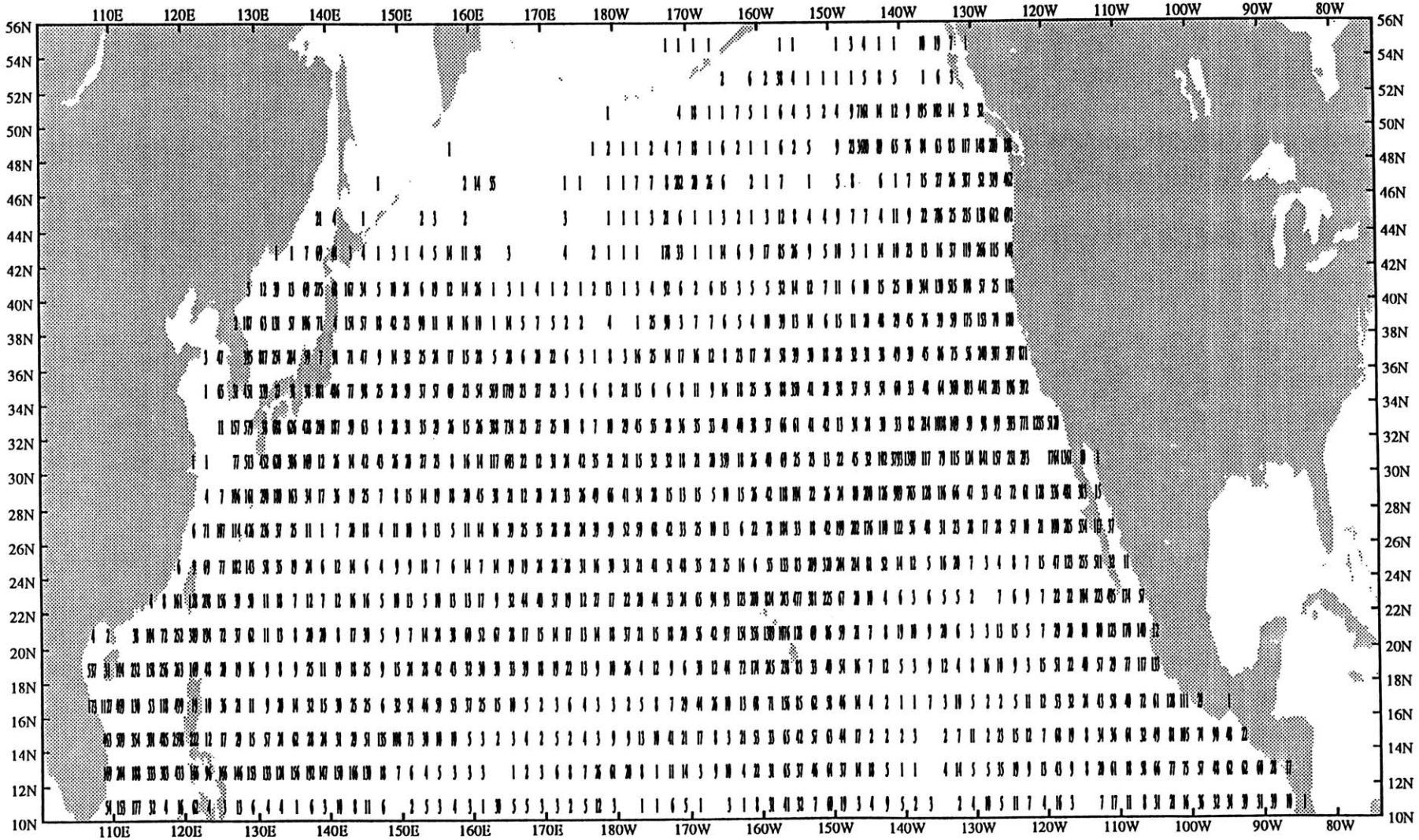

MLD
Max Nr. = 31

Number of years with observation at each grid square

for Spring, 1949 - 1979

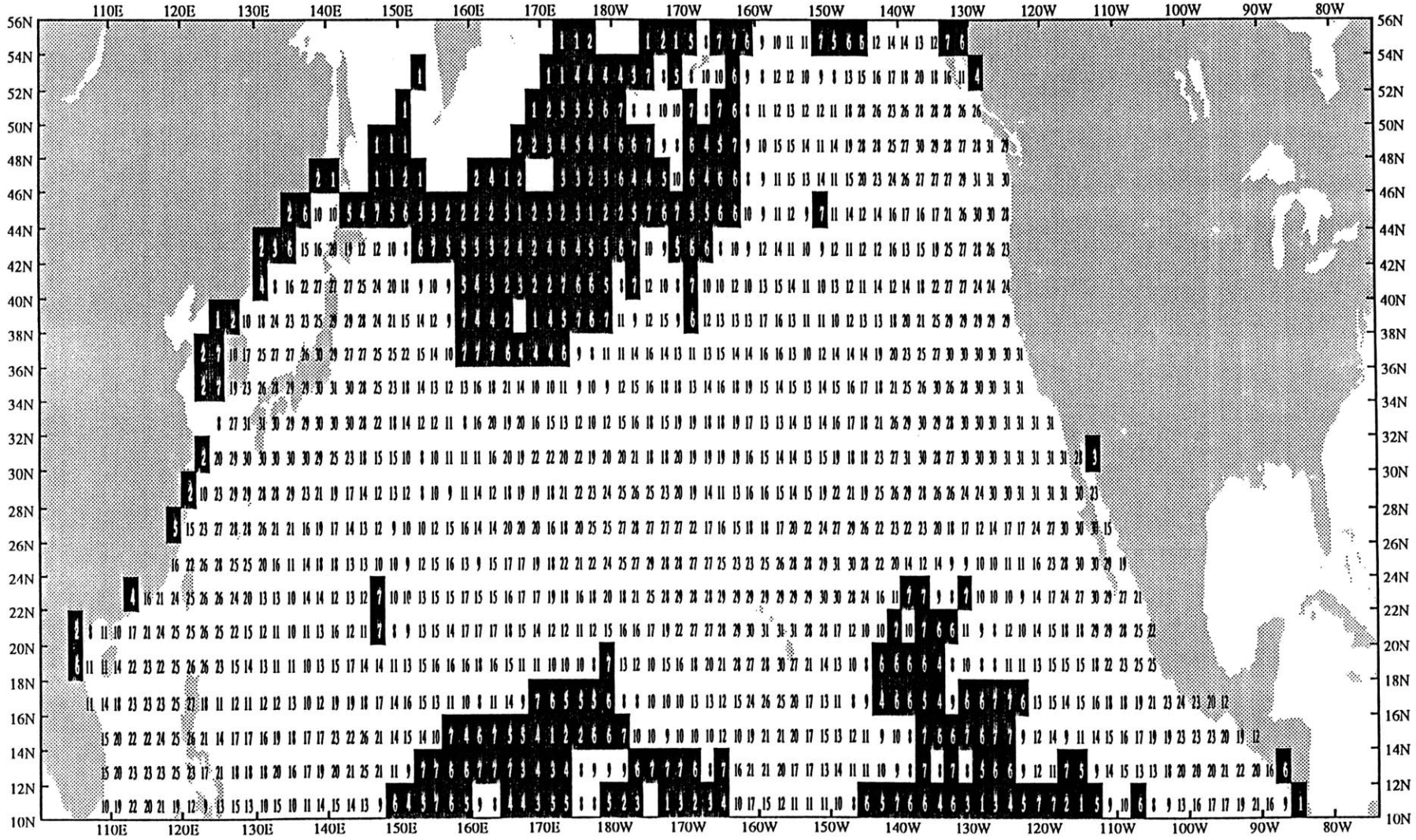

Number of years with observation at each grid square

for Summer, 1949 - 1979

MLD
Max Nr. = 31

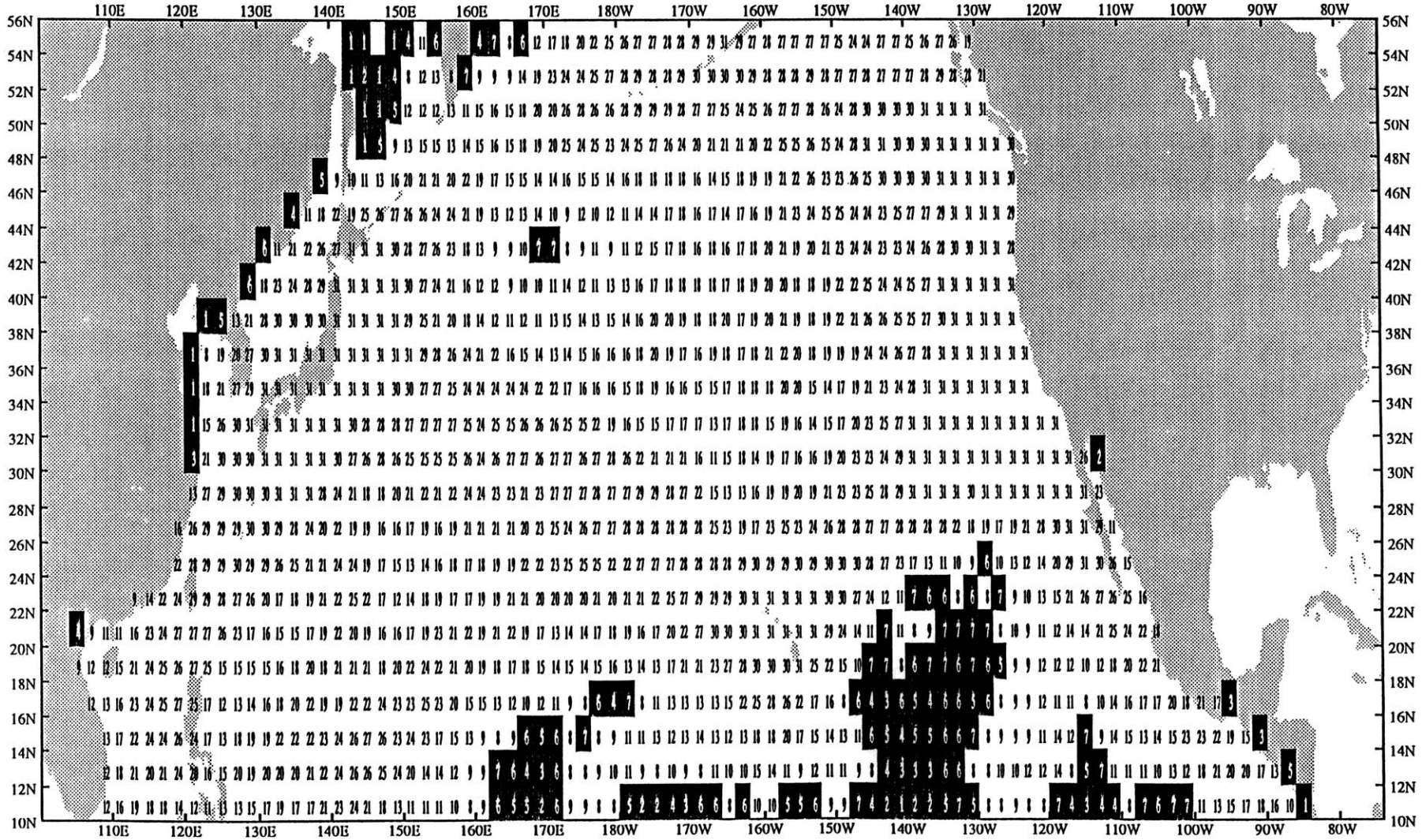

Number of years with observation at each grid square

for Fall, 1949 - 1979

MLD
Max Nr. = 31

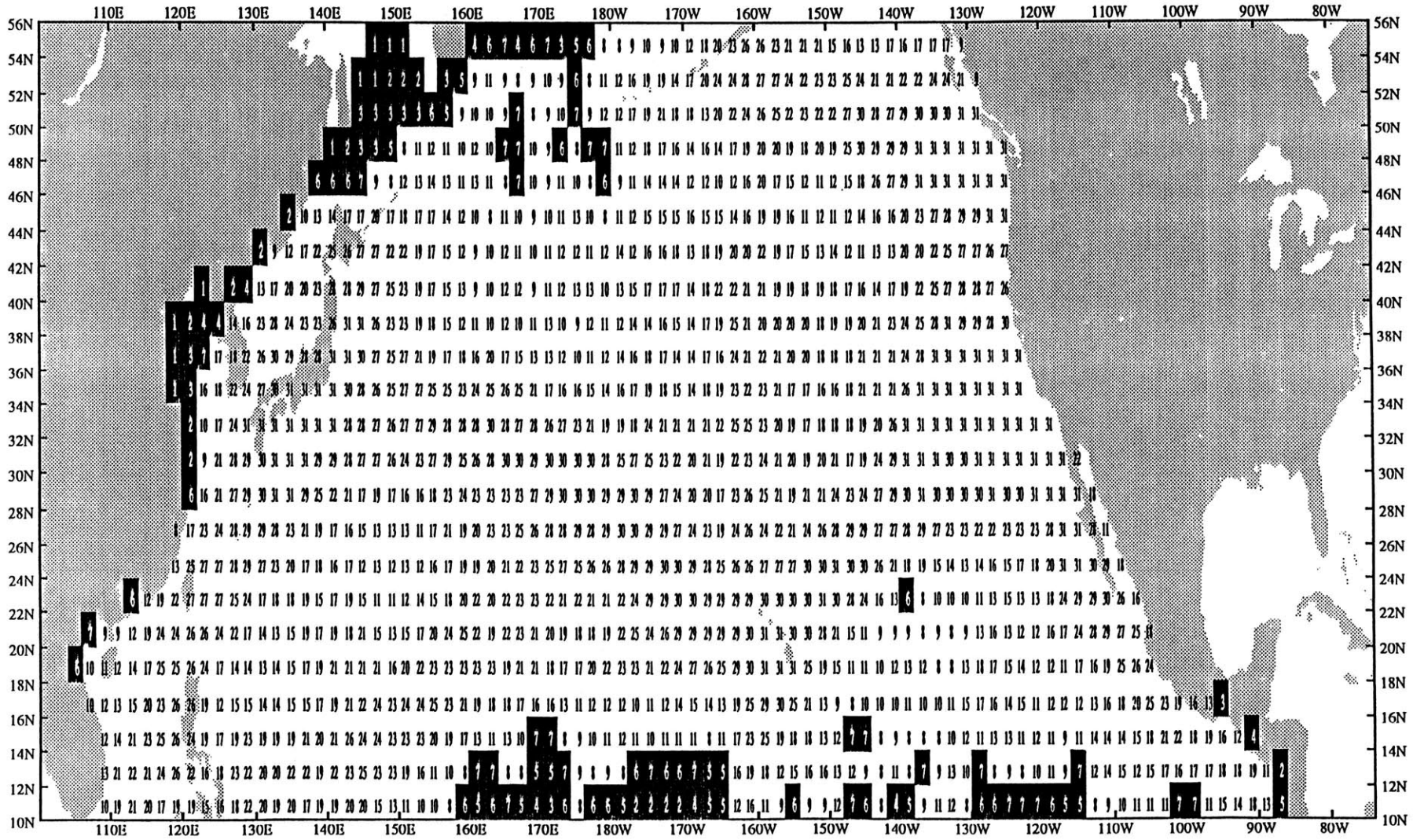

MLD
Max Nr. = 31

Number of years with observation at each grid square

for Winter, 1949 - 1979

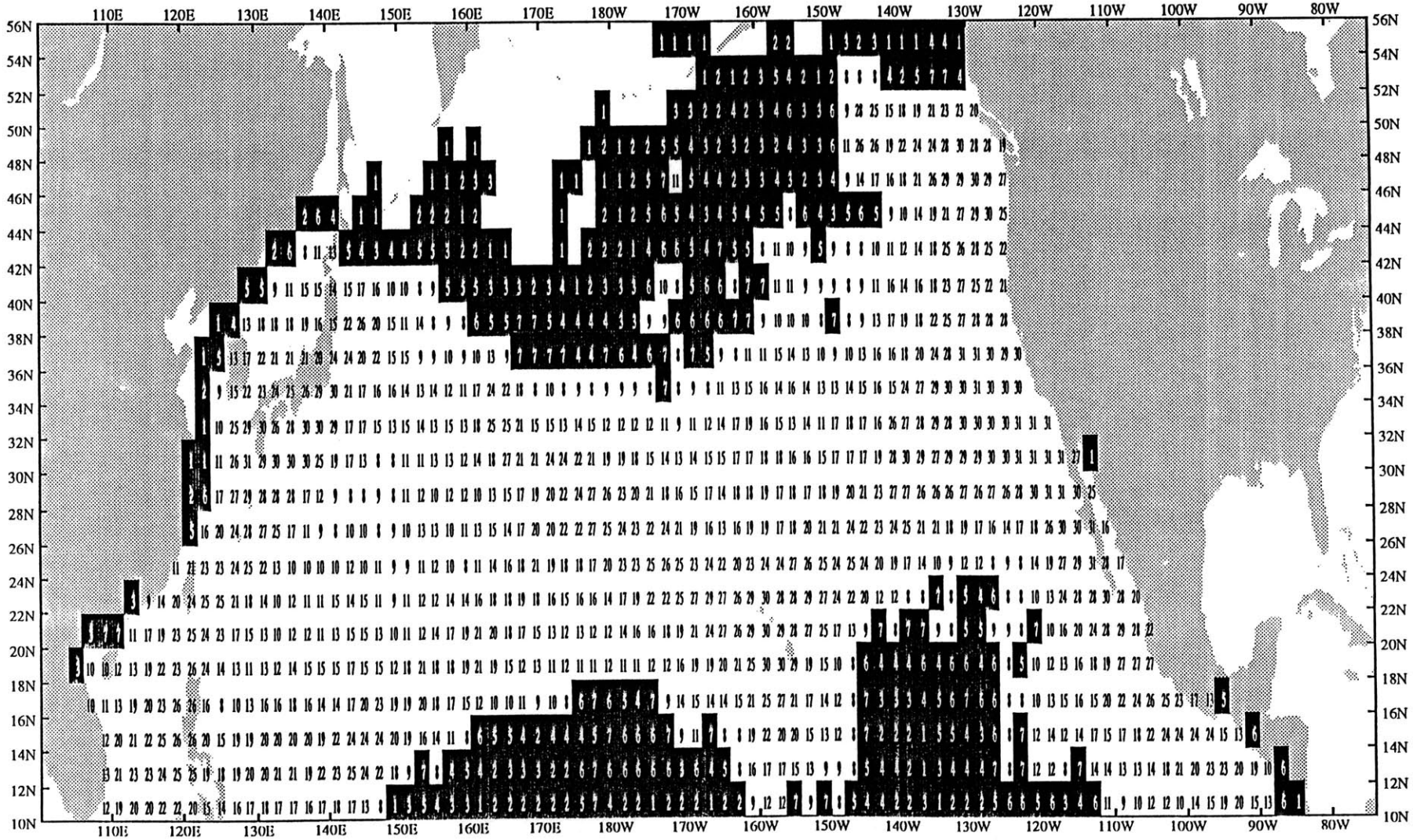

Standard deviation at each grid square
for Fall, 1949 - 1979

MLD
In meter

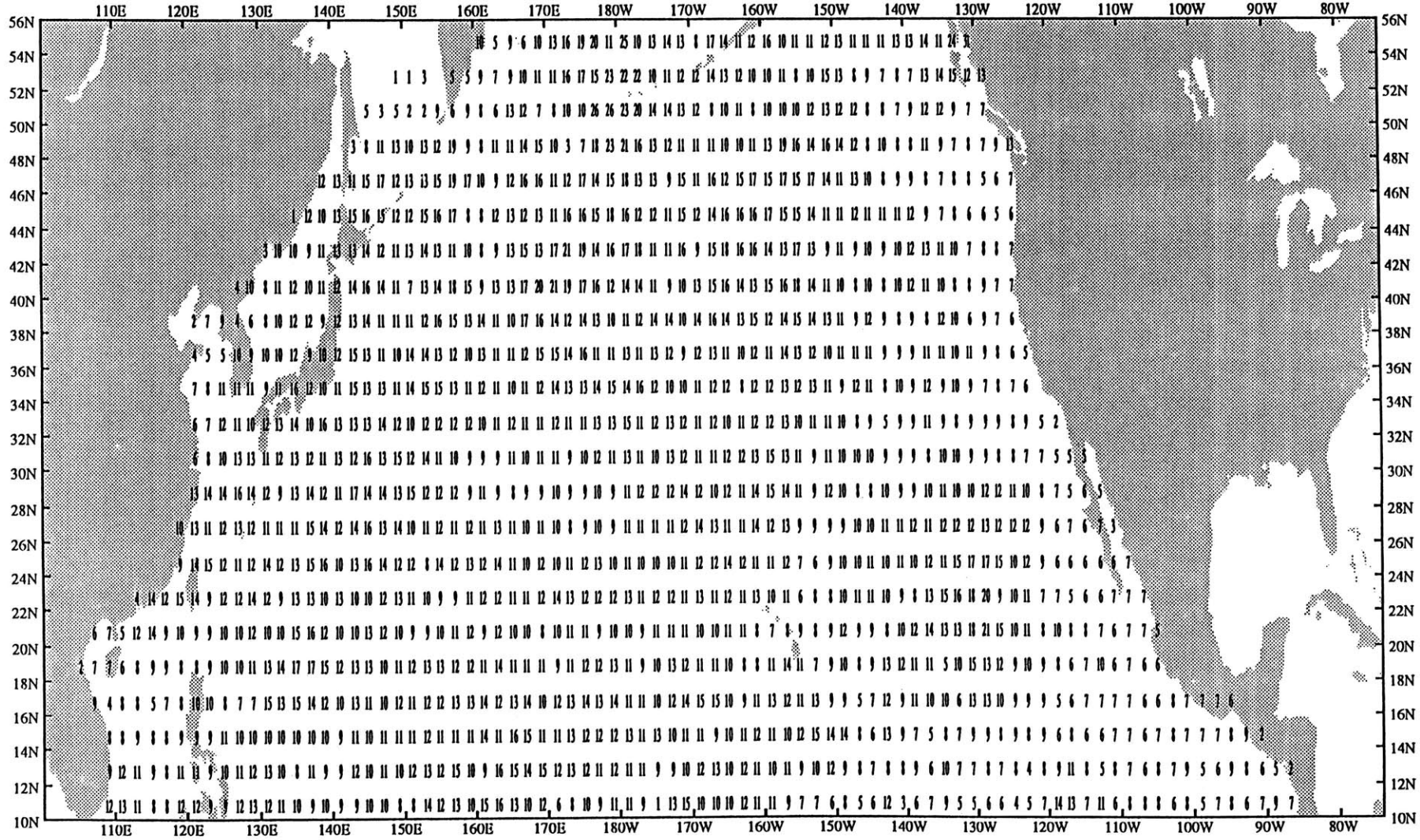

Standard deviation at each grid square
for Summer, 1949 - 1979

MLD
In meter

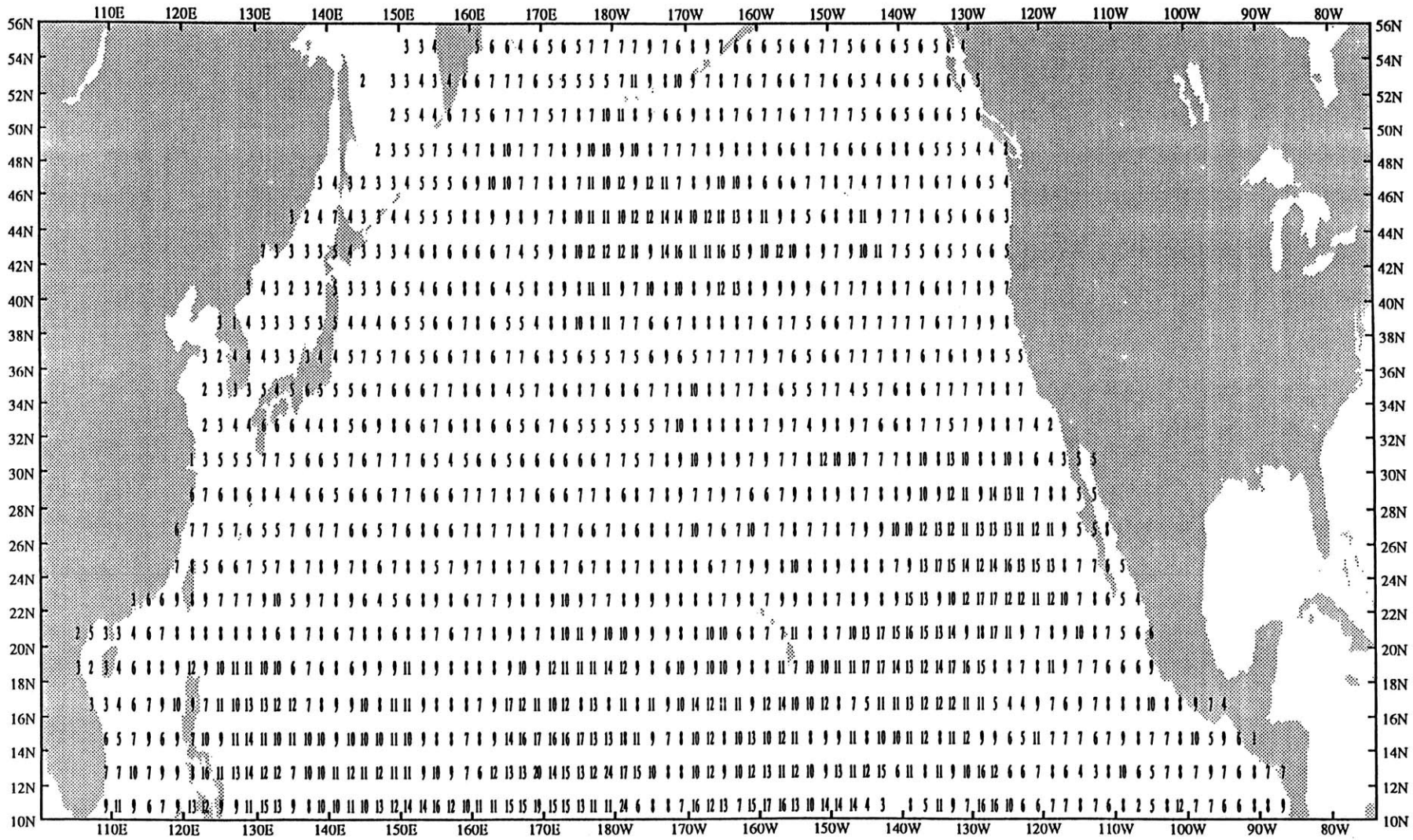

Standard deviation at each grid square for Spring, 1949 - 1979

MLD
In meter

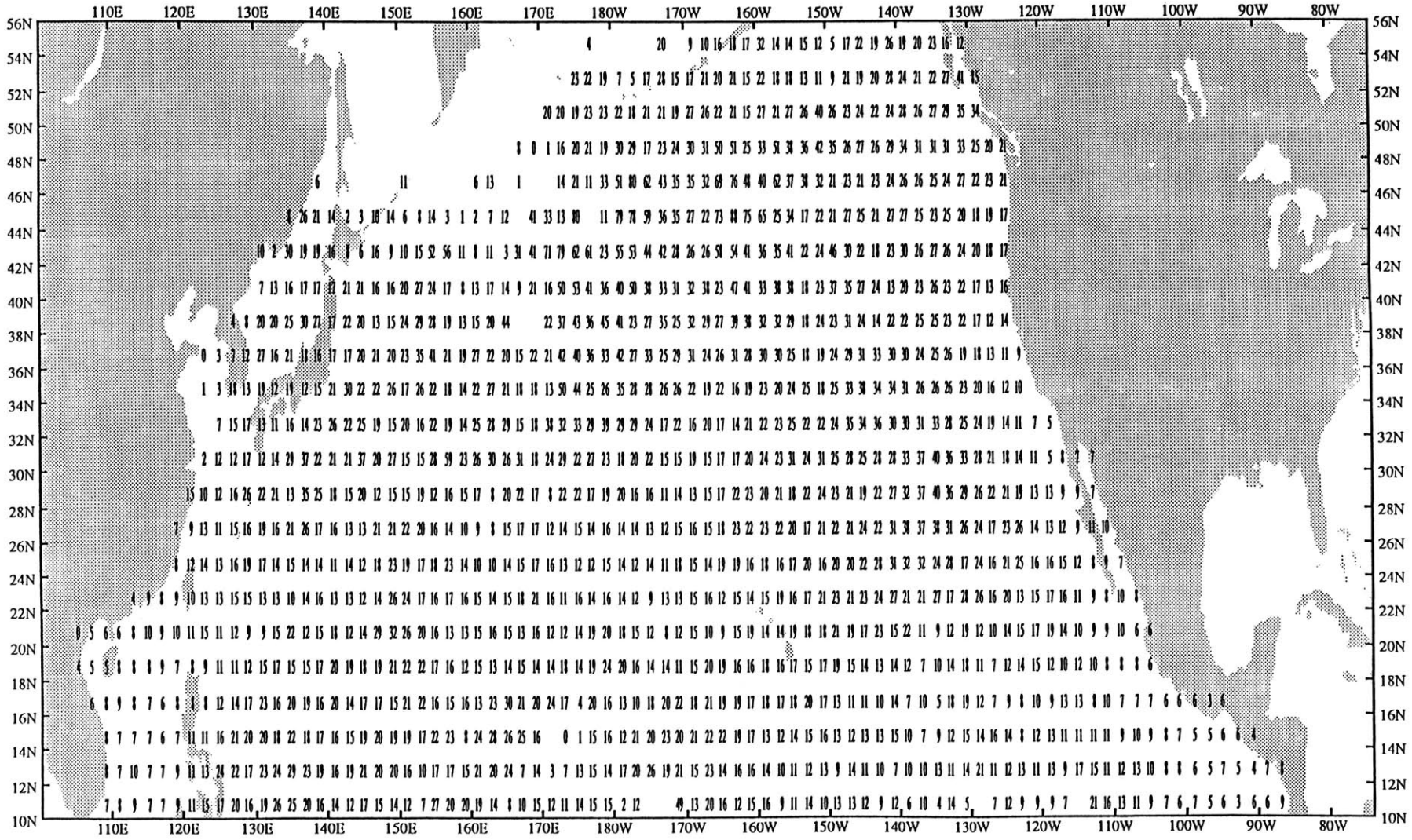

Standard deviation at each grid square for Winter, 1949 - 1979

MLD
In meter